AFFINITY AND SELECTIVITY OF AZACYANINES TO G-QUADRUPLEX FORMING PROMOTER REGIONS

A THESIS SUBMITTED TO
THE GRADUATE SCHOOL OF NATURAL AND APPLIED SCIENCES
OF
MIDDLE EAST TECHNICAL UNIVERSITY

BY

FAHRİYE NUR KIRMACI

IN PARTIAL FULFILLMENT OF THE REQUIREMENTS
FOR
THE DEGREE OF MASTER OF SCIENCE
IN
BIOCHEMISTRY

FEBRUARY 2022

Approval of the thesis:

AFFINITY AND SELECTIVITY OF AZACYANINES TO G-QUADRUPLEX FORMING PROMOTER REGIONS

submitted by **FAHRİYE NUR KIRMACI** in partial fulfillment of the requirements for the degree of **Master of Science** i**n Biochemistry, Middle East Technical University** by,

Prof. Dr. Halil Kalıpçılar
Dean, Graduate School of **Natural and Applied Sciences** _____

Assoc. Prof. Dr. Özgül Persil Çetinkol
Head of the Department, **Biochemistry** _____

Assoc. Prof. Dr. Özgül Persil Çetinkol
Supervisor, **Biochemistry, METU** _____

Examining Committee Members:

Assoc. Prof. Dr. Salih Özçubukçu
Chemistry, METU _____

Assoc. Prof. Dr. Özgül Persil Çetinkol
Biochemistry, METU _____

Prof. Dr. Ayşen Yılmaz
Chemistry, METU _____

Assoc. Prof. Dr. Yeşim Soyer
Food Engineering, METU _____

Assoc. Prof. Dr. Bala Gür Dedeoğlu
Biotechnology, Ankara University _____

Date: 09.02.2022

I hereby declare that all information in this document has been obtained and presented in accordance with academic rules and ethical conduct. I also declare that, as required by these rules and conduct, I have fully cited and referenced all material and results that are not original to this work.

Name Last name : Fahriye Nur Kırmacı

Signature :

ABSTRACT

AFFINITY AND SELECTIVITY OF AZACYANINES TO G-QUADRUPLEX FORMING PROMOTER REGIONS

Kırmacı, Fahriye Nur
Master of Science, Biochemistry
Supervisor : Assoc. Prof. Dr. Özgül Persil Çetinkol

February 2022, 92 pages

DNA has multiple levels of regulations owing to complex regulatory units. Promoters are among the most crucial regulatory sequence units in DNA, altering transcription initiation. Recent studies have shown that secondary structures called G-quadruplexes (G4s) can be found in promoter regions of certain genes along with the common double-helical Watson-Crick DNA. G-quadruplexes are four-stranded helical structures formed by the π-π stacking of G-tetrad structures with a pattern called G-tracts. New findings suggest that these noncanonical structures are transcriptionally altering the expression of critical proteins in healthy cells and possibly involved in the formation of cancerous tissue. For this reason, the promoter regions that have the capacity to form G-quadruplex structures have become the target of many drug development efforts against cancer. Within the scope of this thesis, it is revealed that five Azacyanine derivatives (Azamethyl, Aza4, Aza5, Azabutyl, and Azaisobutyl) were preferentially binding to the c-MYC (Cellular Myelocytomatosis) promoter region over the G4 forming promoter regions of B-Cell CLL/lymphoma 2 (BCL-2), Vascular Endothelial Growth Factor (VEGF), Kirsten Rat Sarcoma (KRAS), Human Epidermal Growth Factor Receptor 2 (HER-2) and

Retinoblastoma (RB) via competition dialysis. Interactions of G4 c-MYC and Azamethyl were investigated further using UV-Vis, Fluorescence, and Circular Dichroism spectroscopy. G4 of c-MYC promoter region was found to be stabilized by Azamethyl via thermal denaturation studies. Thermal denaturation temperature of c-MYC was shifted up to 20°C with varying Azamethyl concentration. Lastly, fluorescence spectroscopy unveiled the association constant between c-MYC and Azamethyl as $2.9 \times 10^5 \pm 1.4 \times 10^4$ M^{-1}.

Keywords: G-Quadruplex, Azacyanine, c-MYC

ÖZ

AZASİYANİNLERİN G-DÖRTLÜ SARMALI OLUŞTURAN PROMOTÖR BÖLGELERİNE OLAN AFİNİTE VE SEÇİCİLİKLERİ

Kırmacı, Fahriye Nur
Yüksek Lisans, Biyokimya
Tez Yöneticisi: Doç. Dr. Özgül Persil Çetinkol

Şubat 2022, 92 sayfa

DNA çok kademeli, kompleks bir düzenlemeye sahiptir. Promotörler, DNA'da transkripsiyonun başlamasını etkinleştirmeden sorumlu en önemli düzenleyici yapılardan biridir. Genel olarak görülen Watson-Crick ikili sarmal DNA yapısından farklı olan G-dörtlü sarmal yapısının da bazı genlerin promotör bölgelerinde bulunduğu yapılan son çalışmalar ile gösterilmiştir. G-dörtlü sarmal (G4) yapıları, belirli guanin dizileriyle oluşan G-dörtlüsü adı verilen yapının π-π istiflemesiyle oluşan dörtlü sarmal helikslerdir. Yeni çalışmalar bu kanonik olmayan yapıların sağlıklı hücrelerde kritik olan proteinlerin ekspresyonlarını değiştirdiğini göstermiştir. Transkripsiyonu değiştirmeleri sebebiyle de bu yapıların hücrelerin kanserli dokuya dönüşmelerinde rol aldığı düşünülmektedir. Bu sebeple, G-dörtlü sarmal yapı oluşturma kapasitesine sahip promotör bölgeler son yıllarda kansere karşı ilaç geliştirme çalışmalarındaki hedeflerden biri haline gelmiştir. Bu tez kapsamında, beş farklı Azasiyanin türevi tarafından (Azametil, Aza4, Aza5, Azabütil ve Azaisobütil), G4 sarmal yapısı oluşturan c-MYC (Cellular Myelocytomatosis), B-Cell CLL/lymphoma 2 (BCL-2), Vascular Endothelial Growth Factor (VEGF), Kirsten Rat Sarcoma (KRAS), Human Epidermal Growth Factor Receptor 2 (HER-2) ve Retinoblastoma (RB) promotör bölgeleri arasında en çok c-MYC bölgesinin

seçildiği rekabetçi diyaliz yöntemi ile gösterilmiştir. Elde edilen bulgular doğrultusunda Azametil ve c-MYC etkileşimleri UV-Vis, Floresans and Dairesel dikroizm spektoskopileri kullanılarak daha detaylı olarak incelenmiştir. Gerçekleştirilen termal denatürasyon çalışmaları, Azametil'in varlığının c-MYC promotör bölgesindeki G-dörtlü yapısının kararlılığını arttırdığını göstermiştir. c-MYC G4'nün termal denatürasyon sıcaklığının farklı derişimlerde Azametil varlığında 20°C'ye kadar arttığı gözlemlenmiştir. Son olarak, c-MYC ile Azametil arasıdaki bağlanma sabiti $2.9 \times 10^5 \pm 1.4 \times 10^4\ M^{-1}$ olarak floresans spektroskopi ile tespit edilmiştir.

Anahtar Kelimeler: G-Dörtlü Sarmal, Azasiyanin, c-MYC

To my family

ACKNOWLEDGMENTS

I would like to express my deepest gratitude to my advisor, Assoc. Prof. Dr. Özgül Persil Çetinkol for her valuable support, encouragement, and guidance. I am also grateful to my committee members Prof. Dr. Ayşen Yılmaz, Assoc. Prof. Dr. Yeşim Soyer, Assoc. Prof. Dr. Salih Özçubukçu and Assoc. Prof. Dr. Bala Gür Dedeoğlu.

I would like to thank Prof. Dr. Ahmet M. Önal and his lab members for their help with the fluorescence experiments.

I am sincerely thankful to my dearest friends Sercan Güloğlu and Mehrdad Forough for their friendship, encouragement and help during my work. I also thank Gözdem Çavdar, Serra Tütüncü, Kübra Doğan, Ecenaz Bilgen, Hatice Müge Usta, Aybüke Gülkaya, Aynur Özel and Buket Sakinci for their help and friendship.

I want to extend my thanks to Deniz Arçak for her help, guidance, and dearest friendship. I want to thank my best friend Aybüke Senbani for her endless support.

I would like to thank all administrative, academic, and technical staff of the Department of Chemistry and the Department of Biology, METU, for their support during my education.

I gratefully acknowledge the Scientific and Technological Research Council of Turkey (TUBITAK) for financial support via project number 116Z219.

Finally, I am immensely grateful to my husband Alper Kırmacı, my mother Şükran Alper, my father Reşit Atilla Alper, my sister Işıl Gül Alper and my brother Kadı Turhan Alper for their love and supports. This thesis study could not be completed without their encouragement and belief. I dedicate this thesis study to my family.

TABLE OF CONTENTS

ABSTRACT v

ÖZ vii

ACKNOWLEDGMENTS x

TABLE OF CONTENTS xi

LIST OF TABLES xiv

LIST OF FIGURES xv

LIST OF ABBREVIATIONS xx

CHAPTERS

1 INTRODUCTION 1

1.1 Content of DNA and Its Primary Structure 1

1.1.1 Biophysical Forms of DNA 3

1.1.1.1 Non-Canonical Structures of DNA 4

1.2 G-Quadruplex Structures 7

1.2.1 G-quadruplex DNA 8

1.2.2 Importance of G-quadruplex Sequences in Telomeric Regions 10

1.2.3 G-quadruplex Bearing Promoter Regions 11

1.3 Targeting G-quadruplexes with Small Molecules 14

1.4 Azacyanine Molecules and Their Structures 15

1.5 Thesis Focus 16

2 MATERIALS AND METHODS 19

2.1 Selectivity of Azacyanine Derivatives Towards G-Quadruplex Forming Sequences 19

2.1.1 Competition Dialysis 20
2.1.2 BPES Buffer and 10% (w/v) SDS Stock Solutions Preparation 21
2.1.3 Oligonucleotide Preparations 22
2.1.4 Calibration Curve Construction 25
2.2 Spectroscopic Investigation of c-MYC:Azamethyl Interactions 27
2.2.1 Thermal Denaturation Experiments 27
2.2.2 Association Constant Determination 28
3 RESULTS AND DISCUSSION 29
3.1 Selectivity of Azacyanine Molecules Against Different G4 forming Sequences Found Mainly in Promoter Regions 29
3.1.1 Azamethyl 30
3.1.2 Aza4 33
3.1.3 Aza5 35
3.1.4 Azabutyl 37
3.1.5 Azaisobutyl 39
3.1.6 Doxorubicin 41
3.1.7 Overall c-MYC Affinities of Azacyanine Derivatives and Doxorubicin . 43
3.2 Spectrophotometric Investigation of Azamethyl Binding to c-MYC 44
3.3 Thermal Denaturation of c-MYC:Azamethyl Samples via Circular Dichroism (CD) Spectroscopy 47
3.4 Determination of Association Constant for c-MYC:Azamethyl 51
3.5 Discussions 53
3.5.1 Selectivity of Azacyanines Against Different Promoter Regions 53
3.5.2 Spectrochemical Analysis of c-MYC:Azamethyl Interactions 55

4 THESIS CONCLUSION 57

REFERENCES 59

APPENDICES

A. Micrococcus lysodeikticus (72% GC) Genomic DNA Purification Procedure 73

B. Azacyanine Derivatives 75

C. Calibration Curves of Molecules 76

D. BPES Buffer and 10% (w/v) SDS Stock Solutions Preparation 82

E. Association Constant Measurements 84

F. Sample Preparation for Thermal Denaturation Experiments 86

G. Interactions of c-MYC:Azamethyl in UV-Vis spectrophotometer 87

H. CD spectra between 15°C and 95°C 91

I. UV-Vis spectra of c-MYC:Azamethyl samples between 15°C and 95°C 92

LIST OF TABLES

TABLES

Table 2.1 BPES buffer content for competition dialysis. 21
Table 2.2 Parameters used in Fluorescence and UV-Vis measurements. 22
Table 2.3 Nucleic acid sequences used (Ragazzon et al., 2007). 24
Table 2.4 Experimental setup used during the Fluorescence measurements. 25
Table 3.1 Calibration curve equations and reference wavelengths. 29
Table 3.2 Competition dialysis results for Azamethyl. 32
Table 3.3 Competition dialysis results for Aza4. 34
Table 3.4 Competition dialysis results for Aza5. 36
Table 3.5 Competition dialysis results for Azabutyl. 38
Table 3.6 Competition dialysis results for Azaisobutyl. 40
Table 3.7 Competition dialysis results for Doxorubicin. 42
Table 3.8 Overall competition dialysis results for c-MYC. 43
Table 3.9 Thermal denaturation temperatures obtained through the differentiation of the thermal denaturation curves given in Figure 3.20. Concentration of c-MYC and Azamethyl is the multiples of 9 µM and 3 µM, respectively, in given ratios. . 49
Table E. 1 Titration table of 1.0 µM Azamethyl solution with 400.0 µM c-MYC G4 with 1.0 µM Azamethyl..... 84
Table F. 1 c-MYC:Azamethyl 1:8 ratio sample preparation for annealing..... 86

LIST OF FIGURES

FIGURES

Figure 1.1. First modelling of DNA structure in B-form (Watson & Crick, 1953).. 2
Figure 1.2. Scheme represents the single stranded DNA from 5' to 3' (Sinden, 2012). 2
Figure 1.3. Scheme represents Hoogsteen face and Watson-Crick face of TAT and C^+GC triplexes (Sinden, 1994). 5
Figure 1.4. C:C+ Hoogsteen bond formation in i-motif (Xu & Sugiyama, 2006).... 6
Figure 1.5. G-tetrad conformation. 'R' stands for Deoxyribose. Figure is created with BioRender.com. 7
Figure 1.6. Different topologies of G-quadruplexes with their strand orientations are illustrated. (A) Formation of G-quadruplexes from four different strands (Tetramer) and two different strands (Dimer). Monomeric (Unimolecular) G4s are illustrated in variable folding types. (B) Mixed parallel-antiparallel G4 type with propeller and diagonal loop conformations, respectively. (C) Antiparallel G4 type with lateral loop. (D) Parallel G4 type with propeller loop at three sides of four-stranded helix. Figures are created with BioRender.com. 10
Figure 1.7. G-quadruplex binders (Dexheimer et al., 2006). 15
Figure 1.8. Structures of (A) Azamethyl, (B) Aza4, (C) Aza5, (D) Azabutyl, (E) Azaisobutyl and (F) Doxorubicin. 16
Figure 2.1. Competition Dialysis set-up. Disposable dialysis cassette, each containing 600.0 µL of a 75.0 µM solution of one of the DNA structures listed in Table 2.3, are placed in a beaker containing 750.0 mL of 1.0 µM ligand solution in 1XBPES. 19
Figure 3.1. Average fluorescence intensity versus wavelength (nm) plots from two independent competition dialysis experiments of Azamethyl. 31
Figure 3.2. Average C_b/C_f values of competition dialysis for Azamethyl. Error bars represent the standard deviations from two independent experiments. 32

Figure 3.3. Average fluorescence intensity versus wavelength (nm) plots from two independent competition dialysis experiments of Aza4. 33
Figure 3.4. Average C_b/C_f values of competition dialysis for Aza4. Error bars represent the standard deviations from two independent experiments. 34
Figure 3.5. Average fluorescence intensity versus wavelength (nm) plots from two independent competition dialysis experiments of Aza5. 35
Figure 3.6. Average C_b/C_f values of competition dialysis for Aza5. Error bars represent the standard deviations from two independent experiments. 36
Figure 3.7. Average fluorescence intensity versus wavelength (nm) plots from two independent competition dialysis experiments of Azabutyl. 37
Figure 3.8. Average C_b/C_f values of competition dialysis for Azabutyl. Error bars represent the standard deviations from two independent experiments. 38
Figure 3.9. Average fluorescence intensity versus wavelength (nm) plots from two independent competition dialysis experiments of Azaisobutyl. 39
Figure 3.10. Average C_b/C_f values of competition dialysis for Azaisobutyl. Error bars represent the standard deviations from two independent experiments. 40
Figure 3.11. Average fluorescence intensity versus wavelength (nm) plots from two independent competition dialysis experiments of Doxorubicin. 41
Figure 3.12. Average C_b/C_f values of competition dialysis for Doxorubicin. Error bars represent the standard deviations from two independent experiments. 42
Figure 3.13. Average C_b/C_f values of competition dialysis against c-MYC. Error bars represent the standard deviations from two independent experiments. 44
Figure 3.14. Fluorescence spectra of of c-MYC:Azamethyl samples with varying concentrations. Each c-MYC:Azamethyl ratio is represented by the corresponding color of the solid line in given caption. Concentration of c-MYC and Azamethyl is the multiples of 9 µM and 3 µM, respectively, in given ratios. 45
Figure 3.15. (A) UV-Vis spectra of 0:1, 1:1 and 1:0 c-MYC:Azamethyl samples at 15°C. Inset in A shows the 300 nm to 400 nm region of the spectra. (B) Fluorescence spectra of c-MYC:Azamethyl samples between 325 nm and 675 nm and (C) CD spectra of c-MYC:Azamethyl samples 240 nm and 290 nm,

respectively. Concentration of c-MYC and Azamethyl is the multiples of 9 µM and 3 µM, respectively, in given ratios..... 46
Figure 3.16. CD spectra of different c:MYC:Azamethyl samples with varying concentrations at 15°C between 240-400 nm (A). Concentration of c-MYC and Azamethyl is the multiples of 9 µM and 3 µM, respectively, in given ratios..... 47
Figure 3.17. CD spectra of different c:MYC:Azamethyl samples with varying concentrations at 95°C between 240-400 nm (A) and blown-up image of the spectra in A in the range of 245-280 nm. Concentration of c-MYC and Azamethyl is the multiples of 9 µM and 3 µM, respectively, in given ratios. 48
Figure 3.18. Thermal denaturation profiles of c-MYC in the presence of varying Azamethyl concentrations between 15°C and 95°C. Concentration of c-MYC and Azamethyl is the multiples of 9 µM and 3 µM, respectively, in given ratios..... 49
Figure 3.19. First derivative of thermal denaturation profiles of c-MYC, in the presence of differing Azamethyl concentrations, used in the calculation of the melting temperatures. Concentration of c-MYC and Azamethyl is the multiples of 9 µM and 3 µM, respectively, in given ratios. 50
Figure 3.20. Integrated fluorescence intensity plotted against G4 concentration obtained from three independent titration experiments (Appendix E). 52
Figure C. 1. Calibration curve construction of Azamethyl. (A) Fluorescence spectra of Azamethyl at varying concentrations between 0.1 µM and 5.5 µM. (B) Calibration curve of Azamethyl obtained from the fluorescence intensity at 378 nm. (C) Calibration curve of Azamethyl obtained from the fluorescence intensity at 440 nm. 76
Figure C. 2. Calibration curve construction of Aza4. (A) Fluorescence spectra of Aza4 at varying concentrations between 0.1 µM and 5.5 µM. (B) Calibration curve of Aza4 obtained from the fluorescence intensity at 445 nm. (C) Calibration curve of Aza4 obtained from the fluorescence intensity at 470 nm. 77
Figure C. 3. Calibration curve construction of Aza5. (A) Fluorescence spectra of Aza5 at varying concentrations between 0.1 µM and 5.5 µM. (B) Calibration curve

of Aza5 obtained from the fluorescence intensity at 480 nm. (C) Calibration curve of Aza5 obtained from the fluorescence intensity at 500 nm. 78
Figure C. 4. Calibration curve construction of Azabutyl. (A) Fluorescence spectra of Azabutyl at varying concentrations between 0.1 µM and 5.5 µM. (B) Calibration curve of Azabutyl obtained from the fluorescence intensity at 379 nm. (C) Calibration curve of Azabutyl obtained from the fluorescence intensity at 440 nm. 79
Figure C. 5. Calibration curve construction of Azaisobutyl. (A) Fluorescence spectra of Azasiobutyl at varying concentrations between 0.1 µM and 5.5 µM. (B) Calibration curve of Azaisobutyl obtained from the fluorescence intensity at 379 nm. (C) Calibration curve of Azasobutyl obtained from the fluorescence intensity at 440 nm. 80
Figure C. 6. Calibration curve construction of Doxorubicin. (A) Fluorescence spectra of Doxorubicin at varying concentrations between 0.1 µM and 5.5 µM. (B) Calibration curve of Doxorubicin obtained from the fluorescence intensity at 593 nm. (C) Calibration curve of Doxorubicin obtained from the fluorescence intensity at 619 nm. 81
Figure E. 1. Fluorescence intensity vs Wavelength (nm) graphics for titration of 1.0 µM Azamethyl with c-MYC 85
Figure G. 1. c-MYC:Azamethyl 1:0 ratio absorbance comparisons at 15 °C (dotted line) and 95 °C (solid line) 87
Figure G. 2. c-MYC:Azamethyl 1:1 ratio absorbance comparisons at 15 °C (dotted line) and 95 °C (solid line) 87
Figure G. 3. c-MYC:Azamethyl 1:2 ratio absorbance comparisons at 15 °C (dotted line) and 95 °C (solid line) 88
Figure G. 4. c-MYC:Azamethyl 1:4 ratio absorbance comparisons at 15 °C (dotted line) and 95 °C (solid line) 88
Figure G. 5. c-MYC:Azamethyl 1:6 ratio absorbance comparisons at 15 °C (dotted line) and 95 °C (solid line) 89

Figure G. 6. c-MYC:Azamethyl 1:8 ratio absorbance comparisons at 15 °C (dotted line) and 95 °C (solid line)..... 89
Figure G. 7. c-MYC:Azamethyl 1:10 ratio absorbance comparisons at 15 °C (dotted line) and 95 °C (solid line)..... 90
Figure H. 1. CD spectra of c-MYC:Azamethyl samples 1:0 (A), 1:1 (B), 1:2 (C), 1:4 (D), 1:6 (E), 1:8 (F) and 1:10 (G) with 5 ˚C intervals from 15 °C (solid line) to 95 °C (dotted line) 91
Figure I. 1. Absorbance spectra of different c-MYC:Azamethyl samples in the range of 240-400 nm at 15°C (A) and 95°C (B) 92

LIST OF ABBREVIATIONS

ABBREVIATIONS

µL	Microliter
µM	Micromolar
A	Adenine
Aza4	Azacyanine 4
Aza5	Azacyanine 5
Azabutyl	Azacyanine Butyl
Azaisobutyl	Azacyanine Isobutyl
Azamethyl	Azacyanine Methyl
BCL-2	Promoter Region of B-Cell CLL/lymphoma 2
BPES	Buffered Phosphate EDTA with Sodium Chloride
C	Cytosine
C_b	Bound Molecule Concentration
CD	Circular Dichroism
C_f	Free Molecule Concentration
c-MYC	Promoter Region of Cellular Myelocytomatosis
C_t	Total Molecule Concentration
°C	Degree Celsius
DMSO	Dimethyl Sulfoxide
DNA	Deoxyribonucleic Acid

Dox	Doxorubicin
ds	Double Stranded
EDTA	Ethylenediamine Tetra Acetic Acid
Ɛ	Epsilon (Extinction Coefficient)
FUSE	Far Upstream Element
G	Guanine
G4	G-Quadruplex
H. Telomere	Human Telomeric Sequence
HCI	Hydrochloric Acid
HER-2	Promoter Region of Human Epidermal Growth Factor Receptor 2
HG	Hoogsteen
IDT	Integrated-DNA Technologies
i-motif	Intercalated Motif
K^+	Potassium Ion
K_a	Association Constant
KRAS	Promoter Region of Kirsten Rat Sarcoma
L	Liter
M	Molar
M. lyso	Genomic DNA of Micrococcus Lysodeikticus
mdeg	Millidegrees
Mg	Magnesium
min	Minute

mL	Milliliter
mM	Millimolar
MW	Molecular Weight
n	Mol
Na^+	Sodium Ion
Na_2EDTA	Disodium Ethylenediamine Tetra Acetic Acid
Na_2HPO_4	Disodium Hydrogen Phosphate
NaCI	Sodium Chloride
NaH_2PO_4	Sodium Phosphate Monobasic
NaOAc	Sodium Acetate
NaOH	Sodium Hydroxide
NHE III (1)	Nuclear Hypersensitive Element III (1)
nm	Nanometer
NMR	Nuclear Magnetic Resonance
Ras	Rat Sarcoma
RB	Promoter Region of Retinoblastoma
rcf	Relative Centrifugal Force
RT	Room Temperature
SDS	Sodium Dodecyl Sulphate
ss	Single Stranded
T	Thymine
T_m	Melting Temperature

UV-Vis	Ultraviolet-Visible
VEGF	Promoter Region of Vascular Endothelial Growth Factor
WC	Watson-Crick
λ	Lambda (Wavelength)
π	Pi

CHAPTER 1

INTRODUCTION

1.1 Content of DNA and Its Primary Structure

Deoxyribonucleic acid (DNA) is a long macromolecule that controls all living life forms and passes the genetic information through generations (Rich, 1982). After long research and confused ideas, the scientific world was able to confirm that it is the inheritance material storing the information in all organisms (Avery, Macleod, & McCarty, 1944; Hershey & Chase, 1951). Its structure was revealed by Watson and Crick in 1953 (Watson & Crick, 1953). The basic structure of DNA was shown as composed of a pentose sugar, a nitrogenous base, and a phosphate, as represented in Figure 1.1 and Figure 1.2. Bases are categorized as purines (A or G) and pyrimidines (T or C). Consequently, it was understood that the large and distinct codes are created by the arrays of four nucleotides in all life forms.

Watson and Crick presented the features of the most common DNA structure, B-form, with its unique hydrogen bonded base pairing. In Watson-Crick (WC) base pairing, A-T and G-C base pairings form a right-handed double-stranded helical structure coming from inherent torsion in phosphodiester bond coupled with hydrogen bonding (Figure 1.3) (Watson & Crick, 1953).

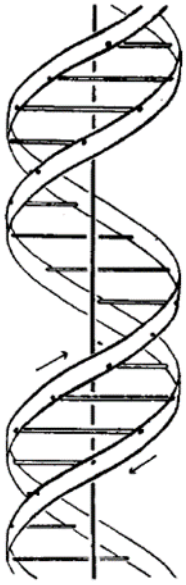

Figure 1.1. First modelling of DNA structure in B-form (Watson & Crick, 1953)

DNA is not the sole possessor of nitrogenous bases in the cell. As a messenger of DNA, ribonucleic acids (RNAs) are also composed of four nucleotides, with Uracil instead of Thymine and the ribose sugar instead of deoxyribose. Uracil has -H group at 5-C of the base instead of -CH_3 group in Thymine, and the pentose sugar ribose has -OH group in 2-C, which is characteristic for all RNAs. Together with RNA, DNA could control almost all cellular activities.

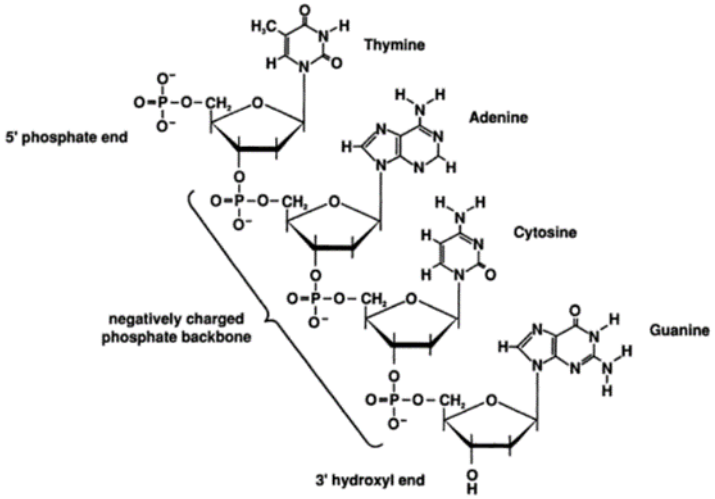

Figure 1.2. Scheme represents the single stranded DNA from 5’ to 3’ (Sinden, 2012).

Regulation by DNA is mainly through transcriptional and translational regulation. In eukaryotes, transcriptional regulation involves several levels; chromatin modifications and epigenetic changes on regulatory sequences (Casamassimi & Ciccodicola, 2019). The ultimate goal of chromatin modifications is to control regulatory elements (promoter regions, enhancer sequences, silencers, and insulators) (Andersson & Sandelin, 2019). The critical importance and complexity of genes make DNA regulations complicated.

1.1.1 Biophysical Forms of DNA

Under normal conditions, B-DNA is known as the common genomic DNA form in vivo. Due to equal interspacing, it is a right-handed helical structure with almost parallel orientation between base pairs. However, this long biopolymer can adopt to different environmental conditions known as stress conditions (Ghosh & Bansal, 2003; Travers & Muskhelishvili, 2015). Specifically, these stress conditions do not necessarily mean to be harmful for the basal state of DNA and its regulations. Besides, they can be induced under an altered environment and are required to keep DNA intact. These forms are also thought to be needed to maintain transcriptional processes where different biophysical forms of DNA are seen simultaneously depending on the transcriptional requirements.

Different stress conditions lead to various DNA forms and, mostly seen forms are called A and Z DNA. A and Z forms arise under dehydrated and high divalent cation and salt concentrations, respectively (Travers & Muskhelishvili, 2015). Z DNA takes its name from standing in zig-zag conformation due to the flipped form of B-DNA during basal processes (Herbert, 2019). This left-handed form forms under the supercoiling stress in the middle of B-form, where glycosylic bonds start to alternate between syn and anti conformations (Bourtayre, Liquier, Pizzomi, & Taillandier, 2012; Safina et al., 2017). These different DNA forms can be identified in vitro using Circular Dichroism studies. In the A form, the double helix partially unwinds to induce flexibility, which results in a decrease in parallel orientation and an increase

in the intensity in CD band at 270 nm. (Ivanov & Krylov, 1992; Kypr et al., 2009). However, Z-form shows a different CD pattern with hypochroism around 275 nm along with a red shift around 295 nm and loss of negative ellipticity around 250 nm (Bourtayre et al., 2012).

Although A, B, and Z DNA occur interchangeably and spontaneously, genomic DNA is thought to be changing its conformation back to native B-form once the altered conditions are removed (Herbert, 2019; Ivanov & Krylov, 1992).

Most of the time, gene sequences are read out in B form rather than A and Z forms so that transition points can be counted as recruitment elements. While alteration from B to Z is thought to enhance gene editing, A form enables dense packing and flexible DNA rotation for other regulatory purposes (Herbert, 2019; Travers & Muskhelishvili, 2015). The presence of different DNA forms is not limited to DNA. dsRNAs and RNA:DNA hybrids can also adopt these forms rather than the B form (Herbert, 2019; Ivanov & Krylov, 1992). Lastly, A, B, and Z forms can be counted as mostly seen or dominant double helical structures in DNA. Yet, secondary structures are not limited to the conventional double stranded anti-parallel structures.

1.1.1.1 Non-Canonical Structures of DNA

Besides anti-parallel double helices, DNA conformations range from parallel stranded DNA to triple helical H-DNA, bubble formation, cruciform, slipped-mispaired DNA loops, and tetraplexes (i-motif and G-Quadruplex) (Jain & Bhattacharya, 2010; Travers & Muskhelishvili, 2015).

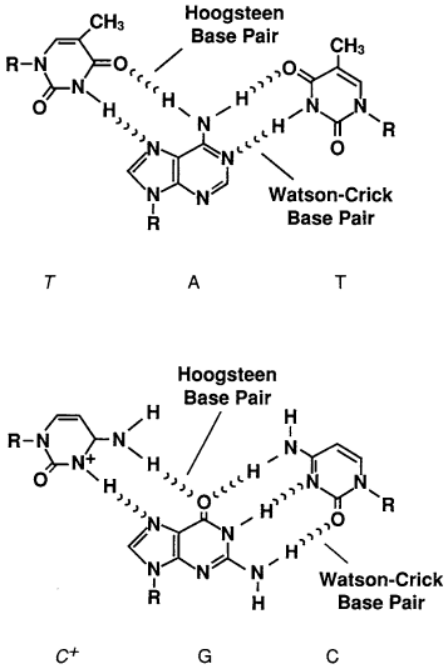

Figure 1.3. Scheme represents Hoogsteen face and Watson-Crick face of TAT and C^{+}GC triplexes (Sinden, 1994).

Conventional double helical strand orientation includes opposite runs of two strands around each other, also called the anti-parallel orientation. On the contrary, mirror sequences can form parallel stranded and reverse Watson-Crick pairings through inter or intra molecular folding (Shchyolkina et al., 2003). A few years later, after the Watson-Crick model was established, Hoogsteen observed different pairing models in DNA where hydrogen bonding faces were flipped 180˚ (Figure 1.3) (Hoogsteen, 1959, 1963). Hoogsteen (HG) base pairing is considered noncanonical since WC base pairing is seen predominantly throughout the genomic DNA (Persil Çetinkol, 2008). DNA is known to have both WC and HG base pairings in its biologically relevant structures as in G-quadruplex and i-motif structures. All these structures are believed to play a role in transcriptional and replicational processes. Their presence is thought not being random due to their availability in promoter regions and telomeres (King et al., 2020; Sun & Hurley, 2009; Zeraati et al., 2018). For instance, triple helical structures can adopt parallel orientation in addition to anti-parallel orientation via reverse Hoogsteen and Hoogsteen base pairings, respectively

(Jain & Bhattacharya, 2010). In either case, transcriptional regulation processes are observed to be activated (Jain & Bhattacharya, 2010).

Along with the Z DNA, other negatively supercoiled conformations interfere with genome rearrangements, repair, and readout mechanisms such as cruciform and slipped loop variants (Minyat et al., 2012; Travers & Muskhelishvili, 2015). Cruciform is another noncanonical secondary structure that involves complementarity between inverted sequences in X shaped manner to be recognized by repair and genome rearrangement systems (Bacolla & Wells, 2004).

Tetraplexes are also common non-canonical structures mostly found in GC rich sequences, and the presence of one structure represses another for genomic regulatory purposes (King et al., 2020). Intercalated motif (i-motif) takes its name from hemi-protonated Cytosine: Cytosine intercalation from four-stranded structure (Figure 1.4). The formation of i-motif is highly related to cell cycle progression and is known to act as a transcriptional scaffold area (Zeraati et al., 2018). In addition, G-quadruplex sequences that involve π-stacking of Guanine bases are known to serve as repressor elements in their stabilized form (Sun & Hurley, 2009).

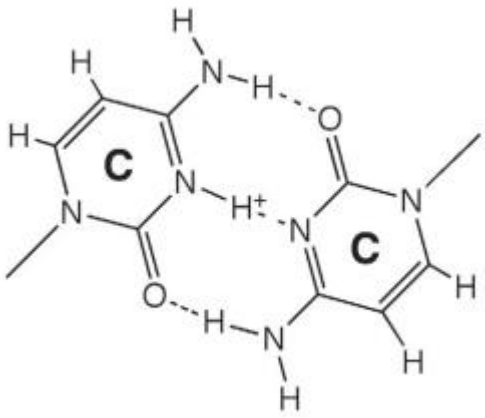

Figure 1.4. C:C+ Hoogsteen bond formation in i-motif (Xu & Sugiyama, 2006).

1.2 G-Quadruplex Structures

Studies about the self-association of guanylic acid can be traced back to the 19th century (Bang, 1910). Bang found out that guanylic acid has a high concentration gelatinous structure. However, a proper folding conformation for G-tetrads was firstly proposed by Gellert and colleagues after almost 50 years (Gellert, Lipsett, & Davies, 1962). In the structure of G-tetrad, the monovalent ion can fit into the middle, which is essential for folding, as seen in Figure 1.5 (Williamson, Raghuraman, & Cech, 1989). These non-canonical secondary structures are planar and four-stranded helices (Chen & Yang, 2012). Multiple G-tetrads can be stacked onto each other by π-π interactions to form G-quadruplex (G4) structures.

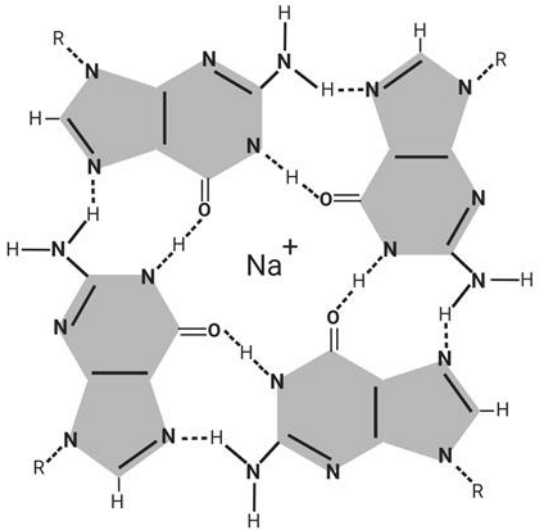

Figure 1.5. G-tetrad conformation. 'R' stands for Deoxyribose. Figure is created with BioRender.com.

G4 conformations are seen in guanine rich sequences with short guanine repeats called G-tracts (Huppert & Balasubramanian, 2005; Sundquist & Klug, 1989). General G-quadruplex sequences are counted as:

$G_3+L_1\ G_3+L_2\ G_3+L_3\ G_3+$

where the number of guanines (G) must be ≥3 in each tract with variable loop (L) sequences and lengths (Huppert & Balasubramanian, 2005; Todd, Johnston, & Neidle, 2005).

Biologically relevant G-quadruplex structures were found for the first time in telomeric regions (Shampay, Szostak, & Blackburn, 1984). Subsequent studies showed that G-quadruplex structures are not limited to telomeric sequences but also gene switch regions, promoters, and RNA sequences are rich in G4 prone sequences (Huppert & Balasubramanian, 2005; Todd et al., 2005). Their involvement in immunological gene regulations, transcription, telomerase activity, and recombination process prove that their presence is nonrandom (Biffi et al., 2013; Maizels & Gray, 2013; Rhodes & Lipps, 2015).

For instance, studies showed that hypomethylation is observed close to G4 regions in many cancer types (De & Michor, 2010). These structures are thought to be regulated and unfolded during basal conditions by protein chaperones and helicases (Gray et al., 2014; Rhodes & Lipps, 2015). Alterations in DNA regulatory systems are believed to lead to an increase in the presence of G4s. However, these regulatory alterations create torsion on DNA and double stranded (ds) and chromosomal breaks at these sites (Biffi et al., 2014; De & Michor, 2011; Katapadi, Nambiar, & Raghavan, 2012). Consequently, stabilization in these sequences is believed to limit and change alterations in DNA conformations and thus the transcription (Sundquist & Klug, 1989).

1.2.1 G-quadruplex DNA

G4s can adopt different conformations depending on the G-tract and loop sequence, G-tract length, loop length, folding direction, and the number of strands involved in G4 formation (Burge et al., 2006; Chen & Yang, 2012).

While intermolecular G4s are called tetramers (4 separate strands) and dimers (2 separate strands), intramolecular G4s are known as monomeric (unimolecular) G-quadruplexes. Each G4 can have multiple conformations (Chen & Yang, 2012; Yang & Okamoto, 2010). For instance, according to the glycosidic bond directions of each loop, unimolecular G4s can be a parallel, antiparallel, and mixed type with loop variations, which are called propeller, diagonal and lateral (Figure 1.6) (Chen & Yang, 2012; Yang & Okamoto, 2010). Different G4 conformations can be identified using spectroscopic techniques such as CD. In the CD spectrum, antiparallel G4 topologies are associated with positive ellipticity at 295 nm and negative minimum at 265 nm. In comparison, parallel topologies are known to give rise to positive ellipticity at 264 nm with a negative minimum at 240 nm (Dexheimer, Sun, & Hurley, 2006). Besides, mixed topologies are identified with positive ellipticity at 264 nm and 295 nm (Dexheimer, Sun, & Hurley, 2006).

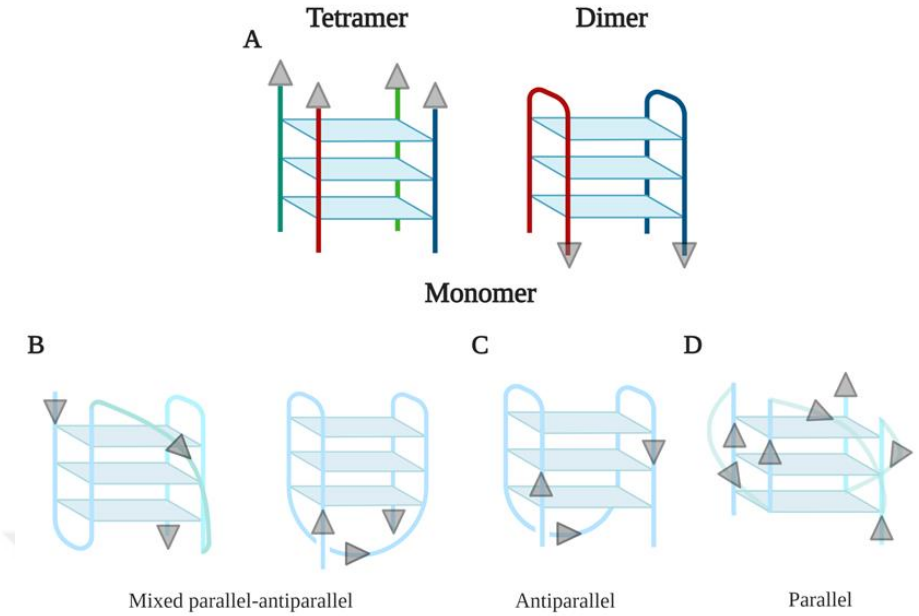

Figure 1.6. Different topologies of G-quadruplexes with their strand orientations are illustrated. (A) Formation of G-quadruplexes from four different strands (Tetramer) and two different strands (Dimer). Monomeric (Unimolecular) G4s are illustrated in variable folding types. (B) Mixed parallel-antiparallel G4 type with propeller and diagonal loop conformations, respectively. (C) Antiparallel G4 type with lateral loop. (D) Parallel G4 type with propeller loop at three sides of four-stranded helix. Figures are created with BioRender.com.

1.2.2 Importance of G-quadruplex Sequences in Telomeric Regions

Studies considering consensus G4 forming sequences revealed that the human genome could form G4s over at 300,000 sites (Rhodes & Lipps, 2015). These structures were found to be conserved through evolution in different species and are found to be localized in significant areas of the genome (König, Evans, & Huppert, 2010; Rhodes & Lipps, 2015). The very first discovered G4 sequences are well-known telomeric repeats followed by promoter and gene switch regions (Blackburn, 1990; Hardin, Watson, Corregan, & Bailey, 2002; Henderson et al., 1987).

Telomeres are unique long single stranded sequences at the 3’ end of chromosomes that protect our genome from nucleolytic degradation, unnecessary recombination, and fusion. They play a vital role in preserving genetic information (Shay & Wright, 2010; Wojtyla, Gladych, & Rubis, 2011). In each cell cycle, telomere length gets shortened due to replication problem. And when telomere length reaches a critical limit, the cell is known to undergo senescence and apoptosis. Telomere length can be taken as the biological clock that determines the lifespan of a cell. Telomeric regions are known to get elongated by the enzyme telomerase that is active only in specific cell types such as germline or stem cells (De Cian et al., 2008). Almost 85% of cancer cells also hijack this mechanism and are known to have active telomerase. Telomerase activity, elongation of the telomeres, is thought to be one of the reasons behind the higher division rates of cancer cells compared to somatic cells (Mergny et al., 2002). Studies showed that inhibition of telomerase activity could be achieved by stabilizing G4 structures (De Cian et al., 2008; Yadav et al., 2017). Consequently, using small molecules as one possible way of stabilizing G4 structures has gained prominence as a recent progressing cancer research area.

1.2.3 G-quadruplex Bearing Promoter Regions

Even though telomeres were the first known possessor of G4 structures, promoter regions, gene bodies, and untranslated regions also constitute G4s in high incidence (Biffi et al., 2013; Huppert & Balasubramanian, 2005; Todd et al., 2005). Promoter regions are regulatory elements in genes where transcription is initiated. Since G4 structures stabilize the area to prevent transcriptional scaffolding, particular helicases are conserved from bacteria to eukaryotes to unwind these conformations (Murat & Balasubramanian, 2014). Unsurprisingly, promoters of proto-oncogene regions also bear G-quadruplex sequences as exploited in this thesis; c-MYC (Cellular Myelocytomatosis), B-Cell CLL/lymphoma 2 (BCL-2), Vascular Endothelial Growth Factor (VEGF), Kirsten Rat Sarcoma (KRAS), Human Epidermal Growth Factor Receptor 2 (HER-2) and Retinoblastoma (RB) (Ragazzon,

Garbett, & Chaires, 2007). There are general characteristics of cancer cells that maintain proliferative signaling, upregulation of growth, invasion to adjacent tissues, immortality, angiogenesis, and evading cell death (Hanahan & Weinberg, 2011). Cancer cells acquire control of transcriptional regulations, commonly exploiting the pro-oncogene regions to conquer all phenotypic traits. This control involves either up or down-regulation of a gene depending on its role.

c-MYC is one of the leading players in cell proliferation by supporting cell growth and division (Miller et al., 2012). It is overexpressed in cancer cells, and over expression is found in at least 40% of tumors (Dang, Le, & Gao, 2009). Former studies showed that G-quadruplex stabilization decreased the c-MYC expression (Brown et al., 2011; Siddiqui-Jain et al., 2002). Besides, the c-MYC promoter sequence recruits Z-DNA binders for G-quadruplex regulation as a direct evidence of its prominent regulatory roles (Herbert, 2019). c-MYC has four main regulatory sequences, P1 promoter, Nuclear Hypersensitive Element (NHE III(1)), Far Upstream Element (FUSE), and P2 promoter, with particularly transcriptional repressor G-quadruplex in NHE III1 (Siddiqui-Jain et al., 2002; Sun & Hurley, 2009). This sequence shows multiple G-quadruplex species in equilibrium with intramolecular propeller parallel type predominantly (Le et al., 2012). At least five different G4 topologies were observed in the c-MYC sequence in equilibrium (Siddiqui-Jain et al., 2002). The putative G-Quadruplex sequence that has been used in this thesis is also called Pu27, known as the predominant expression regulator of c-MYC at 115 bp upstream of the P1 promoter. The sequence that we used in our experiments is also shown to have different G4 folding patterns as in its binding to TMPyP4 (Phan et al., 2004; Seenisamy et al., 2004).

BCL-2 has a role in programmed cell death by preventing apoptosis (Dexheimer et al., 2006). It is used as a target in prostate and pancreatic cancers due to its increased expression and dysregulation, respectively (Răsădean et al., 2019). Upstream of P1

promoter has putative G-quadruplex structures found in three different conformations (Dexheimer et al., 2006).

KRAS is a cell membrane protein from the Ras family and involves in cell growth and apoptosis (Cogoi & Xodo, 2006). Mutations in KRAS are the most frequently observed Ras mutations in overall cancer mutations, especially in the colon and pancreatic cancer (Adjei, 2001).

VEGF is an angiogenic factor that supports new blood vessel formation through increasing survival change, permeability, proliferative, and migration of endothelial cells (Sun et al., 2005). Therefore, it is a crucial factor in maintaining cancerous cell tissue. KRAS and VEGF share similar G-quadruplex topologies; three G-Quadruplex formations in parallel stranded folding patterns (Răsădean et al., 2019; Yang & Okamoto, 2010).

HER-2 is a member of growth factor membrane proteins amplified in primary breast cancer types in almost 30% (Slamon et al., 1989). Elevated HER-2 protein expression leads to aggressive type of cancer progress.

Apart from previous regulatory proteins, RB has an antiproliferative and indirectly apoptotic function in a cell's fate (Nevins, 2001). It bears antiparallel G-quadruplex that shows positive ellipticity at 295 nm and negative ellipticity at 265 nm due to syn/anti-G residue conformations in the secondary structure (Xu & Sugiyama, 2006).

Transcriptional regulations of these sequences contribute hallmarks of cancer, angiogenesis in VEGF; upregulation of growth in c-MYC and KRAS; evading cell death in BCL-2 (Brooks, Kendrick, & Hurley, 2010). Besides, HER-2 involves two sets of hallmarks; evasion of apoptosis and growth upregulation (Cui et al., 2019).

Above mentioned and exploited G-quadruplex sequences mostly show parallel intramolecular topologies. However, different number of G-tracts, loop size and sequence offer distinct patterns to elucidate sequence-dependent binding preferences of Azacyanines, including the promoter region of RB.

1.3 Targeting G-quadruplexes with Small Molecules

G-quadruplexes are one of the critical non-canonical structures that can be folded under basal conditions in the presence of metallic ions, as K^+ and Na^+, and proper chaperones. Their presence can interfere with the transcriptional process, genomic stability, and translations (Dhamodharan & Pradeepkumar, 2019). Their potential in enabling direct regulation of DNA is counted as an efficient technique for chemotherapeutic targeting in recent years.

Partly due to G-quadruplex's planar structure, G-quadruplex targeting molecules display common features. They possess a wide aromatic, electron-poor surface for π-stacking and cationic capability to increase the electrostatic interactions with G-stacks (Pirota et al., 2019). As stated previously, G-quadruplex targeting is shown to repress transcriptional regulations. TMPyP4, TMPyP2, Se2SAP, and telomestatin are well-known G-quadruplex binders (Figure 1.7) (Dexheimer et al., 2006; Sun et al., 2005). Although TMPyP4 is used as one of the most commonly investigated molecules in G-quadruplex stabilization studies, there is no sequence and structure selectivity upon TMPyP4 binding to G-quadruplex structures.

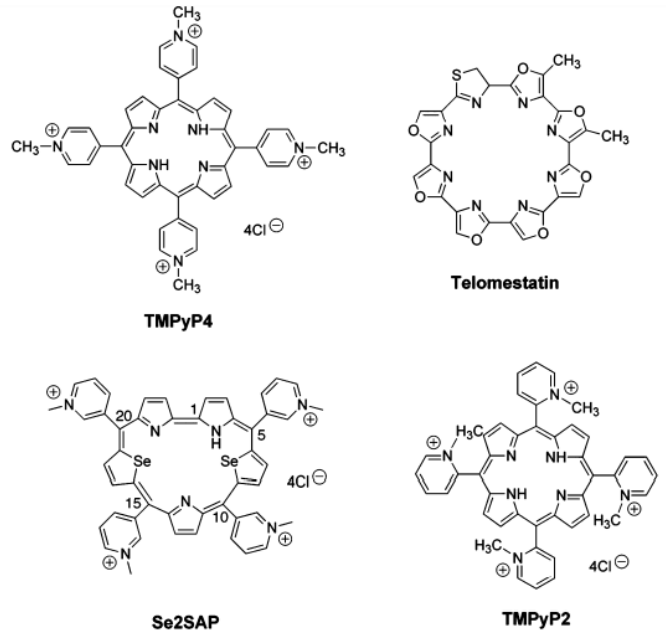

Figure 1.7. G-quadruplex binders (Dexheimer et al., 2006).

1.4 Azacyanine Molecules and Their Structures

Azacyanines are positively charged small planar molecules. According to previous studies, planar molecules can intercalate between bases easily (Persil Çetinkol et al., 2008; Persil et al., 2004). The positive charge on a small Azacyanine molecule enables them to interact with a negatively charged DNA backbone and intercalate between bases or stack on G-tetrads (Persil Çetinkol & Hud, 2009; Tutuncu et al., 2018).

Their potential was realized from the first day of discovery and used to target cancerous tissues involving controlling G-quadruplex sequences (Haddadin, Kurth, & Olmstead, 2000; Huang et al., 2001; Kaulage et al., 2018; Maji et al., 2014; Persil Çetinkol et al.,2008). This thesis study investigates benzimidazole derivatives named Azamethyl, Azabutyl, and Azaisobutyl and benzothiazole derivatives called Aza4 and Aza5. It is known that Azamethyl, Aza4, and Aza5 bind to telomeric G4 sequences, triple-stranded DNA, and poly(A) sequences from previous studies (Persil Çetinkol et al., 2008; Persil Çetinkol & Hud, 2009; Tutuncu et al., 2018).

However, their selectivity toward different G-quadruplex sequences in different promoter regions was not examined previously.

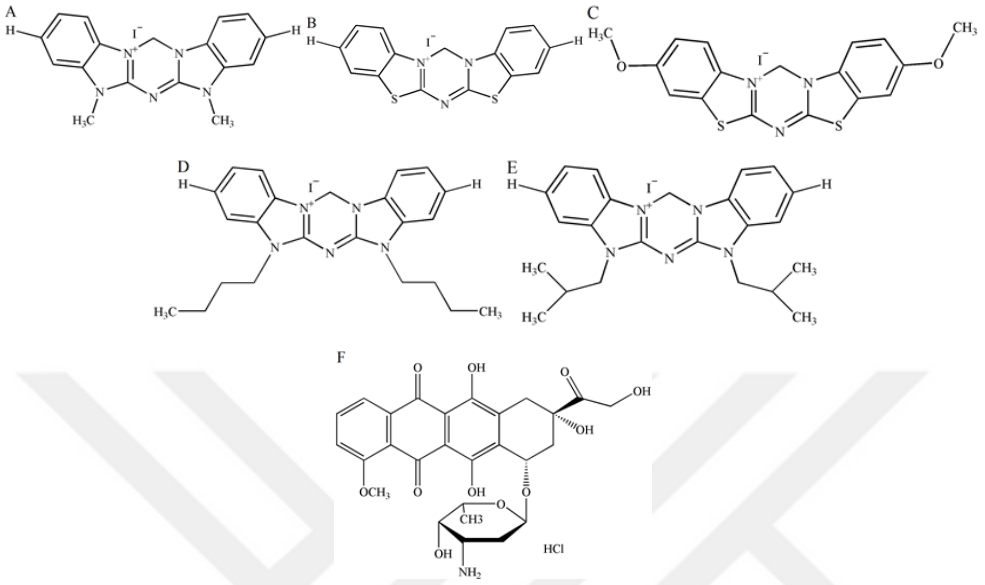

Figure 1.8. Structures of (A) Azamethyl, (B) Aza4, (C) Aza5, (D) Azabutyl, (E) Azaisobutyl and (F) Doxorubicin.

1.5 Thesis Focus

Non-selective binding patterns of cancer therapeutics generally cause challenging side effects and toxicity in cancer treatment. Small molecule binding to genomic DNA with high affinity kills not only cancer cells but also healthy somatic cells. Consequently, in recent years, cancer research in developing small therapeutic agents is shifted more towards the development of small molecules targeting specific DNA regions and noncanonical structures selectively.

The scope of this thesis is to investigate the selectivity and affinity of Azacyanine derivatives toward nucleic acid sequences with varying G-quadruplex structures. Promoter regions of proto-oncogene sequences were selected as target G4 sequences due to their regulatory roles in gene expression and regulation (Chen & Yang, 2012;

Rhodes & Lipps, 2015; Siddiqui-Jain, Grand, Bearss, & Hurley, 2002). Particularly, these G4 secondary structures are detected in critical regions, and their presence is thought to be non-random (Rhodes & Lipps, 2015; Wu & Brosh, 2010; Zhou et al., 2006).

First, the sequence or structure selectivity of Azacyanine derivatives was examined via the competition dialysis method. Since former studies already gave promising results in G-quadruplex selectivity of Azacyanines, the critical sequences were chosen to scan and quantify the selectivity of these molecules (Çetinkol et al., 2008; Küçükakdağ Doğu, 2019). Afterwards, based on the results of competition dialysis experiments, the most preferred sequence and the drug (Azamethyl) were selected to perform further detailed spectrophotometric studies. Benzothiazole derivatives were not even considered during the selection process since Aza4 and Aza5 are sensitive to high temperatures and light. Their decomposition was observed during thermal denaturation studies.

Overall, this thesis aims to reveal out the selectivity of Azacyanines towards G4 forming promoter regions and their potential to stabilize these G4 structures.

CHAPTER 2

MATERIALS AND METHODS

2.1 Selectivity of Azacyanine Derivatives Towards G-Quadruplex Forming Sequences

Dialysis is an ancient but one of the most effective techniques in purifying molecules of different sizes, relying on the selective diffusion of small molecules through a semipermeable membrane while the large molecules are held inside the tube (Craig & King, 1962; De & Michor, 2010). Competition dialysis is one of the straightforward methods evolved from dialysis to detect the selectivity of ligands in a quantitative manner towards different nucleic acid structures (Ragazzon, Garbett, & Chaires, 2007).



Figure 2.1. Competition Dialysis set-up. Disposable dialysis cassette, each containing 600.0 µL of a 75.0 µM solution of one of the DNA structures listed in Table 2.3, are placed in a beaker containing 750.0 mL of 1.0 µM ligand solution in 1XBPES.

In competition dialysis, each of the different nucleic acid structures is placed inside a cassette, and all the cassettes are dialyzed against a ligand solution simultaneously. The cassette holds the nucleotides trapped inside, while the ligand can diffuse freely. Once the system is equilibrated, where nucleic acids are in equilibrium with the free ligand, the amount of the bound ligand directly proportional to the ligand binding affinity is measured via UV-Vis or Fluorescence measurements.

2.1.1 Competition Dialysis

The competition dialysis method used in these studies was optimized according to studies by Ragazzon and colleagues (Ragazzon et al., 2007; Ragazzon & Chaires, 2007). The experiments were conducted with Slide-A-Lyzer G2 Dialysis Cassettes with a 3.5 kDa cutoff point (Thermo Scientific, Rockford, USA, 0.5 mL). Each cassette was labeled and used for a single type of oligonucleotide while examining six different small molecules. A spare cleaning tank was used to clean and hold cassettes in Millipore water (Milli-Q H_2O) kept in the dark and cool place.

600.0 µL nucleotide solutions (75.0 µM) in 1XBPES buffer were prepared and added into clean empty cassettes. A cassette containing only the buffer solution was also prepared as a control. Exposure to air was kept at the minimum for the sustainability of the cassette membranes. After that, the cassettes were immediately placed into a 750.0 mL 1.0 µM ligand in 1XBPES buffer tank (Figure 2.1.). Parafilm was applied to the top of the tank to prevent evaporation. The system was let sit for 24 hours with continuous stirring to reach equilibrium.

After 24 hours, equal volumes of the samples were taken out from the cassettes. 288.0 µL sample was mixed with 32.0 µL 10% SDS and 1680.0 µL 1XBPES, and the fluorescence measurements were performed using the parameters given in Table 2.2. Calibration curves were constructed for each small molecule at two different wavelengths (Appendix C) to minimize the experimental error. The bound ligand C_b

concentrations were determined via the calibration curves using the following equation.

$C_b/C_f = (C_t/C_f)-1$

Where C_t represents total molecule concentration in cassette, C_b is bound molecule concentration, and C_f is free molecule concentration in the cassette (control). The concentration of only buffer cassette (1XBPES) gave C_f value close to the total concentration of azacyanine molecule, 1.0 µM, found in 750.0 mL 1XBPES Buffer at the beginning.

2.1.2 BPES Buffer and 10% (w/v) SDS Stock Solutions Preparation

The buffer solution was prepared in 5 times concentrated (5XBPES) form, and pH was adjusted for both 1XBPES and 5XBPES in each preparation. 200.0 mL 5XBPES was put into a volumetric flask, and volume was completed to 1.0 L with Millipore water (Milli-Q H_2O). NaOH and HCI solutions were used to adjust pH. Preparation of buffer solutions are given in detail in appendix D.

Table 2.1 BPES buffer content for competition dialysis.

	1XBPES Final Conc. (mM)	**5XBPES Final Conc. (mM)**	**Stock Conc. (mM)**	**Stock Vol. In 500 mL 5XBPES (mL)***
NaCI	185	925	2000	231.25
Na_2HPO_4	6	30	600	25.0
Na_2EDTA	1	5	100	25.0
NaH_2PO_4	2	10	400	12.5

* After addition of stock solutions, volume was completed to 500.0 mL with H_2O in volumetric flask.

Table 2.2 Parameters used in Fluorescence and UV-Vis measurements.

	Azamethyl	Aza4	Aza5	Azabutyl	Azaisobutyl	Doxorubicin
Excitation Wavelength (nm)	324	389	399	324	324	480
Emission Wavelength Start (nm)	325	390	400	325	325	500
Emission Wavelength End (nm)	675	650	750	675	675	750
Excitation Slit (nm)	2.5	2.5	2.5	2.5	2.5	5
Emission Slit (nm)	5.0	5.0	5.0	5.0	5.0	10.0
Scan Rate (nm/min)	300	300	300	300	300	600
λ (nm)	343	387	407	343	343	480
Ɛ ($M^{-1}cm^{-1}$)	45700	24240	25000	44000	44700	11500

2.1.3 Oligonucleotide Preparations

The list of nucleic acid sequences used and their extinction coefficients are listed in Table 2.3. G-quadruplex oligonucleotides were obtained from IDT (Europe) in the lyophilized form. Extinction coefficients (Ɛ) given in Table 2.3 either supplied by IDT or reported in were used in concentration calculations (Ren & Chaires, 1999).

Polyd(A) and Polyd(A).Polyd(T) (Sigma-Aldrich, Europe) were prepared according to the same principle used in G-quadruplex forming sequences. *Micrococcus lysodeikticus* (Sigma-Aldrich, Europe) arrived as lyophilized. *Micrococcus lysodeikticus* (*M.lyso*) genomic DNA was purified further according to the previously reported procedure in Appendix A (Chaires, Dattagupta, & Crothers, 1982; Ren & Chaires, 2001). After the oligonucleotides were solubilized, their exact concentrations were measured in UV-Vis spectrophotometer with their given Ɛ ($M^{-1}cm^{-1}$) unit.

For competition dialysis, 75.0 µM oligonucleotide stock solutions were prepared in 1XBPES buffer and annealed before the experiment. The annealing process starts

with holding 75.0 µM oligonucleotide solution tube at 95°C water tank for 5 mins, and then the tube is kept in the same tank for 24 hours for slow cooling to ensure the proper folding.

Table 2.3 Nucleic acid sequences used (Ragazzon et al., 2007).

Conformation	Index	Nucleic Acid	λ (nm)	Ɛ ($M^{-1}cm^{-1}$)*	Monomeric Unit
Single-Stranded DNA	1	Polyd(A)	257	8600	Nucleotide
Double-Stranded DNA	2	Polyd(A).Polyd(T)	260	12000	Base Pair
	3	Micrococcus lysodeikticus (72% GC)	260	13846	Base Pair
Quadruplex DNA	4	5'-$T_2G_{20}T_2$-3'	260	235600	Quartet
	5	Promoter BCL-2 (5'-$AG_4CG_3CGCG_3AG_2A_2G_5CG_3AGCG_4C$-3')	260	41591	Quartet
	6	Promoter c-MYC (5'-$TG_4AG_3TG_4AG_3$ $TG_4A_2G_2$-3')	260	45309	Quartet
	7	Promoter HER-2/neu (5'-$AG_2AGA_2G_2(AG_2)_2TG_2(AG_2)_3GC$-3')	260	42985	Quartet
	8	Promoter KIRAS (5'-$G_3A_2GAG_3A_2GAG_5AG_2$-3')	260	24646	Quartet
	9	Promoter RETINOBLASTOMA (5'-$CG_6T_4G_3CG_2C$-3')	260	9407	Quartet
	10	Promoter VEGF (5'-$G_3CG_3C_2G_5CG_4TC_3G_2CG_4CG_3AG$-3')	260	35778	Quartet
	11	Human Telomere (5'- $(AG_3T_2)_3AG_3$-3')	260	73000	Quartet

2.1.4 Calibration Curve Construction

Calibration curves obtained via fluorescence spectroscopy were used to determine the small molecule concentrations trapped in the cassettes during competition dialysis. For each small molecule, 50.0 μM stock solution was prepared in DMSO (for Azacyanines) or H_2O (for Doxorubicin) using UV-Vis absorbance. DMSO, used in all measurements, was obtained from AppliChem GmbH (Darmstadt, Germany). Cary Eclipse fluorescence spectrophotometer (Varian Company, USA) and Agilent Cary 8454 UV-Vis diode array spectrophotometer equipped with an Agilent 89090A Peltier (Santa Clara, CA, USA) were used in fluorescence and UV-Vis spectroscopy experiments, respectively.

Table 2.4 Experimental setup used during the Fluorescence measurements.

Concentration (μM)	**Added Molecule Volume[a] (μL)**	**Total Molecule Volume (μL)**	**10% SDS Volume (μL)[b]**	**1XBPES Volume (μL)**	**Total Volume (μL)**
0.1	4.0	4.0	32.0	1964	2000
0.2	4.0	8.0	32.0	1964	2004.0
0.3	4.1	12.1	32.0	1964	2008.1
0.4	4.1	16.2	32.0	1964	2012.2
0.5	4.1	20.3	32.0	1964	2016.3
0.6	4.2	24.5	32.0	1964	2020.5
0.7	4.2	28.7	32.0	1964	2024.7
0.8	4.2	32.9	32.0	1964	2028.9

Table 2.4 (cont.)

0.9	4.3	37.2	32.0	1964	2033.2
1.0	4.3	41.5	32.0	1964	2037.5
1.1	4.3	45.8	32.0	1964	2041.8
1.2	4.4	50.2	32.0	1964	2046.2
1.3	4.4	54.6	32.0	1964	2050.6
1.4	4.4	59.1	32.0	1964	2055.1
1.5	4.5	63.6	32.0	1964	2059.6
1.8	11.1	74.7	32.0	1964	2070.7
2.1	11.6	86.3	32.0	1964	2082.3
2.6	23.3	109.6	32.0	1964	2105.6
3.2	24.8	134.4	32.0	1964	2130.4
3.7	26.0	160.4	32.0	1964	2156.4
4.3	27.2	187.5	32.0	1964	2183.5
4.9	28.4	216.0	32.0	1964	2212.0
5.5	29.8	245.8	32.0	1964	2241.8

[a]Added stock concentration was 50.0 µM.

[b]10% SDS was used during the measurements to denature DNA and release the bound molecules.

Measurement starts with 0.1 µM molecule concentration. The calculation can be seen in the following equation.

- 50.0 µM x A µL = 0.10 µM x (1996 + A) µL.

A = 4.0 µL addition from 50 µM stock solution.

For the remaining calculations, the following equation is mediated.

- 50.0 µM x B µL = 0.20 µM x (2000 + B) µL.

B = 8.0 µL is total added 50.0 µM molecule.

C represents added molecule volume, calculated in each addition as explained below.

C = B – A → C = 8 .0– 4.0 = 4.0 µL.

Pipetting was mediated during each step just before the measurement, and 3-minute intervals were mediated between each sample. The parameters used during fluorometer and UV-vis spectrometer measurements are listed in Table 2.2.

In order to reduce error, calibration curves were constructed from two independent experiments at two reference wavelengths (Appendix C). The linear regression method was used to obtain the equations from fluorescence intensity vs. concentration graphs.

2.2 Spectroscopic Investigation of c-MYC:Azamethyl Interactions

c-MYC:Azamethyl interactions at varying concentrations were investigated via thermal denaturation experiments using UV-Vis spectrophotometry and Circular Dichroism Spectroscopy. Plotting and data processing were performed using Igor Pro software (WaveMetrics). Quartz cuvettes with PTFE stoppers (3.5 mL, 111-QS, Hellma) were used in all spectrophotometric measurements.

2.2.1 Thermal Denaturation Experiments

Thermal denaturation experiments were carried out with c-MYC:Azamethyl samples with fixed ratios of 1:0, 0:1, 1:1, 1:2, 1:4, 1:6, 1:8, and 1:10. Calculations for sample preparations can be found in Appendix F.

Agilent Cary 8454 UV-Vis diode array spectrophotometer equipped with an Agilent 89090A Peltier (Santa Clara, CA, USA) was used during thermal denaturation experiments. Samples were heated or cooled between 15°C and 95°C with 1°C rate. Absorbances were collected in the range of 190-1100 nm. Melting profiles of each solution were obtained by plotting the absorbance at a chosen wavelength (nm) versus temperature (°C).

For Circular Dichroism (CD) studies, a Circular Dichroism spectropolarimeter (JASCO J-815, Easton, USA) equipped with a Peltier temperature control system (PTC-423S/15) was used at the laboratory service of Bilkent/UNAM. The CD spectra for almost all samples were obtained between 240-400 nm at 15°C and 95°C with scan rates of 200 nm/min and 1 nm intervals. CD melting points for all samples were obtained by increasing the temperature from 15°C to 95°C with 5°C intervals. The first derivative of the thermal denaturation curves was used to obtain the melting temperatures (°C).

2.2.2 Association Constant Determination

Lastly, Fluorescence experiments were performed to find the binding affinity of Azamethyl to the c-MYC sequence. 1.0 µM Azamethyl solution was titrated with 400.0 µm quadruplex c-MYC solution containing 1.0 µM Azamethyl until the system reached equilibrium where the emission spectrum was not changing any longer (Appendix E). Experiments were mediated with Cary Eclipse fluorescence spectrophotometer (Varian Company, USA) at room temperature (RT). Azamethyl was excited at 324 nm, and the emission spectrum was collected between 325-765 nm with excitation and emission slits of 2.5 and 5.0, respectively. Measurements were performed as triplicates, and given association constants (K_a) were determined by fitting integrated intensity between 325-765 nm as a function of quadruplex DNA concentration using the least squares equations as explained previously (Horowitz & Hud, 2006). Average of the association constants obtained was reported as the association constant of Azamethyl with c-MYC (Figure 3.21).

CHAPTER 3

RESULTS AND DISCUSSION

3.1 Selectivity of Azacyanine Molecules Against Different G4 forming Sequences Found Mainly in Promoter Regions

Competition dialysis experiments were performed to determine the selectivity of Azacyanines towards different G4 forming sequences found in the promoter regions of several key genes, primarily associated with cell cycle and development. Quantification of the small molecules was performed using pre-constructed calibration curves obtained via Fluorescence measurements. The calibration curves were constructed (Section 2.1.4) using two independent experiments at two reference wavelengths (nm). The linear regression method was used to obtain the equations from fluorescence intensity vs. concentration graphs. The equations obtained from calibration curves used in concentration determinations are given in Table 3.1.

Table 3.1 Calibration curve equations and reference wavelengths.

Molecule Name	**1st Reference Wavelength**	**2nd Reference Wavelength**
	378 nm	**440 nm**
Azamethyl	y = 312.93.x + 8.0918	y = 1.48.05x + 13.23
	445 nm	**470 nm**
Aza4	y = 259.98.x + 6.3689	y = 174.39.x + 4.8983
	480 nm	**500 nm**
Aza5	y = 181.49.x + 5.3636	y = 155.09.x + 4.8555
	379.07 nm	**440 nm**
Azabutyl	y = 269.45.x + 13.244	y = 128.95.x + 12.169
Azaisobutyl	y = 329.62.x + 9.2527	y = 146.47.x + 13.898

Table 3.1 (cont.)

	592.94 nm	**618.98 nm**
Doxorubicin	y = 119.44.x + 5.4633	y = 64.859.x + 2.6724

Competition dialysis experiments were also performed in duplicates. Two independent experiments were performed for each small molecule. After the tank reached equilibrium at the end of 24 hours, concentrations of the ligands were determined via Fluorescence measurements, and the C_b/C_f values were calculated using the constructed calibration curves.

In competition dialysis, all of the DNA samples are in equilibrium with the same free ligand concentration. If the ligand has no or very low affinity to a certain DNA structure, the concentration of ligand in the cassette with that sequence is generally found to be equal to the concentration of the ligand free in solution (tank) or to the ligand concentration in control cassette than contains only buffer. On the other hand, if the ligand has affinity to a certain DNA structure, it travels to the cassette with that DNA structure, and binds to it. As a result, the concentration of the ligand in that cassette increases compared to the free ligand concentration in solution. The amount of bound ligand is proportional to the association constant; the higher the concentration of the ligand, the higher the association constant (K_a) for that ligand binding to the particular DNA structure in that cassette (Ren & Chaires, 1999).

3.1.1 Azamethyl

Differing binding abilities of Azamethyl to each nucleic acid structure gave rise to varying C_b/C_f values. Figure 3.1. displays the results of two independent competition dialysis experiments and reveals the binding tendency of Azamethyl to different nucleic acid sequences. The calculated C_b/C_f values along with the average C_b/C_f values and standard deviations are listed in Table 3.2, and the C_b/C_f bar graph is displayed in Figure 3.2.

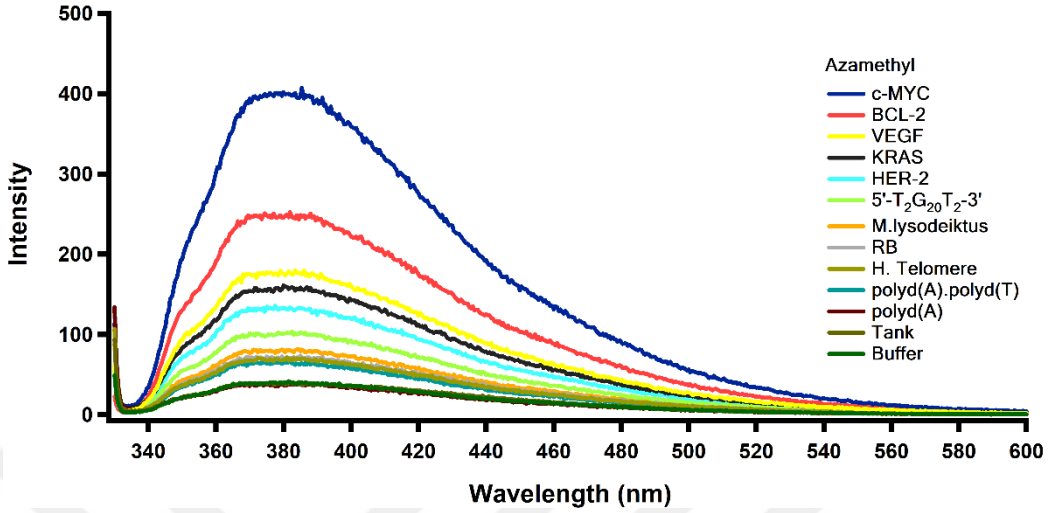

Figure 3.1. Average fluorescence intensity versus wavelength (nm) plots from two independent competition dialysis experiments of Azamethyl.

Table 3.2 Competition dialysis results for Azamethyl.

	C_b/C_f			
Sample Name	**1st Replicate**	**2nd Replicate**	**Average**	**Standard Deviation**
c-MYC	10.24	9.94	10.09	0.21
BCL-2	6.07	6.12	6.10	0.03
VEGF	4.04	4.04	4.04	0.00
KRAS	3.47	3.42	3.45	0.04
HER-2	2.75	2.55	2.65	0.14
5'-$T_2G_{20}T_2$-3'	1.81	1.68	1.75	0.09
M. lysodeikticus	1.27	1.17	1.22	0.07
RB	1.01	0.96	0.99	0.04
H. Telomere	0.90	0.82	0.86	0.06
polyd(A).polyd(T)	0.74	0.71	0.73	0.02
polyd(A)	0.08	0.11	0.09	0.02
Tank	0.11	0.23	0.17	0.09
Buffer	0.00	0.00	0.00	0.00

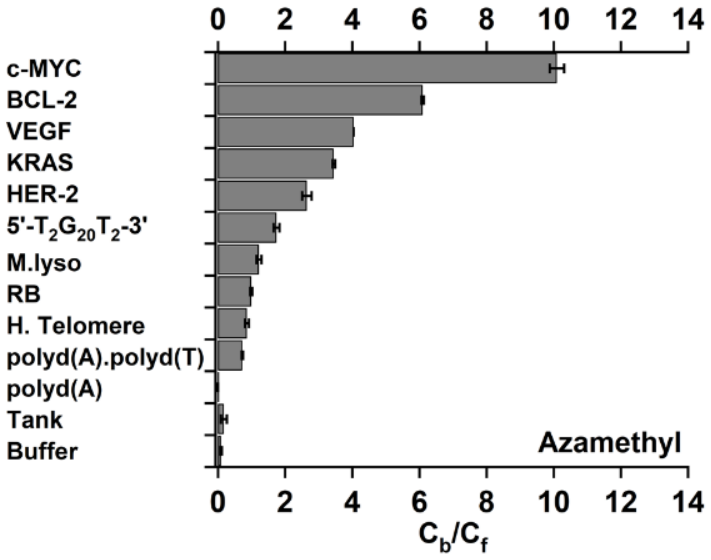

Figure 3.2. Average C_b/C_f values of competition dialysis for Azamethyl. Error bars represent the standard deviations from two independent experiments.

Competition dialysis results of Azamethyl revealed its apparent affinity to G4 bearing sequences. Among them, it had the highest affinity for the c-MYC promoter region with a C_b/C_f value of 10.09. On the other hand, the lowest affinity among G-quadruplex sequences belongs to Retinoblastoma (RB) and Human Telomere (H. Telomere) with 0.99 and 0.86 C_b/C_f values, respectively. Furthermore, the affinity of Azamethyl is observed to be gradually decreasing from the c-MYC promoter region to polyd(A).polyd(T). Its affinity to double-stranded polyd(A).polyd(T) was very low with a C_b/C_f value of 0.73. In accordance with the previous reports, our results also revealed that the Azametyl wasn't binding to single-stranded sequence polyd(A) (Guloglu, 2018). C_b/C_f value for polyd(A) was 0.07, where the C_b/C_f value of the control cassette was 0.17.

3.1.2 Aza4

Aza4's affinity against promoter sequences of proto-oncogenes was also examined via competition dialysis. Average fluorescence spectra of Aza4 from competition dialysis results are depicted in Figure 3.3. C_b/C_f values are given in Table 3.3, and the average C_b/C_f values are plotted as a bar graph in Figure 3.4.

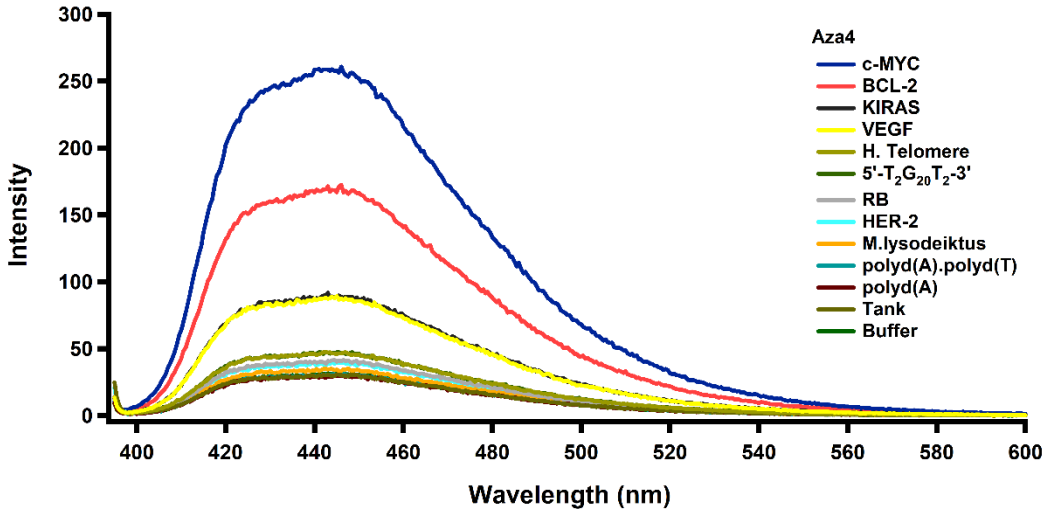

Figure 3.3. Average fluorescence intensity versus wavelength (nm) plots from two independent competition dialysis experiments of Aza4.

Table 3.3 Competition dialysis results for Aza4.

	C_b/C_f			
Sample Name	**1st replicate**	**2nd replicate**	**Average**	**Standard Deviation**
c-MYC	7.78	7.51	7.65	0.19
BCL-2	4.58	4.71	4.64	0.09
VEGF	1.97	1.94	1.95	0.02
KRAS	1.85	2.04	1.94	0.13
HER-2	0.26	0.32	0.29	0.04
5'-$T_2G_{20}T_2$-3'	0.50	0.60	0.55	0.07
M.lysodeikticus	0.11	0.16	0.14	0.04
RB	0.28	0.40	0.34	0.09
H. Telomere	0.21	0.85	0.53	0.45
polyd(A).polyd(T)	-0.01	0.02	0.01	0.03
polyd(A)	-0.06	-0.06	-0.06	0.00
Tank	-0.03	0.03	0.00	0.04
Buffer	0.00	0.00	0.00	0.00

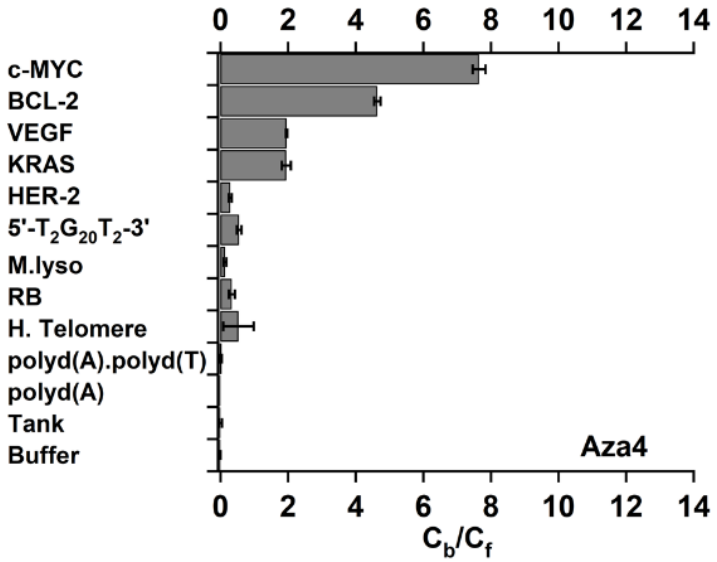

Figure 3.4. Average C_b/C_f values of competition dialysis for Aza4. Error bars represent the standard deviations from two independent experiments.

Our experiments revealed that Aza4 also has the highest affinity toward the c-MYC promoter region among other promoter sequences with C_b/C_f value of 7.65. Its relatively high affinity and selectivity to G4 c-MYC, BCL-2, VEGF, and KRAS sequences is apparent (Figure 3.3). However, there is a dramatic decrease in affinity when we compare the affinity of Aza4 for HER-2, '$T_2G_{20}T_2$-3', *M. lyso*, RB, and H. Telomere with those sequences. Among them, the lowest affinity belongs to *M. lyso* with 0.14 C_b/C_f value. Lastly, we can say that Aza4 also showed no affinity towards polyd(A).polyd(T) and polyd(A) with C_b/C_f values of 0.01 and -0.06. Here, one should be noted that the negative values are due to experimental errors.

3.1.3 Aza5

The second benzothiazole derivative, Aza5, showed a similar profile to Aza4. However, the affinity of Aza5 to G4 sequences was significantly higher than Aza4's. The average fluorescence measurements were displayed in Figure 3.5, the obtained C_b/C_f values are given in Table 3.4, and average C_b/C_f values are depicted as a bar graph in Figure 3.6.

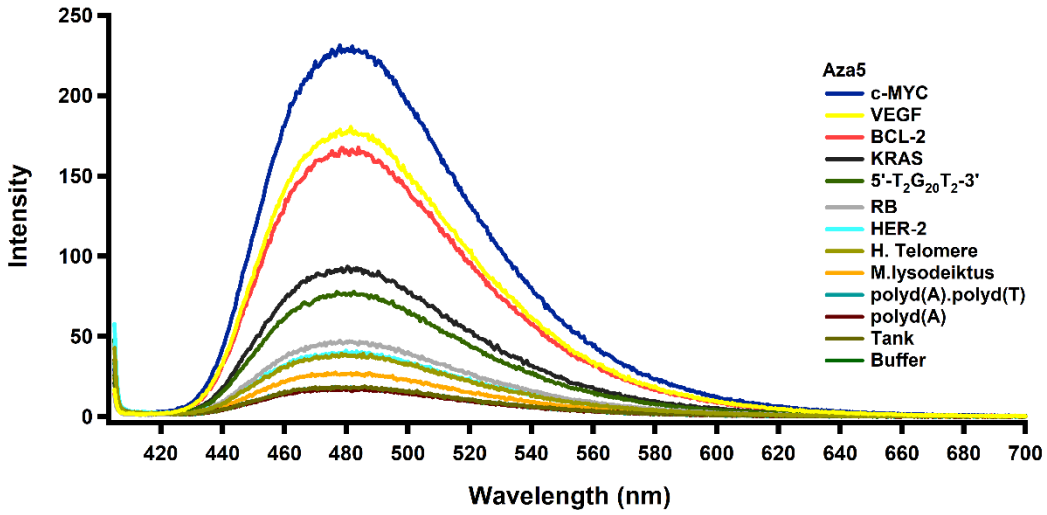

Figure 3.5. Average fluorescence intensity versus wavelength (nm) plots from two independent competition dialysis experiments of Aza5.

Table 3.4 Competition dialysis results for Aza5.

	C_b/C_f			
Sample Name	**1st Replicate**	**2nd Replicate**	**Average**	**Standard Deviation**
c-MYC	12.32	11.52	11.92	0.56
BCL-2	9.67	8.83	9.25	0.59
VEGF	9.25	8.59	8.92	0.47
KRAS	4.14	4.14	4.14	0.00
HER-2	1.25	1.38	1.31	0.09
5'-$T_2G_{20}T_2$-3'	3.55	3.05	3.30	0.35
M.lysodeikictus	0.61	0.47	0.54	0.10
RB	1.72	1.62	1.67	0.07
H. Telomere	1.23	1.14	1.19	0.06
polyd(A).polyd(T)	0.06	-0.01	0.02	0.05
polyd(A)	0.01	-0.04	-0.01	0.03
Tank	0.06	0.10	0.08	0.03
Buffer	0.00	0.00	0.00	0.00

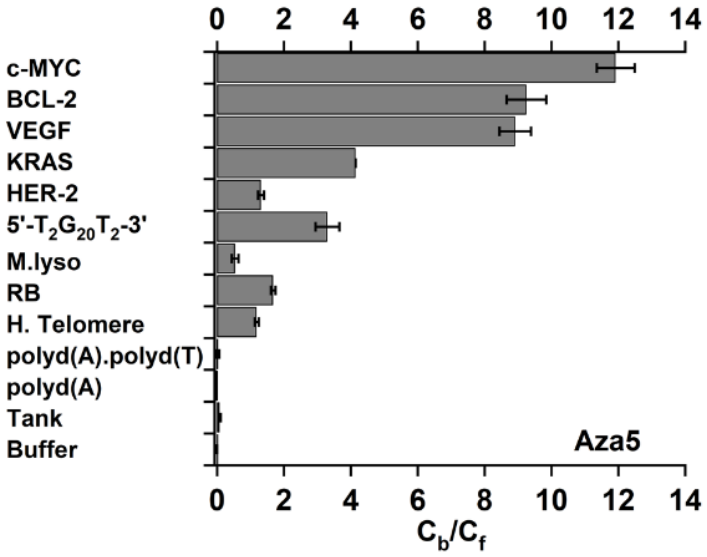

Figure 3.6. Average C_b/C_f values of competition dialysis for Aza5. Error bars represent the standard deviations from two independent experiments.

According to Aza5 competition dialysis results, Aza5 has a higher affinity toward c-MYC, BCL-2, VEGF, KRAS, 5'-$T_2G_{20}T_2$-3', RB, and H. Telomere than Azamethyl with C_b/C_f values of 11.92, 9,25, 8.92, 4.14, 3.30, 1,67 and 1.19, respectively. According to the results, exceptionally, it has lower affinity towards HER-2. Still, Aza5 did not show any affinity as Azamethyl and Aza4 towards polyd(A).polyd(T) and polyd(A).

3.1.4 Azabutyl

Azabutyl is another small molecule candidate in the class of benzimidazole derivatives. Compared to Azamethyl, it has longer alkyl chain in the benzimidazole ring. Azabutyl has been shown to be a very weak binder of triplex polyd(A).polyd(T).polyd(A) structure compared to Azamethyl (Tütüncü et al., 2018). The average fluorescence measurement results of the competition dialysis experiments are displayed in Figure 3.7; the obtained C_b/C_f values are given in Table 3.8 and depicted as a bar graph in Figure 3.8.

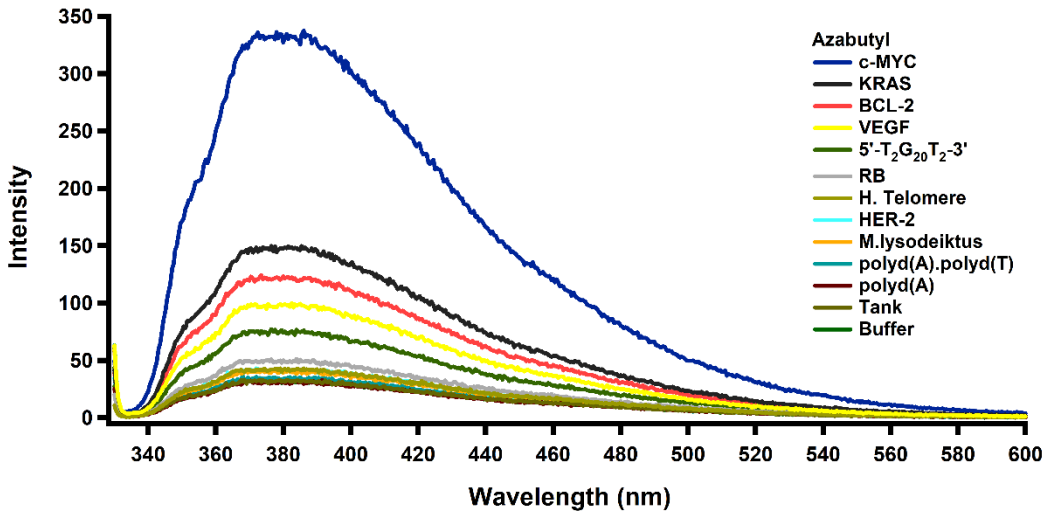

Figure 3.7. Average fluorescence intensity versus wavelength (nm) plots from two independent competition dialysis experiments of Azabutyl.

Table 3.5 Competition dialysis results for Azabutyl.

	C_b/C_f			
Sample Name	**1st Replicate**	**2nd Replicate**	**Average**	**Standard Deviation**
c-MYC	12.32	11.52	11.92	0.56
BCL-2	9.67	8.83	9.25	0.59
VEGF	9.25	8.59	8.92	0.47
KRAS	4.14	4.14	4.14	0.00
HER-2	1.25	1.38	1.31	0.09
5'-$T_2G_{20}T_2$-3'	3.55	3.05	3.30	0.35
M.lysodeikticus	0.61	0.47	0.54	0.10
RB	1.72	1.62	1.67	0.07
H. Telomere	1.23	1.14	1.19	0.06
polyd(A).polyd(T)	0.06	-0.01	0.02	0.05
polyd(A)	0.01	-0.04	-0.01	0.03
Tank	0.06	0.10	0.08	0.03
Buffer	0.00	0.00	0.00	0.00

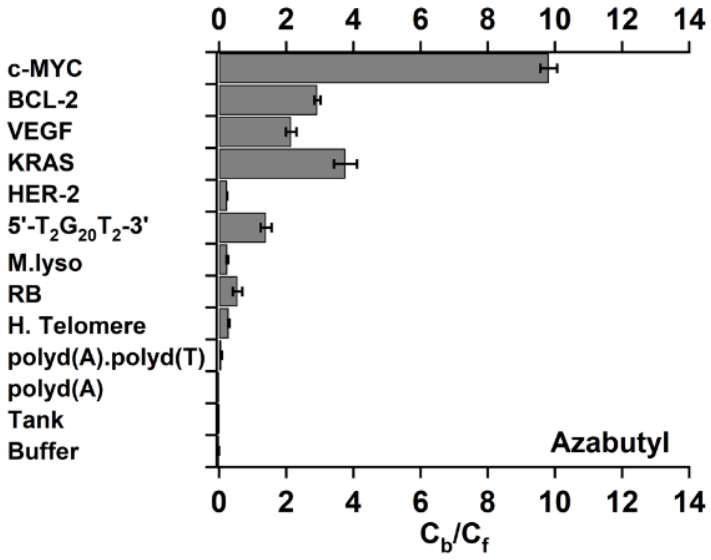

Figure 3.8. Average C_b/C_f values of competition dialysis for Azabutyl. Error bars represent the standard deviations from two independent experiments.

Competition dialysis results revealed that Azabutyl has the highest affinity toward the c-MYC promoter region compared to Azamethyl, Aza4, and Aza5. It was also the most selective. Azabutyl showed higher affinity than Azamethyl toward c-MYC and KRAS sequences with C_b/C_f values of 9.86 and 3.76, respectively. It showed lowered affinity to other sequences when compared to Azamethyl. Binding affinities of Azabutyl toward HER-2, *M. lyso*, RB, and H. Telomere were much lower than c-MYC, BCL-2, VEGF, KRAS, and 5'-$T_2G_{20}T_2$-3' with C_b/C_f values of 0.24, 0.25, 0.55, respectively.

3.1.5 Azaisobutyl

The affinity of Azaisobutyl to different G4s was also investigated. From fluorescence intensity measurements given in Figure 3.9, C_b/C_f values were calculated (Table 3.6), and their average results are shown in Figure 3.10 with standard deviations from two independent experiments.

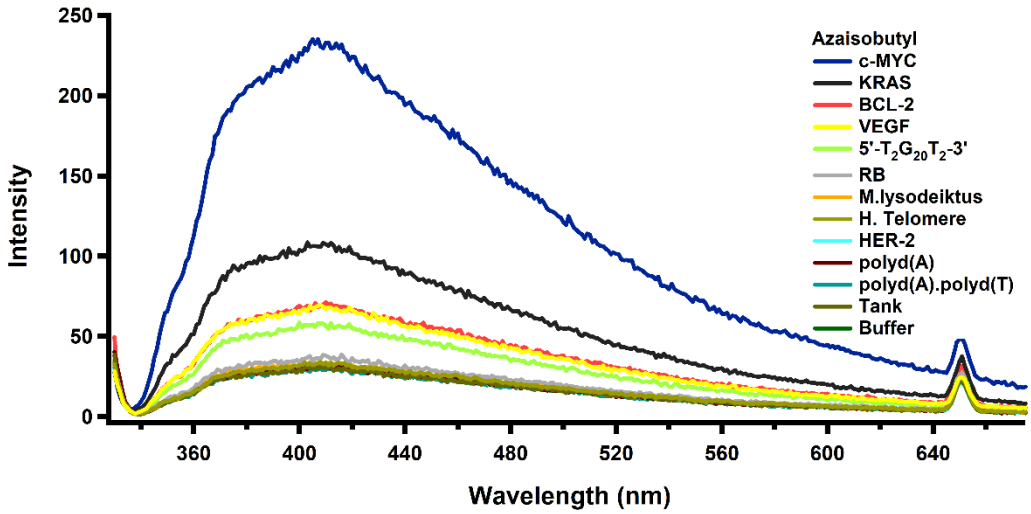

Figure 3.9. Average fluorescence intensity versus wavelength (nm) plots from two independent competition dialysis experiments of Azaisobutyl.

Table 3.6 Competition dialysis results for Azaisobutyl.

	C_b/C_f			
Sample Name	**1st Replicate**	**2nd Replicate**	**Average**	**Standard Deviation**
c-MYC	6.64	7.17	0.37	6.91
BCL-2	1.12	1.42	0.21	1.27
VEGF	1.19	1.36	0.12	1.28
KRAS	2.54	2.67	0.09	2.60
HER-2	0.01	0.03	0.02	0.02
5'-$T_2G_{20}T_2$-3'	0.79	1.04	0.17	0.91
M.lysodeikticus	0.13	0.09	0.03	0.11
RB	0.15	0.27	0.08	0.21
H. Telomere	-0.06	0.15	0.15	0.04
polyd(A).polyd(T)	-0.14	0.01	0.11	-0.06
polyd(A)	-0.06	0.01	0.05	-0.03
Tank	-0.09	0.06	0.11	-0.02
Buffer	0.00	0.00	0.00	0.00

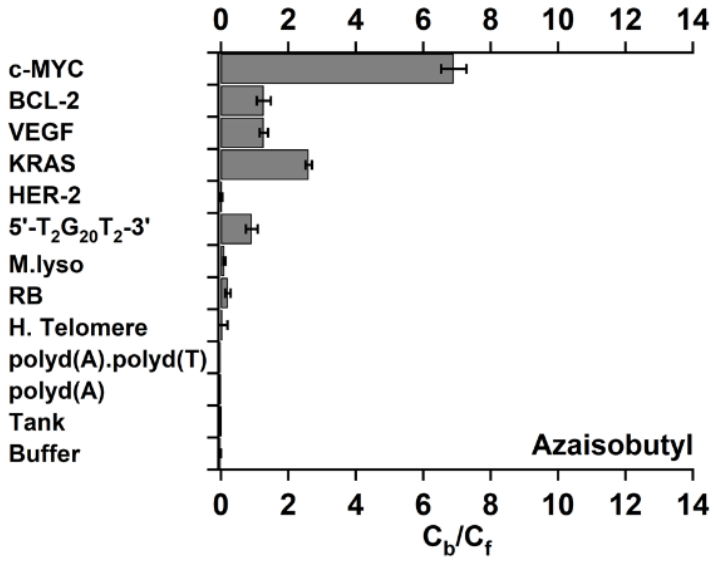

Figure 3.10. Average C_b/C_f values of competition dialysis for Azaisobutyl. Error bars represent the standard deviations from two independent experiments.

Among all Azacyanine derivatives, Azaisobutyl showed the lowest affinity towards the c-MYC promoter region with C_b/C_f value of 6.91. On the other hand, it showed almost no binding to other sequences except KRAS. Overall, these results reveal the importance of alkyl chains in terms of the binding ability of small molecules to a particular DNA structure.

3.1.6 Doxorubicin

In order to comprehend the binding ability of Azacyanines to G4s, we also performed competition dialysis experiments using the anticancer clinical agent Doxorubicin. Doxorubicin is known to exert its effects by binding to genomic DNA that is double stranded (Tacar, Sriamornsak, & Dass, 2013). The results were given in Figure 3.11, Table 3.7, and Figure 3.12.

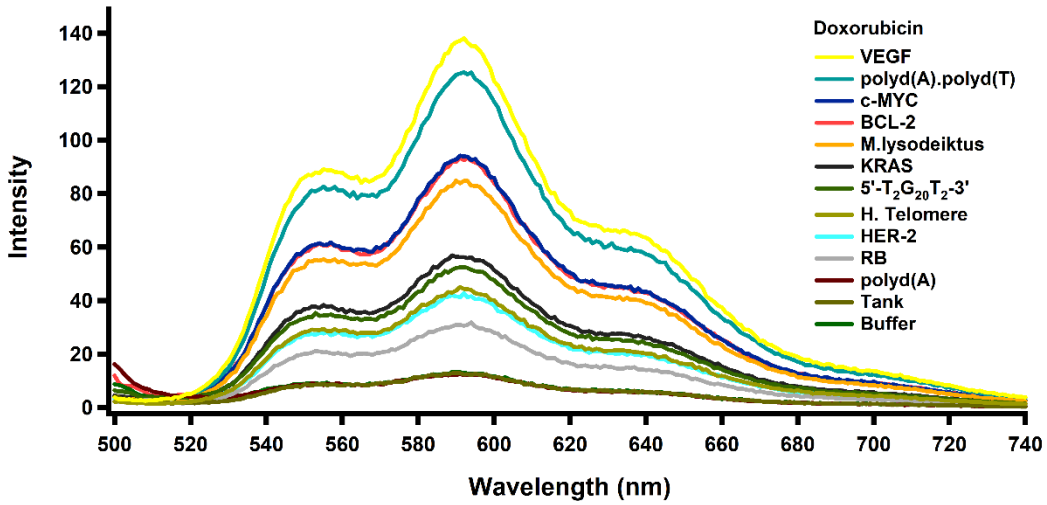

Figure 3.11. Average fluorescence intensity versus wavelength (nm) plots from two independent competition dialysis experiments of Doxorubicin.

Table 3.7 Competition dialysis results for Doxorubicin.

	C_b/C_f			
Sample Name	**1st Replicate**	**2nd Replicate**	**Average**	**Standard Deviation**
c-MYC	6.62	6.58	6.58	0.03
BCL-2	6.85	6.16	6.16	0.49
VEGF	10.42	9.73	9.73	0.49
KRAS	3.36	3.72	3.72	0.26
HER-2	2.23	2.54	2.54	0.22
5'-$T_2G_{20}T_2$-3'	3.20	3.20	3.20	0.00
M.lysodeikticus	6.00	5.65	5.65	0.24
RB	1.54	1.41	1.41	0.10
H. Telomere	3.00	2.06	2.06	0.67
polyd(A).polyd(T)	9.38	8.76	8.76	0.44
polyd(A)	-0.03	-0.10	-0.10	0.05
Tank	-0.04	-0.03	-0.03	0.01
Buffer	0.00	0.00	0.00	0.00

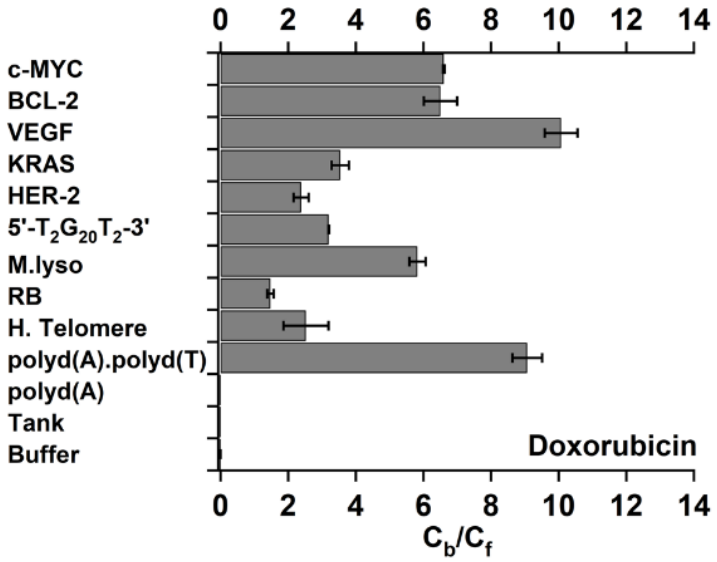

Figure 3.12. Average C_b/C_f values of competition dialysis for Doxorubicin. Error bars represent the standard deviations from two independent experiments.

Competition dialysis results revealed that Doxorubicin showed affinity to all samples except polyd(A) (C_b/C_f value -0.03). As expected, it showed a very high affinity to polyd(A).polyd(T) with C_b/C_f value of 8.76 (Tacar et al., 2013). To our surprise, its affinity to the VEGF G4 sequence was higher than polyd(A).polyd(T)'s. C_b/C_f value of 9.73 was obtained for its binding to VEGF G4. Besides, the affinity of Doxorubicin to c-MYC and BCL-2 sequences was close to each other, with C_b/C_f values of 6.58 and 6.16, respectively.

3.1.7 Overall c-MYC Affinities of Azacyanine Derivatives and Doxorubicin

All Azacyanine derivatives showed the highest affinity to c-MYC among other promoter sequences. Results are depicted in Figure 3.13 with tabulated version (Table 3.8). And all Azacyanines displayed a higher affinity to G4 of c-MYC than Doxorubicin. Small molecule affinities against the c-MYC promoter sequence can be ordered from highest to lowest as Aza5 > Azamethyl > Azabutyl > Aza4 > Azaisobutyl > Doxorubicin.

Table 3.8 Overall competition dialysis results for c-MYC.

Small Molecule	**C_b/C_f**	**Standard Deviation**
Azamethyl	10.09	0.21
Aza4	7.65	0.19
Aza5	11.92	0.56
Azabutyl	9.82	0.25
Azaisobutyl	6.91	0.37
Doxorubicin	6.60	0.03

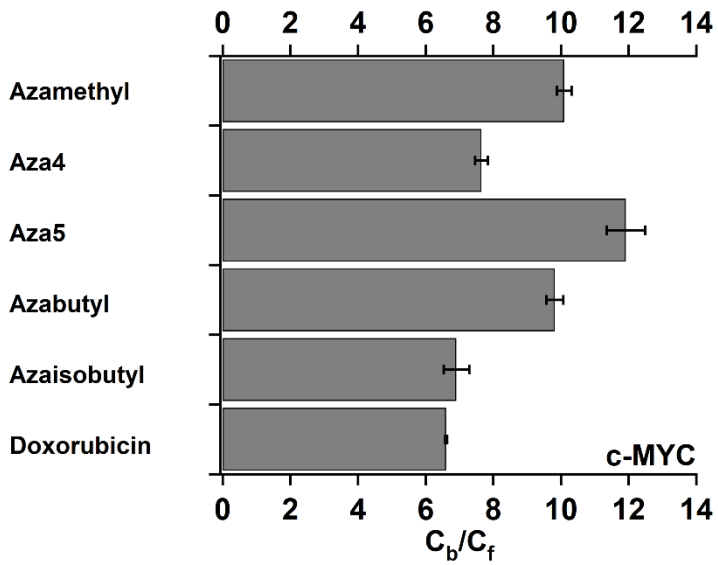

Figure 3.13. Average C_b/C_f values of competition dialysis against c-MYC. Error bars represent the standard deviations from two independent experiments.

3.2 Spectrophotometric Investigation of Azamethyl Binding to c-MYC

Competition dialysis experiments revealed the high affinity and the selective binding of Azacyanines, especially to the c-MYC promoter sequence. Accordingly, to have a deeper understanding of their interactions with c-MYC, the interactions of Azamethyl with c-MYC were further evaluated. The competition dialysis experiments revealed that both Azamethyl and Aza5 had a very high affinity to c-MYC. And, Azamethyl was chosen to be used in further investigations since the benzothiazole derivative Aza5 was not thermally stable.

Samples of c-MYC:Azamethyl with varying concentrations were first investigated using Fluorescence spectroscopy. Azamethyl is a high fluorescencent molecule. Upon binding of Azamethyl to G4 structures, mainly due to its stacking on top of the G4 structure, its fluorescence is quenched (Figure 3.14 and Figure 3.15A).

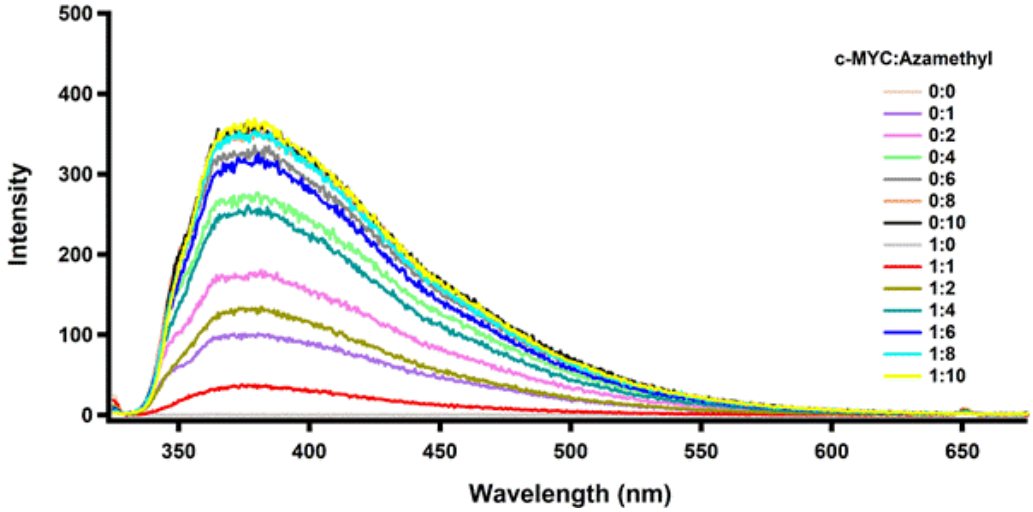

Figure 3.14. Fluorescence spectra of of c-MYC:Azamethyl samples with varying concentrations. Each c-MYC:Azamethyl ratio is represented by the corresponding color of the solid line in given caption. Concentration of c-MYC and Azamethyl is the multiples of 9 µM and 3 µM, respectively, in given ratios.

Changes are also observed in the UV-Vis spectrum of Azamethyl upon binding to DNA. The UV-Vis absorbance of Azamethyl between 300 nm and 360 nm is decreased upon binding of Azamethyl to c-MYC (Figure 3.15B). UV-Vis spectra of all the samples of c-MYC with varying concentrations of Azamethyl at 15°C and 95°C are also given in Appendix I. To calculate the UV-Vis melting profile of G4, absorbance at 295 nm is monitored with varying temperature (Mergny, Phan, & Lacroix, 1998). Although the binding of Azamethyl to c-MYC was clearly evident from changes in UV-Vis absorbance, UV-Vis spectrometry did not discriminate the changes in melting profiles of each sample at 295 nm (not given data). Hence, the thermal denaturation experiments were also performed using CD spectroscopy to evaluate changes in the stability of c-MYC G4 upon Azamethyl binding.

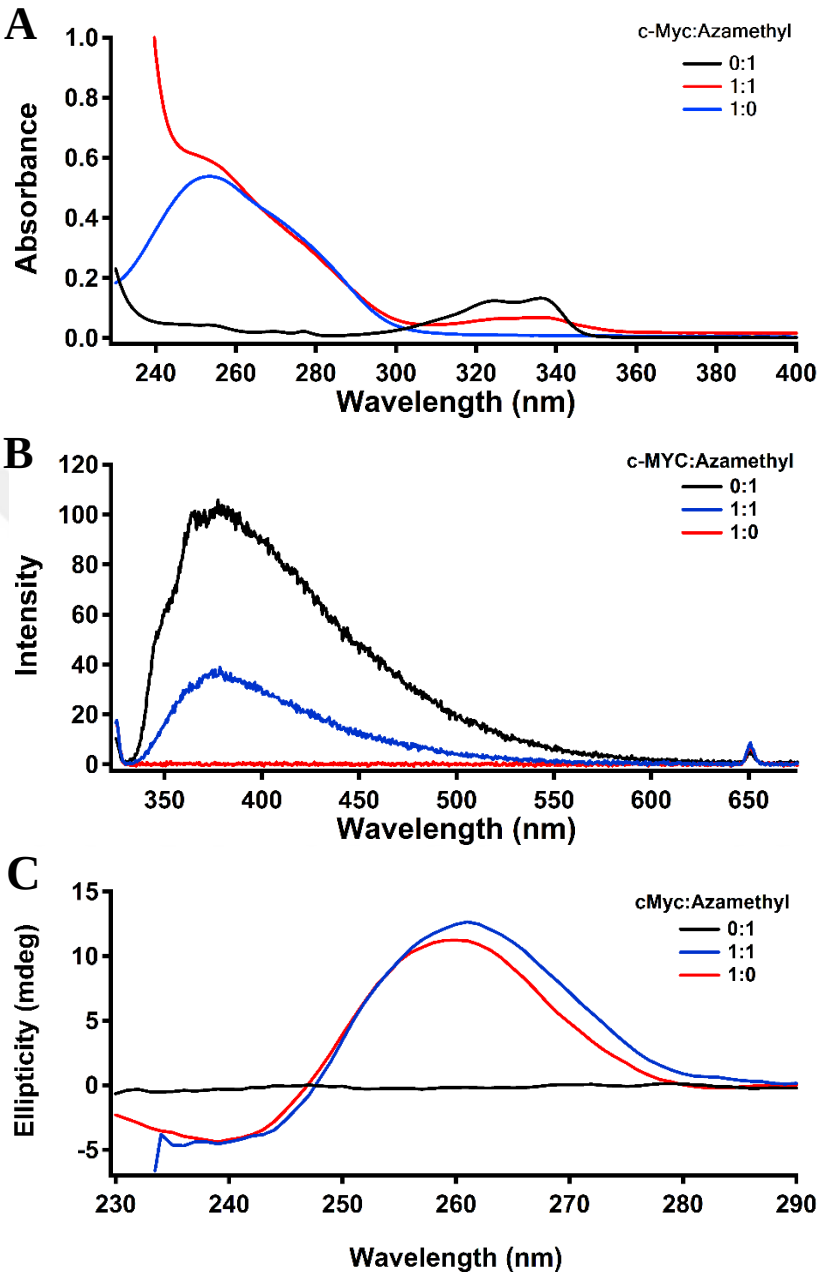

Figure 3.15. (A) UV-Vis spectra of 0:1, 1:1 and 1:0 c-MYC:Azamethyl samples at 15°C. Inset in A shows the 300 nm to 400 nm region of the spectra. (B) Fluorescence spectra of c-MYC:Azamethyl samples between 325 nm and 675 nm and (C) CD spectra of c-MYC:Azamethyl samples 240 nm and 290 nm, respectively. Concentration of c-MYC and Azamethyl is the multiples of 9 µM and 3 µM, respectively, in given ratios.

3.3 Thermal Denaturation of c-MYC:Azamethyl Samples via Circular Dichroism (CD) Spectroscopy

Samples with varying concentrations of c-MYC:Azamethyl were also prepared and investigated via CD spectroscopy. Only the chiral molecules give rise to CD bands. Asymmetry of sugar backbone in DNA gives negative and positive bands depending on DNA form and secondary structure (Vorlíčková et al., 2012). Azamethyl is the achiral molecule; therefore, it does not give rise to CD bands.

CD spectra for G4 sequences are given in Figure 3.18 and Figure 3.19. Unfortunately, due to high voltage problems, CD spectra could not be collected below 240 nm.

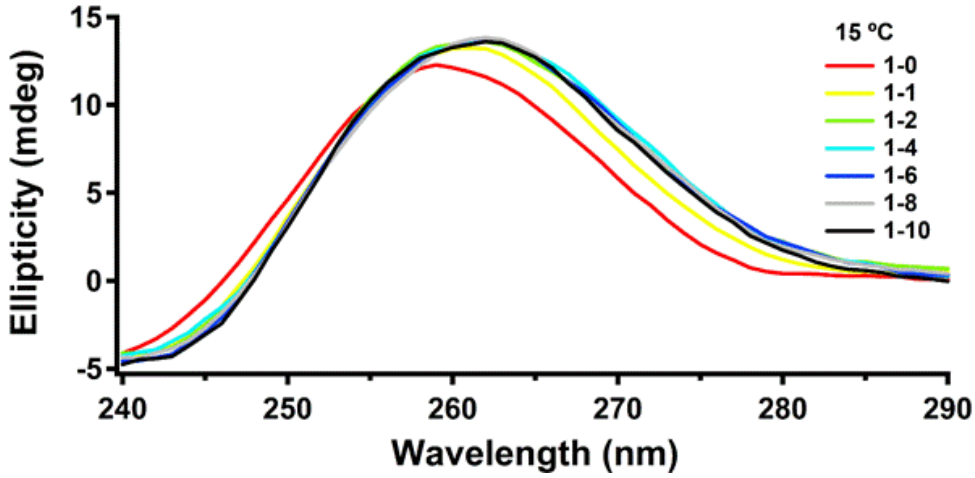

Figure 3.16. CD spectra of different c:MYC:Azamethyl samples with varying concentrations at 15°C between 240-400 nm (A). Concentration of c-MYC and Azamethyl is the multiples of 9 µM and 3 µM, respectively, in given ratios.

c-MYC sample by itself (1:0) has the maximum ellipticity at 259 nm with an intensity of 12.28 mdeg. The wavelength of maximum ellipticity is shifted slightly

to 261 nm (2 nm shift) in 1:1 sample with an increase in intensity to 13.23 mdeg. The wavelength of maximum ellipticity is shifted further to 262 nm in the samples with increasing Azamethyl concentrations. The highest intensity also increased slightly up to 13.82 mdeg.

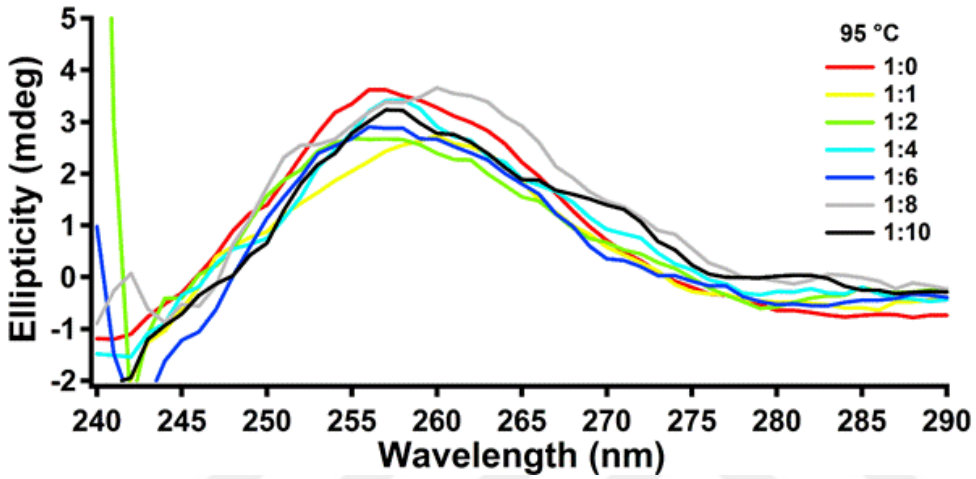

Figure 3.17. CD spectra of different c:MYC:Azamethyl samples with varying concentrations at 95°C between 240-400 nm (A) and blown-up image of the spectra in A in the range of 245-280 nm. Concentration of c-MYC and Azamethyl is the multiples of 9 µM and 3 µM, respectively, in given ratios.

At 95°C, where the G4 structures are thermally denatured, the ellipticity value at around 256 nm is decreased. The intensities for all the samples in that wavelength are close to each other, around 3.6 mdeg. Thermal denaturation profiles between 5°C and 95°C were obtained by plotting the change in ellipticity at 260 nm with varying temperatures (Figure 3.20). During thermal denaturation experiments, the ellipticity at 260 nm was decreased. For instance, in the c-MYC sample in the absence of Azamethyl, it dropped from 12.28 mdeg at 15°C to 3.61 mdeg at 95°C (Appendix H). For the 1:10 c-Myc:Azamethyl sample, the ellipticity decreased from 10.38 mdeg to 4 mdeg. The melting profiles were normalized for better comparison, and the T_m of samples were determined from the first derivative of the melting profiles (Table

3.9). As depicted, c-MYC G4 was stabilized by Azamethyl, where the T_m is increased from 60°C to 80°C in the presence of 10 fold Azamethyl.

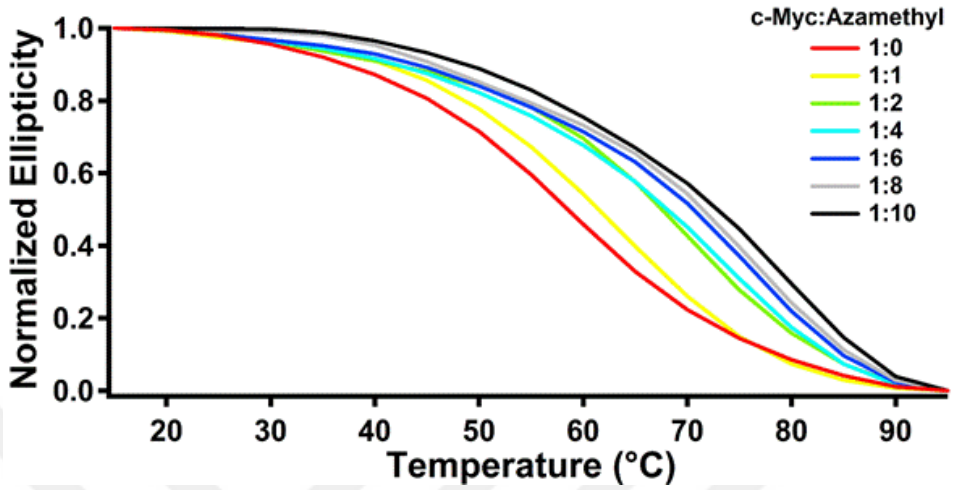

Figure 3.18. Thermal denaturation profiles of c-MYC in the presence of varying Azamethyl concentrations between 15°C and 95°C. Concentration of c-MYC and Azamethyl is the multiples of 9 µM and 3 µM, respectively, in given ratios.

The temperature range was chosen with 5°C steps during CD thermal denaturation experiments, and the melting temperature of c-MYC was calculated by differentiated melting profiles of differing c-MYC:Azamethyl samples in that range. At the peak of differentiated ellipticity, half of the DNA is counted as melted, which gives us T_m after all. These results are tabulated in Table 3.9 to demonstrate the melting pattern of c-MYC with increasing Azamethyl concentration in solution.

Table 3.9 Thermal denaturation temperatures obtained through the differentiation of the thermal denaturation curves given in Figure 3.20. Concentration of c-MYC and Azamethyl is the multiples of 9 µM and 3 µM, respectively, in given ratios.

c-MYC:Azamethyl Ratio	**1:0**	**1:1**	**1:2**	**1:4**	**1:6**	**1:8**	**1:10**
T_m (°C)	60.0	65.0	70.0	75.0	75.0	75.0	80.0

As a result of CD thermal denaturation measurements, the melting temperature of c-MYC was observed to be shifted by around 20°C.

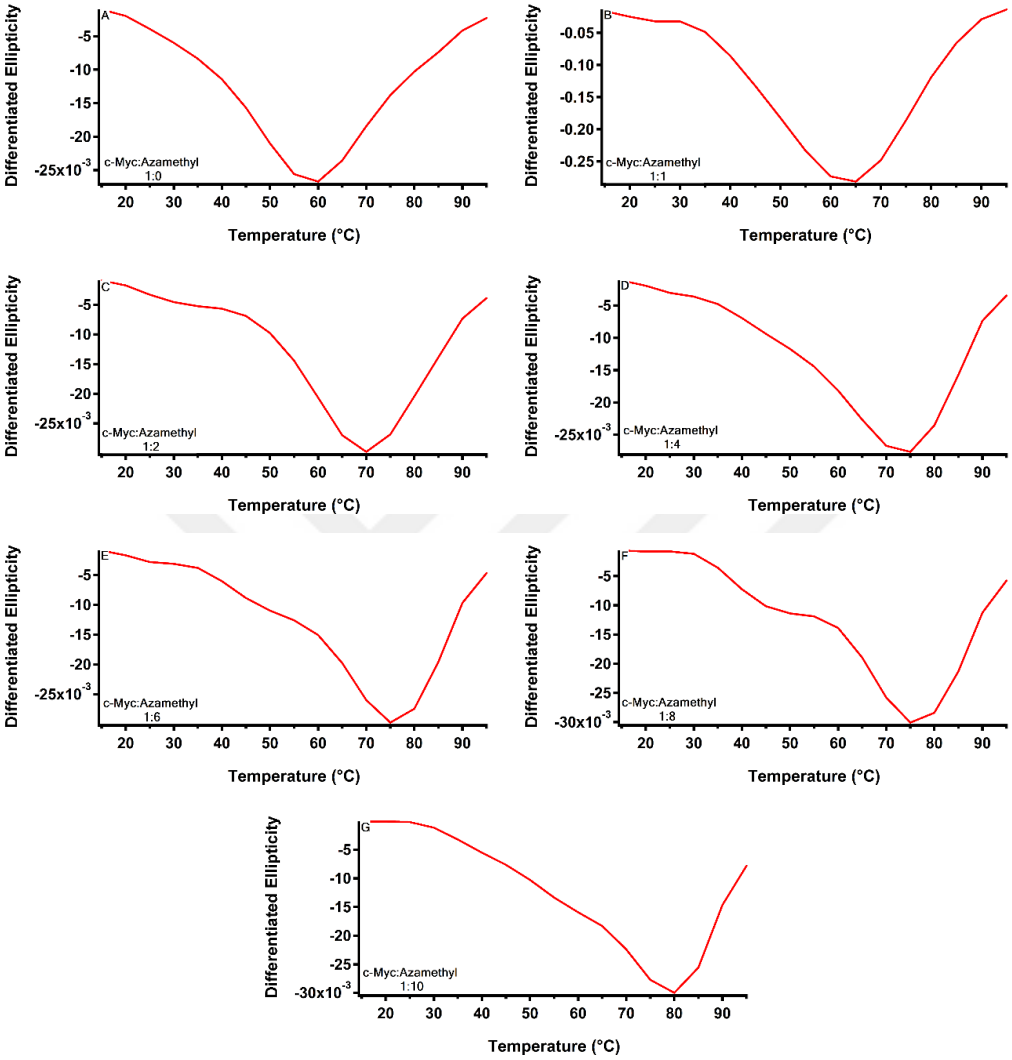

Figure 3.19. First derivative of thermal denaturation profiles of c-MYC, in the presence of differing Azamethyl concentrations, used in the calculation of the melting temperatures. Concentration of c-MYC and Azamethyl is the multiples of 9 µM and 3 µM, respectively, in given ratios.

3.4 Determination of Association Constant for c-MYC:Azamethyl

Finally, in order to determine the binding constant, titration experiments were performed where Azamethyl was titrated with c-MYC:Azamethyl solution. The association constant was calculated by plotting integrated fluorescence intensity as a function of Quadruplex DNA concentration by Igor Pro software (Wavemetrics Inc, USA). The association constant of c-MYC:Azamethyl was determined as $2.9 \times 10^5 \pm 1.4 \times 10^4$ $M^{-1,}$ which is the mean of three independent measurements, represented in Figure 3.21.

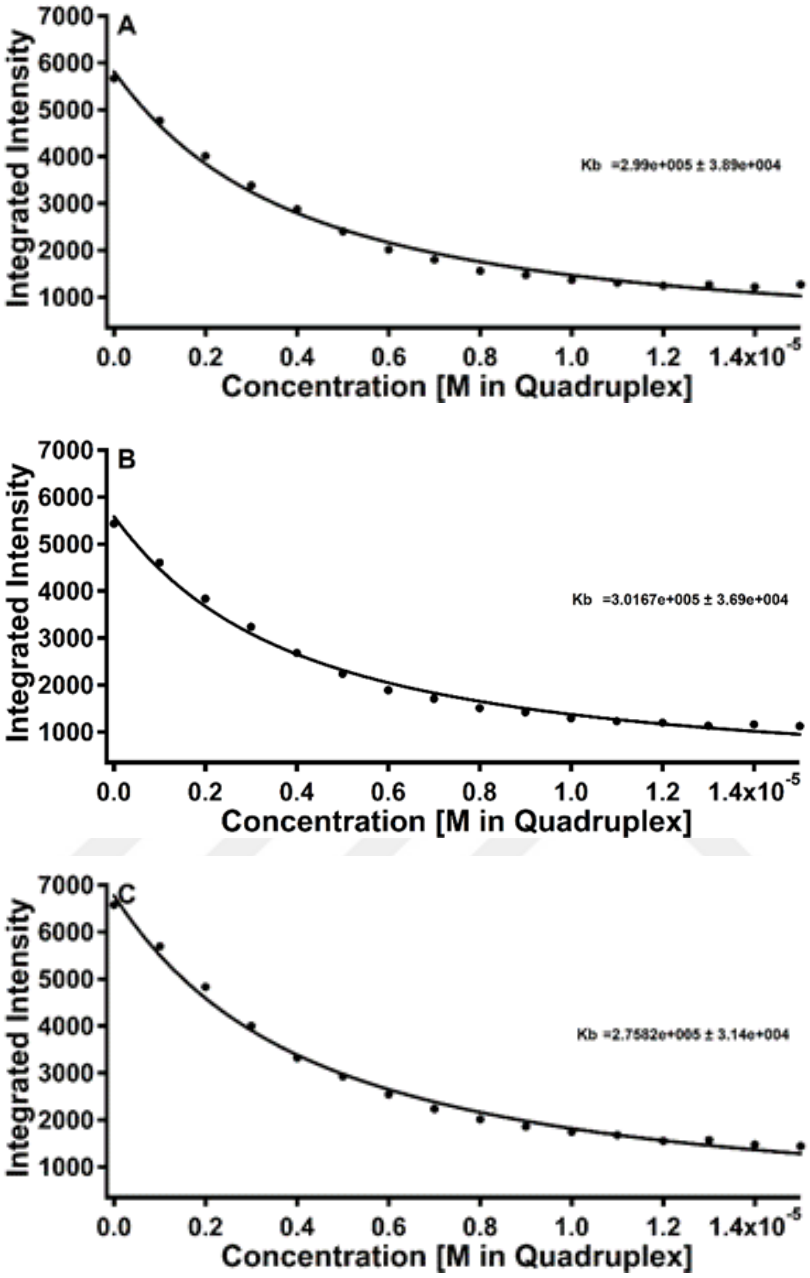

Figure 3.20. Integrated fluorescence intensity plotted against G4 concentration obtained from three independent titration experiments (Appendix E).

3.5 Discussions

3.5.1 Selectivity of Azacyanines Against Different Promoter Regions

Here, the affinity and selectivity of 5 Azacyanine derivatives towards different nucleic acid sequences were first determined via competition dialysis experiments. C-MYC, BCL-2, VEGF, KRAS, HER-2, and RB sequences used in the competition dialysis are the promoter regions of proto-oncogene sequences with G-quadruplex structures. 5'-$T_2G_{20}T_2$-3' and H. Telomere sequences were also used as G-quadruplex forming sequences. As high GC content genomic DNA and non G4 forming control groups, genomic DNA of *M.lyso*, ds polyd(A).polyd(T), and ss polyd(A) were used.

Along with Azacyanine derivatives, a known intercalator and anti-neoplastic agent, Doxorubicin, was also evaluated for its ability to bind to the selected G4 forming sequences as a small molecule control. It is known that Doxorubicin can intercalate both AT-rich and GC-rich double-stranded sequences without known sequence tendency (Airoldi et al., 2014; Thorn et al., 2011). As we expected, it exhibited non-selective binding toward double stranded GC-rich sequences (*M. lyso*) and polyd(A).polyd(T). It did also show relatively high affinity towards G4 sequences.

On the other hand, the competition dialysis experiments revealed that the Azacyanines generally had a high affinity and selectivity towards G4 forming sequences. Among all the sequences, they especially preferred binding to the c-MYC promoter sequence as denoted by high C_b/C_f values. Besides that, affinities of Azacyanines toward BCL-2, VEGF, and KRAS were also higher than the remaining sequences. They showed almost no or very low binding to genomic DNA of *M.lyso*, polyd(A).polyd(T), and polyd(A).

Azamethyl, Azabutyl, and Azaisobutyl were chosen as benzimidazole derivatives used in our assay. Our results revealed that the changes in the alkyl chain of the benzimidazole results in changes in affinity and selectivity of these molecules towards different nucleic acid structures. Azamethyl with the shorter alkyl chain had

a relatively higher affinity towards all G4 sequences. Azabutyl, a longer alkyl chain, was more selective. Its affinity to c-MYC was more than two-fold compared to the KRAS, which has the second-highest C_b/C_f value. Previous studies showed that a longer and flexible alkyl chain on the benzimidazole ring could increase non-covalent interactions during intercalation and stacking with G4 structures (Küçükakdağ Doğu, 2019). However, we have seen that it can also disrupt affinity in different G-quadruplex sequences. Azabutyl showed higher affinity towards only two of the G4 forming sequences than Azamethyl. Azaisobutyl displayed a very low affinity towards G4 structures compared to Azamethyl or Azabutyl. According to the results shown, Azamethyl generally has a higher tendency to stabilize G4 forming sequences among three of them. Although Azaisobutyl and Azabutyl have the same length in the alkyl chain on the benzimidazole ring, the branching and thus the bulkier chain in the benzimidazole ring is thought to be decreasing the non-covalent stacking interactions of the Azacyanines with G4s. Yet, it seemed also to be more selective.

Benzothiazole derivatives Aza4 and Aza5 also showed promising affinities toward the c-MYC promoter sequence. However, according to our observations during our laboratory investigations, their structure quickly breaks down with temperature and light. Therefore, they might not be suitable drug candidates.

Overall, all the Azacyanines were found to be binding to G4 structures, especially the c-MYC G4 sequence. Their large surface area plausibly favors their stacking on G4 tetrads, resulting in relatively high selectivity towards G4 structures. On the other hand, their larger surface area compared to prevents their intercalation in between the bases of the double helical DNA structure, resulting in a very low binding affinity towards double helical structures (Persil Çetinkol & Hud, 2009). Yet, both the small molecule structure and the G4 structure and sequence is found to be a determinant in G4-small molecule interactions.

Consequently, Azamethyl, mainly due to its high affinity and stability, was chosen as the small molecule to further investigate its interactions with the c-MYC G4 sequence.

3.5.2 Spectrochemical Analysis of c-MYC:Azamethyl Interactions

The interactions of Azamethyl with the c-MYC G4 sequence were further investigated with UV-Vis, CD, and Fluorescence spectroscopy.

Studies of Persil Çetinkol and coworkers revealed red shift and hypochromic effect between 305-360 nm of Azamethyl's absorbance in UV-Vis spectrometric studies upon Azamethyl binding to 24 bp human G4 forming telomeric sequence (Persil Çetinkol et al., 2008). These UV-Vis spectral changes are generally verified as intercalative mode of binding or stacking in NMR studies (Hernández-Luis et al., 2010). In the scope of this thesis, we showed Azamethyl has higher affinity and selectivity toward the c-MYC G4 sequence than the human telomeric G4 sequence (22 bp) by competition dialysis experiments. The binding was apparent in changes of the UV-Vis absorbance of Azamethyl upon binding to G4 of c-MYC. However, we were not able to detect stabilization of G4 from UV-Vis thermal denaturation studies (Appendix G) (Figure 3.15 A). To be able to see the stabilization effect of Azamethyl on c-MYC G4 structure, Circular Dichroism measurements were performed

Both UV-Vis and CD studies revealed the binding of Azamethyl to c-MYC G4. CD spectra of c-MYC in the presence of Azamethyl showed that the binding of Azamethyl was not altering the DNA structure. Only a slight shift in the maximum absorption wavelength and intensity change was observed upon Azamethyl binding to c-MYC from CD studies. In the presence and the absence of c-MYC, Azamethyl fluorescence intensities were shifted upon interaction (Figure 3.15). Thermal denaturation experiments revealed the stabilization of c-MYC in the presence of

Azamethyl. T_m of c-MYC was increased up to 20^oC with increasing Azamethyl concentration.

Our studies have proceeded with determining the association constant of Azamethyl with the c-MYC sequence. The gradual addition of 400.0 µM c-MYC: 1.0 µM Azamethyl onto 1.0 µM Azamethyl solution induces a decline in small molecule fluorescence intensity due to interactions with the c-MYC sequence. The fluorescence titrations revealed an association constant of c-MYC:Azamethyl as 2.9 x 10^5 ±1.4 x 10^4 M^{-1} as a mean of three independent experiments (Figure 3. 22). Compared to the other G4 binders, Azamethyl gave promising binding affinity toward c-MYC promoter sequence. Association constant of c-MYC:Azamethyl is in the association constant range of well-known G4 binder, TMPyP4, which is between 10^4 and 10^6 M^{-1} (Mita et al., 2006).

CHAPTER 4

THESIS CONCLUSION

In the scope of this thesis, interactions between Azacyanines and G-quadruplex bearing sequences were investigated, followed by understanding c-MYC:Azamethyl interactions. Firstly, the binding tendencies of Azacyanine derivatives towards different G4 forming sequences were investigated through the competition dialysis method. From previous studies, it has been already known that Azamethyl interacts with multiple DNA secondary structures and topologies; triple helical structures, homoadenine sequences, and G4 forming human telomeric sequences (Çetinkol & Hud, 2009; Küçükakdağ Doğu, 2019; Tütüncü, 2020). Here, G-quadruplex bearing proto-oncogene sequences were dialyzed against five Azacyanine derivatives and Doxorubicin to compare sequence affinity and selectivity. Doxorubicin was used as a control drug, a chemotherapeutic anthracycline agent with known high cytotoxic side effects due to high DNA binding capacity (Tacar et al., 2013). Among all G4 forming sequences, all Azacyanine derivatives showed the highest selectivity toward the c-MYC promoter sequence. Although Aza5 has more affinity than any other Azacyanine derivative with C_b/C_f value of 11.92, its unstable nature does not allow it to be a suitable small molecule agent for future studies. On the contrary, benzimidazole derivative Azamethyl has both stable nature and following highest affinity toward c-MYC with C_b/C_f value of 10.09. It has also higher affinity to c-MYC and more specific in general than Doxorubicin. To this respect, c-MYC:Azamethyl interactions were further investigated via spectrophotometric methods in the scope of the thesis.

Secondly, spectroscopic analysis via Fluorescence, UV-Vis, and CD clearly demonstrated the interactions of Azamethyl with c-MYC G4. Thermal denaturation experiments were mediated to understand the association of c-MYC:Azamethyl. Even though stabilizing effect of Azamethyl was not detected using UV-Vis

spectroscopy, thermal denaturation profiles obtained via CD showed the stabilization of c-MYC G4 in the presence of Azamethyl. In the CD spectrum of c-MYC, an apparent positive peak at 260 nm and a negative peak at 240 nm indicate parallel G4 structure formation. Besides, the ellipticity of G4 was decreased from 12-14 mdeg to 2-4 mdeg upon melting at 95°C due to the denaturation of the G4 structure as expected. The thermal denaturation temperature of c-MYC was obtained as 60°C in the absence of Azametyhl. T_m was shifted up 20°C upon 10 fold Azamethyl addition. Despite all, promoter sequence has multiple equilibrated G-quadruplex topologies under physiological conditions, and it is not known which topologies might be stabilized by Azamethyl under physiological conditions.

In agreement with thermal denaturation results, the association constant was determined to be $2.9 \times 10^5 \pm 1.4 \times 10^4\ M^{-1}$ via Fluorescence spectroscopy.

Ultimately, the design of sequence specific cancer agents is gaining attention to reduce high toxicity in recent targeting approaches of cancer. Azacyanines are potential therapeutic agents with large surface area for stacking, relatively small size, and molecular weight. They display a very weak binding affinity to genomic DNA, which results in nontoxic behavior. Within this thesis, it has been shown that the benzimidazole derivative Azamethyl shows selective binding to the c-MYC gene sequence, which has critical regulatory activities which are disrupted in almost half of cancer types. Therefore, targeting the c-MYC promoter sequence via Azacyanines can be used as a possible approach in the future. An Azacyanine molecule with such selectivity but with a higher affinity will be a better candidate. For the sequence chosen here, CD studies indicated the parallel G4 formation under these conditions. However, c-MYC G4 has been shown to adopt different G4 conformations based on environmental conditions. It might be helpful also to evaluate the interactions of Azamethyl with these conformations. In addition, the mode of binding of Azamethyl to the c-MYC promoter sequence is still not resolved. In order to reveal the exact mode of binding, the changes in the folding pattern of the G4 sequence and G4:Azacyanine interactions in detail. X-ray diffraction analysis and NMR studies will be required in the future.

REFERENCES

Adjei, A. A. (2001). Blocking Oncogenic Ras Signaling for Cancer Therapy. *JNCI: Journal of the National Cancer Institute*, *93*(14), 1062–1074. https://doi.org/10.1093/JNCI/93.14.1062

Airoldi, M., Barone, G., Gennaro, G., Giuliani, A. M., & Giustini, M. (2014). Interaction of doxorubicin with polynucleotides. a spectroscopic study. *Biochemistry*, *53*(13), 2197–2207. https://doi.org/10.1021/bi401687v

Andersson, R., & Sandelin, A. (2020). Determinants of enhancer and promoter activities of regulatory elements. *Nature Reviews Genetics*. Nature Publishing Group. https://doi.org/10.1038/s41576-019-0173-8

Avery, O. T., Macleod, C. M., & McCarty, M. (1944). Studies on the chemical nature of the substance inducing transformation of Pneumococcal types : Induction of transformation by a desoxyribonucleic acid fraction isolated from Pneumococcus Type III. *The Journal of Experimental Medicine*, *79*(2), 137–158. https://doi.org/10.1084/jem.79.2.137

Bacolla, A., & Wells, R. D. (2004). Non-B DNA Conformations, Genomic Rearrangements, and Human Disease. *Journal of Biological Chemistry*, *279*(46), 47411–47414. https://doi.org/10.1074/JBC.R400028200

Bang, I. (1910). Untersuchungen über die Guanylsäure. *Biochemische Zeitschrift*, *26*, 293–311.

Biffi, G., Tannahill, D., McCafferty, J., & Balasubramanian, S. (2013). Quantitative visualization of DNA G-quadruplex structures in human cells. *Nature Chemistry*, *5*(3), 182–186. https://doi.org/10.1038/nchem.1548

Biffi, G., Tannahill, D., Miller, J., Howat, W. J., & Balasubramanian, S. (2014). Elevated levels of G-quadruplex formation in human stomach and liver cancer tissues. *PLoS ONE*, *9*(7), e102711.

https://doi.org/10.1371/journal.pone.0102711

Blackburn, E. H. (1990). Telomeres: Structure and synthesis. *Journal of Biological Chemistry*. 5919-5921. https://doi.org/10.1016/s0021-9258(19)39264-6

Bourtayre, P., Liquier, J., Pizzomi, L., & Taillandier, E. (1987). Z form of poly d(A-t) o poly d(a-t) in solution studied by cd and uv spectroscopies. *Journal of Biomolecular Structure and Dynamics*, *5*(1), 097–104. https://doi.org/10.1080/07391102.1987.10506378

Brooks, T. A., Kendrick, S., & Hurley, L. (2010). Making sense of G-quadruplex and i-motif functions in oncogene promoters. The *FEBS Journal*. *277*(17), 3459–3469. https://doi.org/10.1111/j.1742-4658.2010.07759.x

Brown, R. V., Danford, F. L., Gokhale, V., Hurley, L. H., & Brooks, T. A. (2011). Demonstration that drug-targeted down-regulation of MYC in non-Hodgkins lymphoma is directly mediated through the promoter G-quadruplex. *Journal of Biological Chemistry*, *286*(47), 41018–41027. https://doi.org/10.1074/jbc.M111.274720

Burge, S., Parkinson, G. N., Hazel, P., Todd, A. K., & Neidle, S. (2006). Quadruplex DNA: sequence, topology and structure. *Nucleic Acids Research*, *34*(19), 5402–5415. https://doi.org/10.1093/nar/gkl655

Casamassimi, A., & Ciccodicola, A. (2019). Transcriptional regulation: Molecules, involved mechanisms, and misregulation. *International Journal of Molecular Sciences*. *20*(6), 1281. https://doi.org/10.3390/ijms20061281

Chaires, J. B., Dattagupta, N., & Crothers, D. M. (1982). Studies on Interaction of Anthracycline Antibiotics and Deoxyribonucleic Acid: Equilibrium Binding Studies on Interaction of Daunomycin with Deoxyribonucleic Acid. *Biochemistry*, *21*(17), 3933–3940. https://doi.org/10.1021/bi00260a005

Chen, Y., & Yang, D. (2012). Sequence, stability, and structure of G-Quadruplexes and their interactions with drugs. *Current Protocols in Nucleic Acid Chemistry*,

50(1), 17-5. https://doi.org/10.1002/0471142700.nc1705s50

Cogoi, S., & Xodo, L. E. (2006). G-quadruplex formation within the promoter of the KRAS proto-oncogene and its effect on transcription. *Nucleic Acids Research*, *34*(9), 2536–2549. https://doi.org/10.1093/nar/gkl286

Craig, L. C., & King, T. P. (1962). Dialysis. In *Methods of biochemical analysis* (Vol. 10, pp. 175–199). https://doi.org/10.1002/9780470110270.ch6

Cui, X., Chen, H., Zhang, Q., Xu, M., Yuan, G., & Zhou, J. (2019). Exploration of the Structure and Recognition of a G-quadruplex in the her2 Proto-oncogene Promoter and Its Transcriptional Regulation. *Scientific Reports*, *9*(1), 1–12. https://doi.org/10.1038/s41598-019-39941-5

Dang, C. V., Le, A., & Gao, P. (2009). MYC-induced cancer cell energy metabolism and therapeutic opportunities. *Clinical Cancer Research*, *15*(21), 6479–6483. https://doi.org/10.1158/1078-0432.CCR-09-0889

De Cian, A., Lacroix, L., Douarre, C., Temime-Smaali, N., Trentesaux, C., Riou, J. F., & Mergny, J. L. (2008). Targeting telomeres and telomerase. *Biochimie*, *90*(1), 131–155. https://doi.org/10.1016/j.biochi.2007.07.011

De, S., & Michor, F. (2011). DNA secondary structures and epigenetic determinants of cancer genome evolution. *Nature Structural and Molecular Biology*, *18*(8), 950–955. https://doi.org/10.1186/gb-2010-11-s1-p10

Dexheimer, T. S., Sun, D., & Hurley, L. H. (2006). Deconvoluting the structural and drug-recognition complexity of the G-quadruplex-forming region upstream of the bcl-2 P1 promoter. *Journal of the American Chemical Society*, *128*(16), 5404–5415. https://doi.org/10.1021/ja0563861

Dhamodharan, V., & Pradeepkumar, P. I. (2019). Specific Recognition of Promoter G-Quadruplex DNAs by Small Molecule Ligands and Light-up Probes. *ACS Chemical Biology*, *14*(10), 2102–2114. https://doi.org/10.1021/acschembio.9b00475

Gellert, M., Lipsett, M. N., & Davies, D. R. (1962). Helix formation by guanylic acid. *Proceedings of the National Academy of Sciences of the United States of America*, *48*(12), 2013–2018. https://doi.org/10.1073/pnas.48.12.2013

Ghosh, A., & Bansal, M. (2003). A glossary of DNA structures from A to Z. *Acta Crystallographica Section D:Biological Crystallography*, *59*(4), 620–626. https://doi.org/10.1107/S0907444903003251

Gray, L. T., Vallur, A. C., Eddy, J., & Maizels, N. (2014). G quadruplexes are genomewide targets of transcriptional helicases XPB and XPD. *Nature Chemical Biology*, *10*(4), 313–318. https://doi.org/10.1038/nchembio.1475

Guloglu, S. (2018). *Insights into The Action Mechanism Of Azacyanines: Their Topoisomerase IIα Inhibition Potential and Nucleic Acid Selectivity*.. Middle East Technical University.

Haddadin, M. J., Kurth, M. J., & Olmstead, M. M. (2000). One-step synthesis of new heterocyclic azacyanines. *Tetrahedron Letters*, *41*(30), 5613–5616. https://doi.org/10.1016/S0040-4039(00)00908-4

Hanahan, D., & Weinberg, R. A. (2011). Hallmarks of cancer: The next generation. *Cell*, *144*(5), 646–674. https://doi.org/10.1016/j.cell.2011.02.013

Hardin, C. C., Watson, T., Corregan, M., & Bailey, C. (2002). Cation-dependent transition between the quadruplex and Watson-Crick hairpin forms of d(CGCG3GCG). *Biochemistry*, *31*(3), 833–841. https://doi.org/10.1021/BI00118A028

Henderson, E., Hardin, C. C., Walk, S. K., Tinoco, I., & Blackburn, E. H. (1987). Telomeric DNA oligonucleotides form novel intramolecular structures containing guanine·guanine base pairs. *Cell*, *51*(6), 899–908. https://doi.org/10.1016/0092-8674(87)90577-0

Herbert, A. (2019). Z-DNA and Z-RNA in human disease. *Communications Biology*, *2*(1), 1–10. https://doi.org/10.1038/s42003-018-0237-x

Hernández-Luis, F., Hernández-Campos, A., Castillo, R., Navarrete-Vázquez, G., Soria-Arteche, O., Hernández-Hernández, M., & Yépez-Mulia, L. (2010). Synthesis and biological activity of 2-(trifluoromethyl)-1H-benzimidazole derivatives against some protozoa and Trichinella spiralis. *European Journal of Medicinal Chemistry*, *45*(7), 3135–3141. https://doi.org/10.1016/J.EJMECH.2010.03.050

Hershey, A. D., & Chase, M. (1951). Genetic recombination and heterozygosis in bacteriophage. *Cold Spring Harbor Symposia on Quantitative Biology*, *16*, 471–479. https://doi.org/10.1101/SQB.1951.016.01.034

Hoogsteen, K. (1959). The structure of crystals containing a hydrogen-bonded complex of 1-methylthymine and 9-methyladenine. *Acta Crystallographica*, *12*(10), 822–823. https://doi.org/10.1107/s0365110x59002389

Hoogsteen, K. (1963). The crystal and molecular structure of a hydrogen-bonded complex between 1-methylthymine and 9-methyladenine. *Acta Crystallographica*, *16*(9), 907–916. https://doi.org/10.1107/s0365110x63002437

Huang, K. S., Haddadin, M. J., Olmstead, M. M., & Kurth, M. J. (2001). Synthesis and reactions of some heterocyclic azacyanines. *Journal of Organic Chemistry*, *66*(4), 1310–1315. https://doi.org/10.1021/jo001484k

Huppert, J. L., & Balasubramanian, S. (2005). Prevalence of quadruplexes in the human genome. *Nucleic Acids Research*, *33*(9), 2908–2916. https://doi.org/10.1093/nar/gki609

Ivanov, V. I., & Krylov, D. Y. (1992). [6] A-DNA in solution as studied by diverse approaches. *Methods in Enzymology*, *211*, 111–127. https://doi.org/10.1016/0076-6879(92)11008-7

Jain, A. K., & Bhattacharya, S. (2010). Groove Binding Ligands for the Interaction with Parallel-Stranded ps-Duplex DNA and Triplex DNA. *Bioconjugate Chemistry*, *21*(8), 1389–1403. https://doi.org/10.1021/BC900247S

Katapadi, V. K., Nambiar, M., & Raghavan, S. C. (2012). Potential G-quadruplex formation at breakpoint regions of chromosomal translocations in cancer may explain their fragility. *Genomics*, *100*(2), 72–80. https://doi.org/10.1016/j.ygeno.2012.05.008

Kaulage, M. H., Maji, B., Pasadi, S., Ali, A., Bhattacharya, S., & Muniyappa, K. (2018). Targeting G-quadruplex DNA structures in the telomere and oncogene promoter regions by benzimidazole–carbazole ligands. *European Journal of Medicinal Chemistry*, *148*, 178–194. https://doi.org/10.1016/j.ejmech.2018.01.091

King, J. J., Irving, K. L., Evans, C. W., Chikhale, R. V., Becker, R., Morris, C. J., … Smith, N. M. (2020). DNA G-Quadruplex and i-Motif Structure Formation Is Interdependent in Human Cells. *Journal of the American Chemical Society*, *142*(49), 20600–20604. https://doi.org/ 10.1021/jacs.0c11708

König, S. L. B., Evans, A. C., & Huppert, J. L. (2010). Seven essential questions on G-quadruplexes. *Biomolecular Concepts*, *1*(2), 197–213. https://doi.org/10.1515/BMC.2010.011

Küçükakdağ Doğu, A. (2019). *Targeting Human Telomeric DNA with Azacyanines*. Midddle East Technical University.

Küçükakdağ Doğu, A., & Persil Çetinkol, Ö. (2019). Targeting human telomeric DNA with azacyanines. *Turkish Journal of Chemistry*, *43*(4), 1040–1051. https://doi.org/10.3906/kim-1903-6

Kypr, J., Kejnovská, I., Renčiuk, D., & Vorlíčková, M. (2009). Circular dichroism and conformational polymorphism of DNA. *Nucleic Acids Research*, *37*(6), 1713. https://doi.org/10.1093/nar/gkp026

Le, H. T., Miller, M. C., Buscaglia, R., Dean, W. L., Holt, P. A., Chaires, J. B., & Trent, J. O. (2012). Not all G-quadruplexes are created equally: An investigation of the structural polymorphism of the c-Myc G-quadruplex-forming sequence and its interaction with the porphyrin TMPyP4. *Organic and*

Biomolecular Chemistry, *10*(47), 9393–9404. https://doi.org/10.1039/c2ob26504d

Maizels, N., & Gray, L. T. (2013). The G4 Genome. *PLoS Genetics*, *9*(4), e1003468. https://doi.org/10.1371/journal.pgen.1003468

Maji, B., Kumar, K., Kaulage, M., Muniyappa, K., & Bhattacharya, S. (2014). Design and synthesis of new benzimidazole-carbazole conjugates for the stabilization of human telomeric DNA, telomerase inhibition, and their selective action on cancer cells. *Journal of Medicinal Chemistry*, *57*(16), 6973–6988. https://doi.org/10.1021/jm500427n

Mergny, J. L., Phan, A. T., & Lacroix, L. (1998). Following G-quartet formation by UV-spectroscopy. The *FEBS Letters*, *435*(1), 74–78. https://doi.org/10.1016/S0014-5793(98)01043-6

Mergny, J. L., Riou, J. F., Mailliet, P., Teulade-Fichou, M. P., & Gilson, E. (2002). Natural and pharmacological regulation of telomerase. *Nucleic Acids Research*. Nucleic Acids Res, *30*(4), 839–865. https://doi.org/10.1093/nar/30.4.839

Miller, D. M., Thomas, S. D., Islam, A., Muench, D., & Sedoris, K. (2012). c-Myc and cancer metabolism. *Clinical Cancer Research*, *18*(20), 5546–5553. https://doi.org/10.1158/1078-0432.CCR-12-0977

Minyat, E. E., Khomyakova, E. B., Petrova, M. V., Zdobnov, E. M., & Ivanov, V. I. (1995). Experimental evidence for slipped loop dna, a novel folding type for polynucleotide chain. *Journal of Biomolecular Structure and Dynamics*, *13*(3), 523–527. https://doi.org/10.1080/07391102.1995.10508862

Mita, H., Ohyama, T., Tanaka, Y., & Yamamoto, Y. (2006). Formation of a complex of 5, 10, 15, 20-tetrakis (N-methylpyridinium-4-yl)-21 H, 23 H-porphyrin with G-quadruplex DNA. Biochemistry, 45(22), 6765-6772. https://doi.org/10.1021/bi052442z

Murat, P., & Balasubramanian, S. (2014). Existence and consequences of G-

quadruplex structures in DNA. *Current Opinion in Genetics and Development*, *25*, 22–29. https://doi.org/10.1016/j.gde.2013.10.012

Nevins, J. R. (2001). The Rb/E2F pathway and cancer. *Human Molecular Genetics*, *10*(7), 699–703. https://doi.org/10.1093/hmg/10.7.699

Persil Çetinkol, Ö. (2008). *Small Molecule Recognition of Homopurine Nucleic Acid Structures Small Molecule Recognition of Homopurine*. Georgia Institute of Technology.

Persil Çetinkol, Ö., Engelhart, A. E., Nanjunda, R. K., Wilson, W. D., & Hud, N. V. (2008). Submicromolar, selective G-quadruplex ligands from one pot: Thermodynamic and structural studies of human telomeric DNA binding by azacyanines. *ChemBioChem*, *9*(12), 1889–1892. https://doi.org/10.1002/cbic.200800234

Persil Çetinkol, Ö., & Hud, N. V. (2009). Molecular recognition of poly(A) by small ligands: An alternative method of analysis reveals nanomolar, cooperative and shape-selective binding. *Nucleic Acids Research*, *37*(2), 611–621. https://doi.org/10.1093/nar/gkn977

Persil Çetinkol, Ö., Santai, C. T., Jain, S. S., & Hud, N. V. (2004). Assembly of an antiparallel homo-adenine DNA duplex by small-molecule binding. *Journal of the American Chemical Society*, *126*(28), 8644–8645. https://doi.org/10.1021/ja0492891

Phan, A. T., Modi, Y. S., & Patel, D. J. (2004). Propeller-type parallel-stranded G-quadruplexes in the human c-myc promoter. *Journal of the American Chemical Society*, *126*(28), 8710–8716. https://doi.org/10.1021/ja048805k

Pirota, V., Nadai, M., Doria, F., & Richter, S. N. (2019). Naphthalene diimides as multimodal G-quadruplex-selective ligands. *Molecules*, *24*(3), 426. https://doi.org/10.3390/molecules24030426

Ragazzon, P. A., Garbett, N. C., & Chaires, J. B. (2007). Competition dialysis: A

method for the study of structural selective nucleic acid binding. *Methods*, *42*(2), 173–182. https://doi.org/10.1016/j.ymeth.2006.09.010

Ragazzon, P.A., & Chaires, J. B. (2007). Use of competition dialysis in the discovery of G-quadruplex selective ligands. *Methods*, *43*(4), 313–323. https://doi.org/10.1016/j.ymeth.2007.08.003

Răsădean, D. M., Harrison, S. W. O., Owens, I. R., Miramont, A., Bromley, F. M., & Dan Pantos, G. (2019). Importance of chiral recognition in designing metal-free ligands for G-quadruplex DNA. *Molecules*, *24*(8), 1473. https://doi.org/10.3390/molecules24081473

Ren, J., & Chaires, J. B. (2001). Rapid screening of structurally selective ligand binding to nucleic acids. *Methods in Enzymology*, *340*, 99–108. https://doi.org/10.1016/S0076-6879(01)40419-8

Ren, J., & Chaires, J. B. (1999). Sequence and structural selectivity of nucleic acid binding ligands. Biochemistry, 38(49), 16067-16075. https://doi.org/10.1021/bi992070s

Rhodes, D., & Lipps, H. J. (2015). G-quadruplexes and their regulatory roles in biology. *Nucleic Acids Research*, *Nucleic Acids Research*, *43*(18), 8627–8637. https://doi.org/10.1093/nar/gkv862

Rich, A. (1982). Right-handed and left-handed DNA: Conformational information in genetic material. *Cold Spring Harbor Symposia on Quantitative Biology*, *47*(1), 1–12. https://doi.org/10.1101/SQB.1983.047.01.003

Safina, A., Cheney, P., Pal, M., Brodsky, L., Ivanov, A., Kirsanov, K., … Gurova, K. (2017). FACT is a sensor of DNA torsional stress in eukaryotic cells. *Nucleic Acids Research*, *45*(4), 1925–1945. https://doi.org/10.1093/nar/gkw1366

Seenisamy, J., Rezler, E. M., Powell, T. J., Tye, D., Gokhale, V., Joshi, C. S., … Hurley, L. H. (2004). The dynamic character of the G-quadruplex element in the c-MYC promoter and modification by TMPyP4. *Journal of the American*

Chemical Society, *126*(28), 8702–8709. https://doi.org/10.1021/ja040022b

Shampay, J., Szostak, J. W., & Blackburn, E. H. (1984). DNA sequences of telomeres maintained in yeast. *Nature*, *310*(5973), 154–157. https://doi.org/10.1038/310154a0

Shay, J. W., & Wright, W. E. (2010, September). Telomeres and telomerase in normal and cancer stem cells. The *FEBS Letters*, *584*(17), 3819–3825. https://doi.org/10.1016/j.febslet.2010.05.026

Shchyolkina, A. K., Borisova, O. F., Livshits, M. A., & Jovin, T. M. (2003). Parallel-Stranded DNA with Natural Base Sequences. *Molecular Biology*, *37*(2), 223–231. https://doi.org/10.1023/A:1023393521207

Siddiqui-Jain, A., Grand, C. L., Bearss, D. J., & Hurley, L. H. (2002). Direct evidence for a G-quadruplex in a promoter region and its targeting with a small molecule to repress c-MYC transcription. *Proceedings of the National Academy of Sciences of the United States of America*, *99*(18), 11593–11598. https://doi.org/10.1073/PNAS.182256799

Sinden, R. R. (1994). DNA Structure and Function. In *DNA Structure and Function* (pp. 1–398). Gulf Professional Publishing. https://doi.org/10.1016/C2009-0-02451-9

Slamon, D. J., Godolphin, W., Jones, L. A., Holt, J. A., Wong, S. G., Keith, D. E., … Press, M. F. (1989). Studies of the HER-2/neu proto-oncogene in human breast and ovarian cancer. *Science*, *244*(4905), 707–712. https://doi.org/10.1126/science.2470152

Sun, D., Guo, K., Rusche, J. J., & Hurley, L. H. (2005). Facilitation of a structural transition in the polypurine/polypyrimidine tract within the proximal promoter region of the human VEGF gene by the presence of potassium and G-quadruplex-interactive agents. *Nucleic Acids Research*, *33*(18), 6070–6080. https://doi.org/10.1093/nar/gki917

Sun, D., & Hurley, L. H. (2009). The importance of negative superhelicity in inducing the formation of G-quadruplex and i-motif structures in the c-Myc promoter: Implications for drug targeting and control of gene expression. *Journal of Medicinal Chemistry*, *52*(9), 2863–2874. https://doi.org/10.1021/jm900055s

Sundquist, W. I., & Klug, A. (1989). Telomeric DNA dimerizes by formation of guanine tetrads between hairpin loops. *Nature*, *342*(6251), 825–829. https://doi.org/10.1038/342825a0

Tacar, O., Sriamornsak, P., & Dass, C. R. (2013). Doxorubicin: An update on anticancer molecular action, toxicity and novel drug delivery systems. *Journal of Pharmacy and Pharmacology*, *65*(2), 157–170. https://doi.org/10.1111/j.2042-7158.2012.01567.x

Thorn, C. F., Oshiro, C., Marsh, S., Hernandez-Boussard, T., McLeod, H., Klein, T. E., & Altman, R. B. (2011). Doxorubicin pathways: Pharmacodynamics and adverse effects. *Pharmacogenetics and Genomics*, *21*(7), 440–446. https://doi.org/10.1097/FPC.0b013e32833ffb56

Todd, A. K., Johnston, M., & Neidle, S. (2005). Highly prevalent putative quadruplex sequence motifs in human DNA. *Nucleic Acids Research*, *33*(9), 2901–2907. https://doi.org/10.1093/nar/gki553

Travers, A., & Muskhelishvili, G. (2015a). DNA structure and function. The *FEBS Journal*, *282*(12), 2279–2295. https://doi.org/10.1111/febs.13307

Tütüncü, S. (2020). *Investigating The Interactions Of Azacyanines With Triplex Nucleic Acids*. Middle East Technical University.

Tütüncü, S., Guloglu, S., Kucukakdag, A., & Persil Çetinkol, Ö. (2018). Selective High Binding Affinity of Azacyanines to polyd(A) polyd(T)·polyd(T) Triplex: The Effect of Chain Length and Branching on Stabilization, Selectivity and Affinity. *ChemistrySelect*, *3*(45), 12878–12887. https://doi.org/10.1002/slct.201802802

Vorlíčková, M., Kejnovská, I., Bednářová, K., Renčiuk, D., & Kypr, J. (2012). Circular dichroism spectroscopy of DNA: From duplexes to quadruplexes. *Chirality*, *24*(9), 691–698. https://doi.org/10.1002/chir.22064

Watson, J.D., Crick, F. H. C. (1953). A structure for deoxyribose nucleic acid. *Nature*, *171*(737–738), 3.

Williamson, J. R., Raghuraman, M. K., & Cech, T. R. (1989). Monovalent cation-induced structure of telomeric DNA: The G-quartet model. *Cell*, *59*(5), 871–880. https://doi.org/10.1016/0092-8674(89)90610-7

Wojtyla, A., Gladych, M., & Rubis, B. (2011). Human telomerase activity regulation. *Molecular Biology Reports*, *38*(5), 3339–3349. https://doi.org/10.1007/s11033-010-0439-x

Wu, Y., & Brosh, R. M. (2010). G-quadruplex nucleic acids and human disease. *The FEBS Journal*, *277*(17), 3470–3488. https://doi.org/10.1111/j.1742-4658.2010.07760.x

Xu, Y., & Sugiyama, H. (2006). Formation of the G-quadruplex and i-motif structures in retinoblastoma susceptibility genes (Rb). *Nucleic Acids Research*, *34*(3), 949–954. https://doi.org/10.1093/nar/gkj485

Yadav, K., Meka, P. N. R., Sadhu, S., Guggilapu, S. D., Kovvuri, J., Kamal, A., … Nagesh, N. (2017). Telomerase Inhibition and Human Telomeric G-Quadruplex DNA Stabilization by a β-Carboline-Benzimidazole Derivative at Low Concentrations. *Biochemistry*, *56*(33), 4392–4404. https://doi.org/10.1021/acs.biochem.7b00008

Yang, D., & Okamoto, K. (2010). Structural insights into G-quadruplexes: Towards new anticancer drugs. *Future Medicinal Chemistry*, *2*(4), 619–646. https://doi.org/10.4155/fmc.09.172

Zeraati, M., Langley, D. B., Schofield, P., Moye, A. L., Rouet, R., Hughes, W. E., … Christ, D. (2018). I-motif DNA structures are formed in the nuclei of human

cells. *Nature Chemistry, 10*(6), 631–637. https://doi.org/10.1038/s41557-018-0046-3

Zhou, J. M., Zhu, X. F., Lu, Y. J., Deng, R., Huang, Z. S., Mei, Y. P., … Zeng, Y. X. (2006). Senescence and telomere shortening induced by novel potent G-quadruplex interactive agents, quindoline derivatives, in human cancer cell lines. Oncogene, 25(4), 503–511. https://doi.org/10.1038/sj.onc.1209067

APPENDICES

A. Micrococcus lysodeikticus (72% GC) Genomic DNA Purification Procedure

1. Put glycogen to room temperature from -20°C.

2. Prepare an ice bowl.

3. Make a mixture of phenol and chloroform (1:1 ratio), where each one is 2000.0 µL.

4. Put ice cubes into the sonicator. The temperature must be 10°C.

5. Make 3.0 mL 70 % ethanol solution (2800.0 µL ethanol and 1200.0 µL H_2O).

6. Take a full spoon of lyophilized *Micrococcus lysodeikticus* (72% GC) to a tube and add 1000.0 µL H_2O. Vortex for at least 10 minutes until it is dissolved.

7. Put it into the sonicator at 10°C and sonicate six times (5 min. sonication 5 min breaks).

8. Divide it into two separate tubes with equal volumes.

9. Before adding phenol-chloroform solution, vortex it.

10. Add freshly prepared phenol-chloroform solution 1:1 (v/v) ratio with the sample.

11. After addition, vortex it shortly.

12. Incubate samples 5 mins at room temperature to wait for phase separation.

13. Centrifuge at 14000 rcf for 5 mins (if there is a problem taking the upper phase, apply it again).

14. Take the upper phase to a new tube and measure its volume.

15. Add 3.0 M NaOAc on to samples at 1:10 (v:v) ratio.

16. Add glycogen as a final concentration of 0.5 mg/ml.

17. Add 1:1 ratio of 100% isopropanol or 100% ethanol.

18. Shortly vortex and shortly centrifuge the samples.

19. Incubate at -20°C for at least 1 hour.

20. Centrifuge samples at 4°C and 14000 rcf for 30 mins.

21. Remove the supernatant and dry pellet for a maximum of 10 mins.

22. Add 1000.0 µL of 70% ethanol to wash pellet for each sample.

23. Centrifuge samples at 4°C and 14000 rcf for 3 mins.

24. Remove the supernatant and dry it max 10 mins.

25. Add 1000.0 µL of 70% ethanol to wash pellet for each sample.

26. Centrifuge at 4°C and 14000 rcf for 3 mins.

27. Remove supernatant and dry entirely for 15min.

28. Put 500.0 µL water into each sample, vortex them, and put into a small centrifuge.

29. Take one of the samples to another tube to mix them.

30. Vortex well and spin down.

31. Store at -20°C.

B. Azacyanine Derivatives

All Azacyanines were synthesized, purified, and characterized in our laboratory by Ayça Küçükakdağ Doğu in accordance with previously published methods (Çetinkol & Hud, 2009; Huang et al., 2001; Küçükakdağ Doğu & Persil Çetinkol, 2019). Names of Azacyanine derivatives are:

Azamethyl: 7H-1,13 dimethyldibenzoimidazolo [1,2-a:2′,1′-d] [1,3,5]- triazin-6-ium

Aza4: 7H-dibenzothiazolo[1,2-a:2′,1′-d] [1,3,5]triazin-6-ium

Aza5: 7H-3,11-dimethoxydibenzothiazolo[1,2-a:2′,1′-d] [1,3,5]-triazin-6-ium

Azabutyl: 7H-1,13 dibutyldibenzoimidazolo [1,2-a:2′,1′-d] [1,3,5]- triazin-6-ium

Azaisobutyl: 7H-1,13 diisobutyldibenzoimidazolo [1,2-a:2′,1′-d] [1,3,5]- triazin-6-ium

Doxorubicin hydrochloride (DOX, C27H30ClNO11, 98.8%) was acquired from Zhejiang Hisun Pharmaceutical CO., LTD (Zhejiang,China).

C. Calibration Curves of Molecules

Calibration Curves of Azamethyl

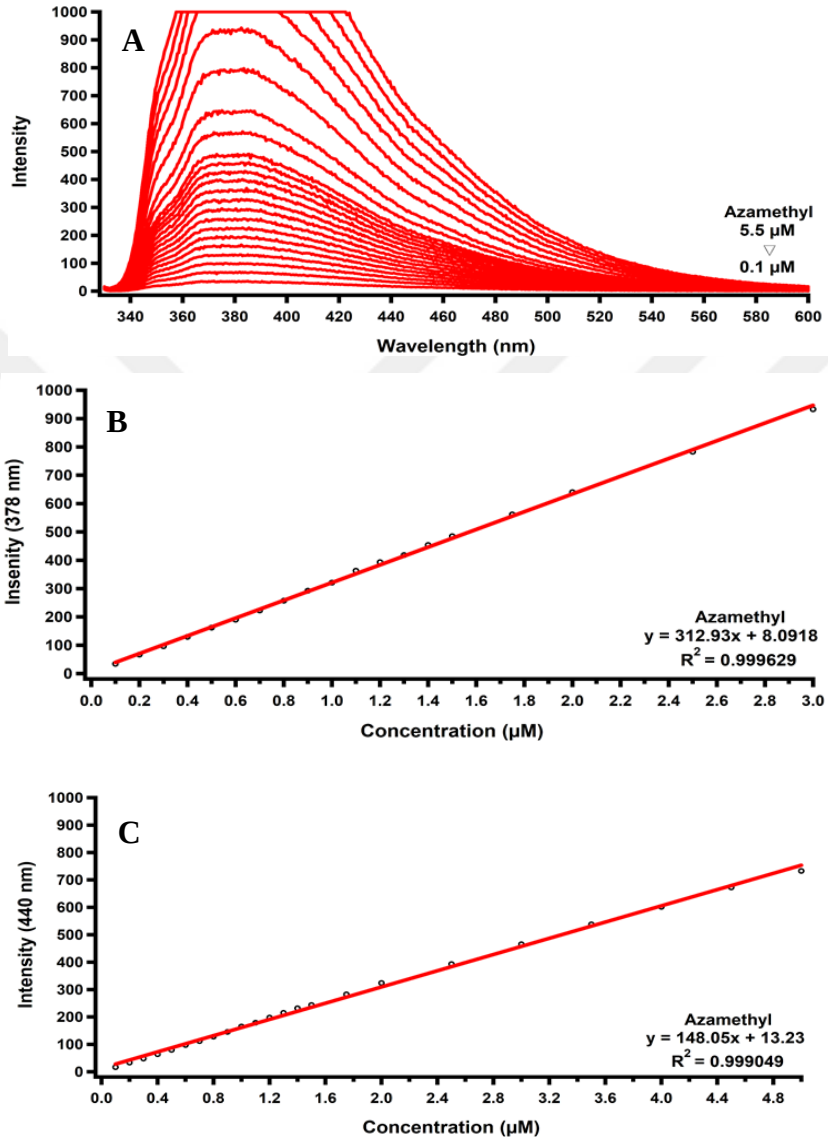

Figure C. 1. Calibration curve construction of Azamethyl. (A) Fluorescence spectra of Azamethyl at varying concentrations between 0.1 µM and 5.5 µM. (B) Calibration curve of Azamethyl obtained from the fluorescence intensity at 378 nm. (C) Calibration curve of Azamethyl obtained from the fluorescence intensity at 440 nm.

Calibration Curves of Aza4

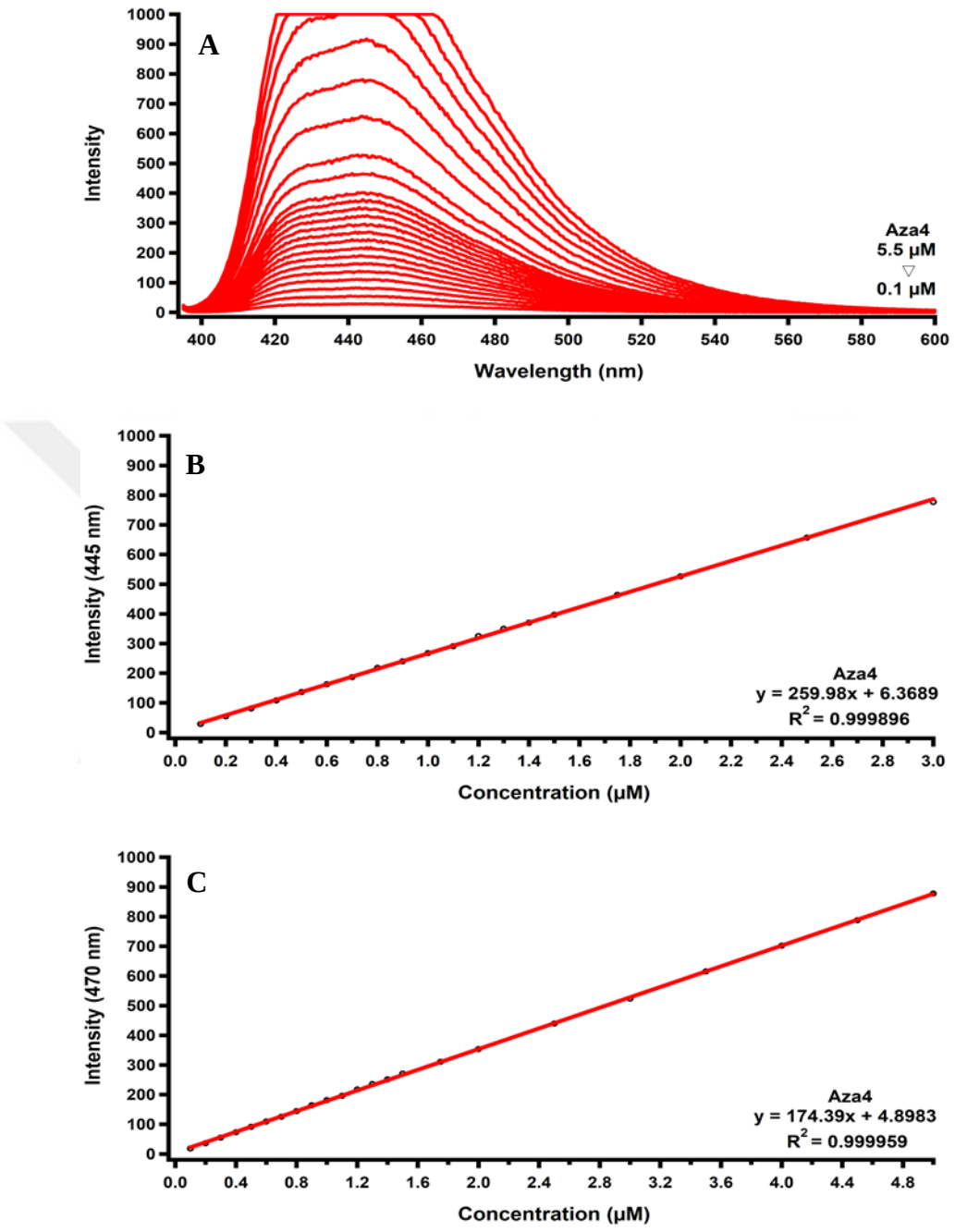

Figure C. 2. Calibration curve construction of Aza4. (A) Fluorescence spectra of Aza4 at varying concentrations between 0.1 µM and 5.5 µM. (B) Calibration curve of Aza4 obtained from the fluorescence intensity at 445 nm. (C) Calibration curve of Aza4 obtained from the fluorescence intensity at 470 nm.

Calibration Curve of Aza5

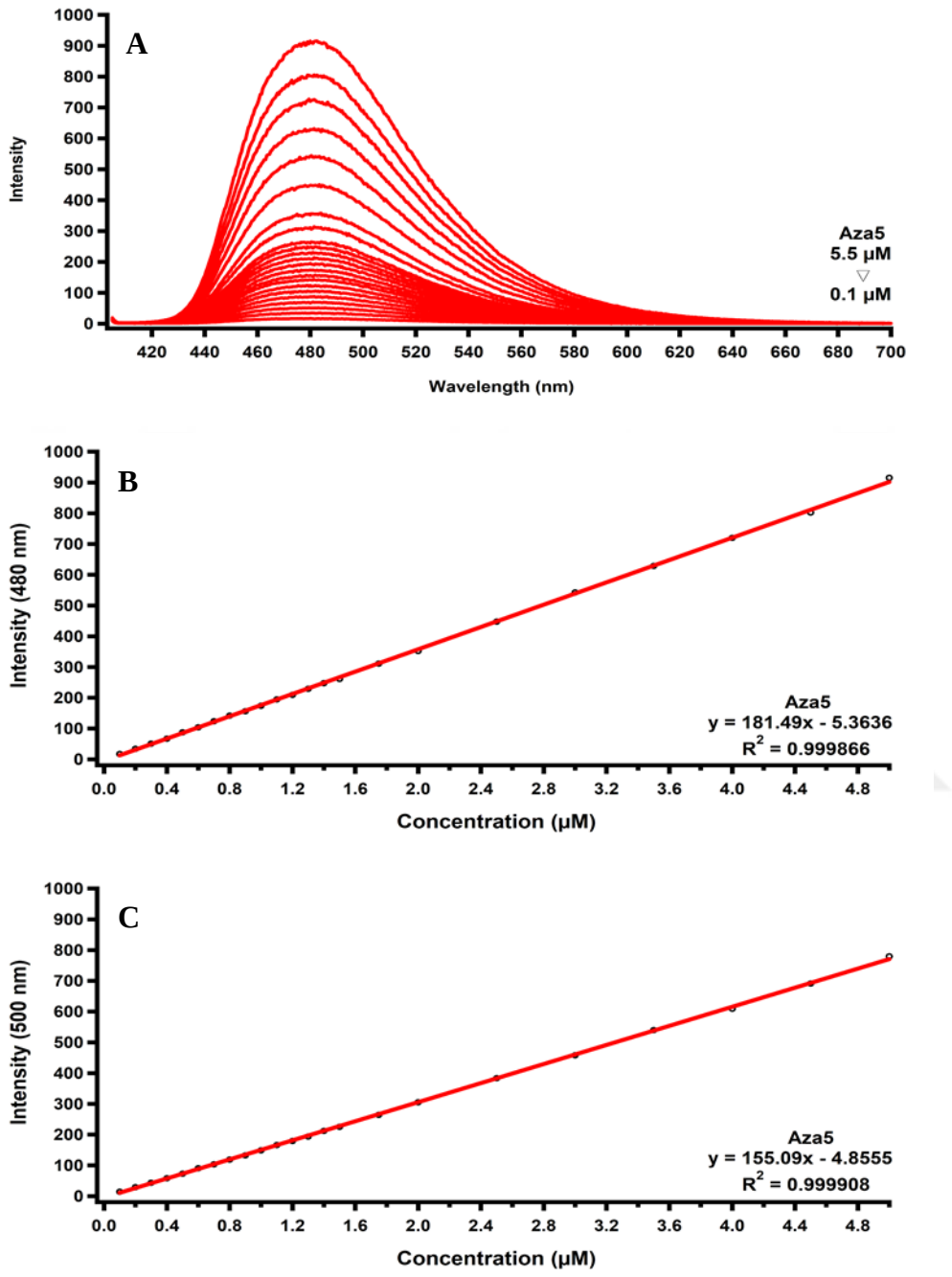

Figure C. 3. Calibration curve construction of Aza5. (A) Fluorescence spectra of Aza5 at varying concentrations between 0.1 µM and 5.5 µM. (B) Calibration curve of Aza5 obtained from the fluorescence intensity at 480 nm. (C) Calibration curve of Aza5 obtained from the fluorescence intensity at 500 nm.

Calibration Curve of Azabutyl

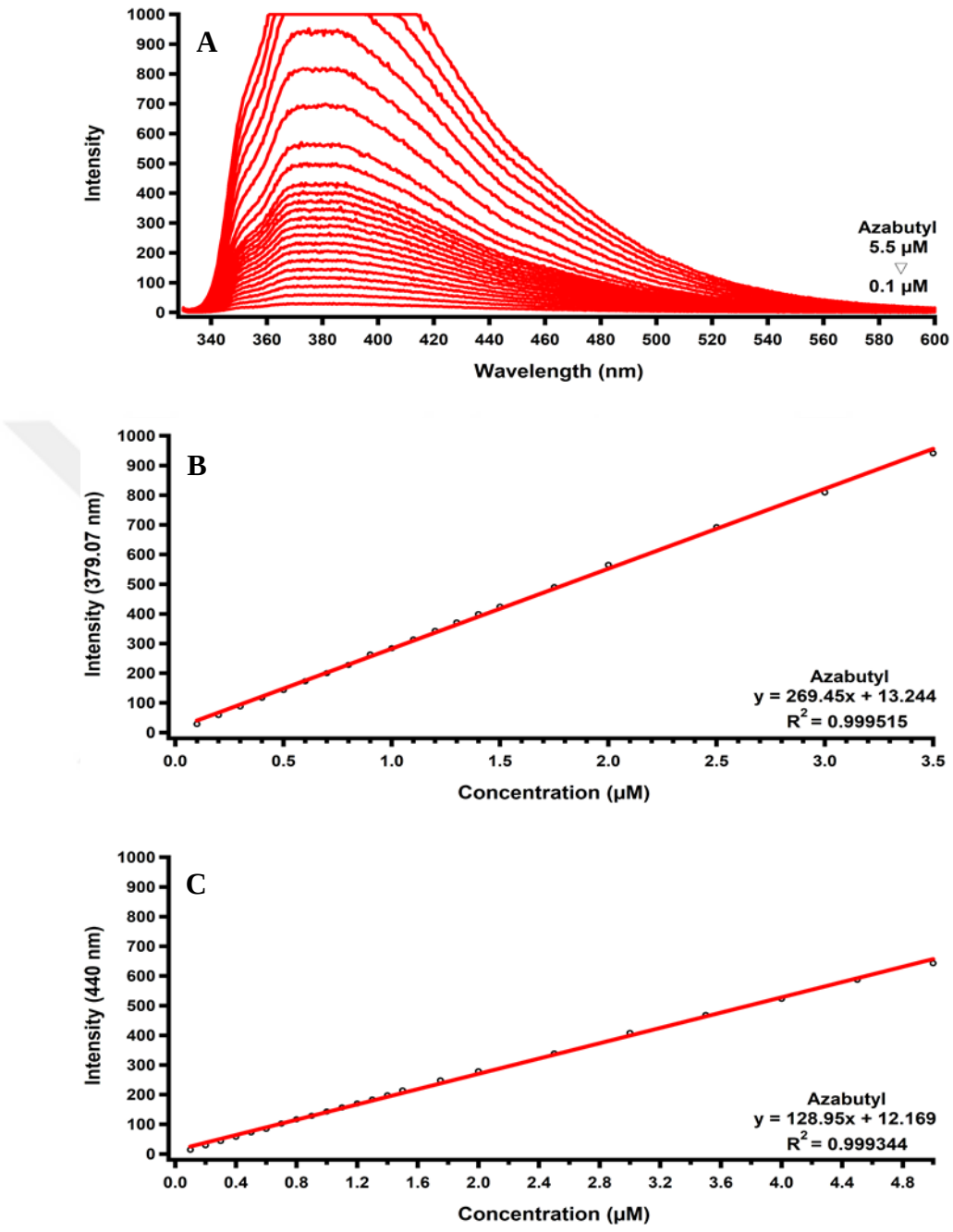

Figure C. 4. Calibration curve construction of Azabutyl. (A) Fluorescence spectra of Azabutyl at varying concentrations between 0.1 µM and 5.5 µM. (B) Calibration curve of Azabutyl obtained from the fluorescence intensity at 379 nm. (C) Calibration curve of Azabutyl obtained from the fluorescence intensity at 440 nm.

Calibration Curve of Azaisobutyl

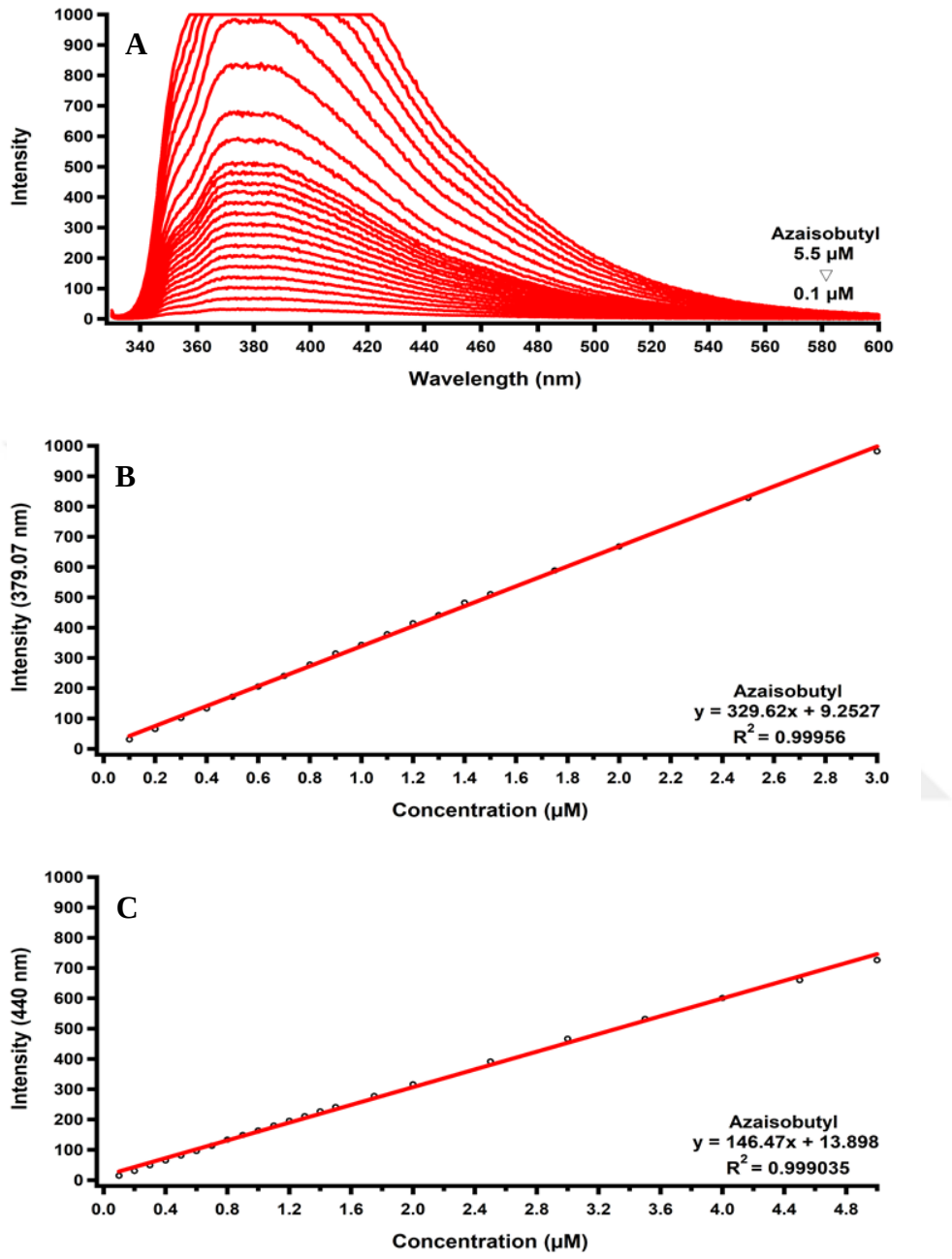

Figure C. 5. Calibration curve construction of Azaisobutyl. (A) Fluorescence spectra of Azasiobutyl at varying concentrations between 0.1 µM and 5.5 µM. (B) Calibration curve of Azaisobutyl obtained from the fluorescence intensity at 379 nm. (C) Calibration curve of Azasobutyl obtained from the fluorescence intensity at 440 nm.

Calibration Curve of Doxorubicin

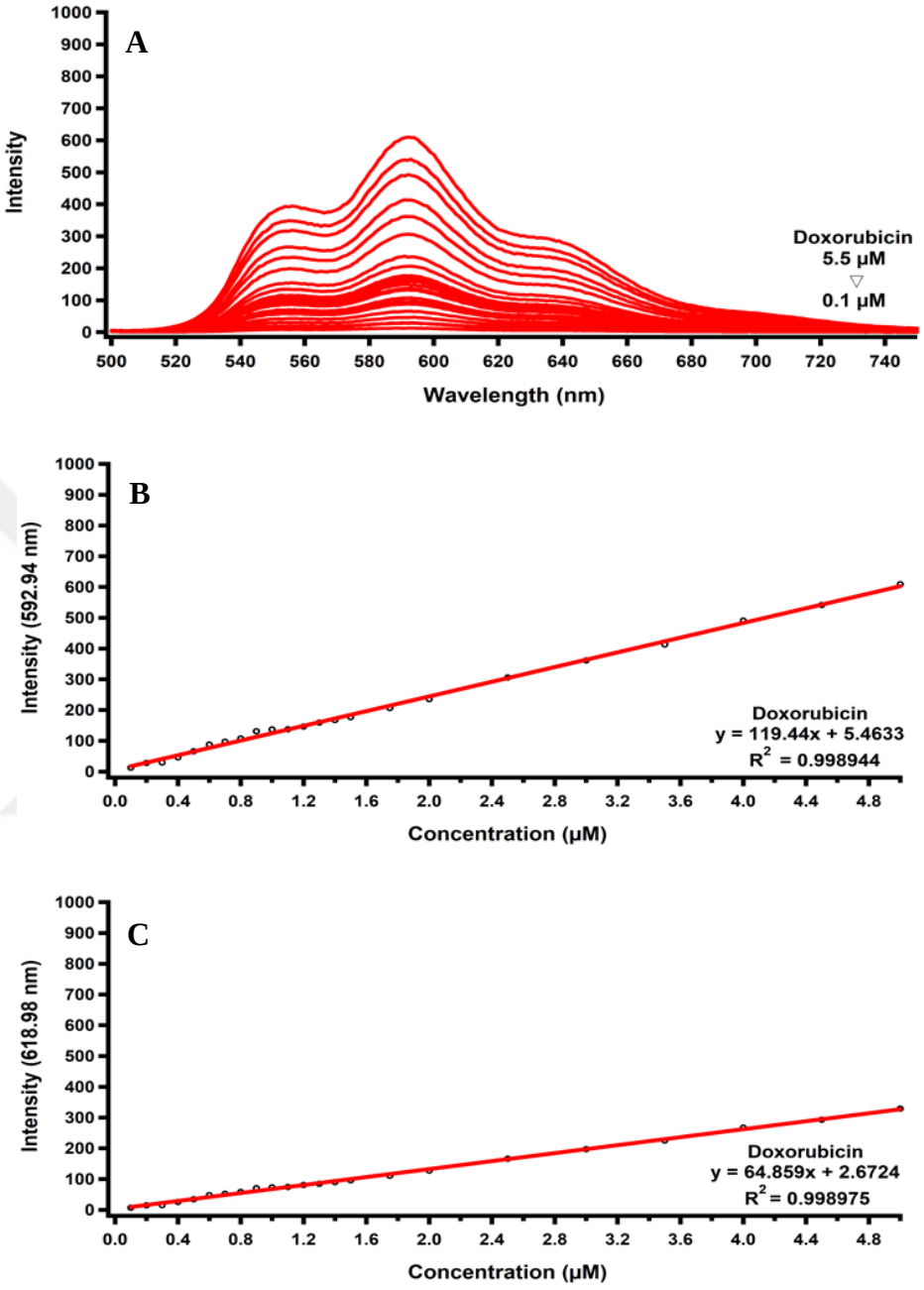

Figure C. 6. Calibration curve construction of Doxorubicin. (A) Fluorescence spectra of Doxorubicin at varying concentrations between 0.1 µM and 5.5 µM. (B) Calibration curve of Doxorubicin obtained from the fluorescence intensity at 593 nm. (C) Calibration curve of Doxorubicin obtained from the fluorescence intensity at 619 nm.

D. BPES Buffer and 10% (w/v) SDS Stock Solutions Preparation

D.1 BPES Buffer and 10% (w/v) SDS Stock Solutions Preparation

The following equations were applied for preparations of NaCI, Na_2HPO_4, Na_2EDTA, and NaH_2PO_4 stock solutions and their volumes in 5XBPES, respectively.

1. n (mol) = M (molarity) x L (volume)

m = n (mol) x MW

2. M1 x V1 = M2 x V2

D.2 2000.0 mM NaCI Stock Solution Preparation

1. n (mol) NaCI = 2.000 M x 0.5000 L gives n (mol) NaCI = 1.000 mol

m NaCI = 1 mol x 58.44 g/mol (MW of NaCI) = 58.44 g

58.44 g NaCI was solubilized in H2O and completed to 500.0 mL in a volumetric flask

2. 2 M x V1 = 9.250 M x 500.0 mL

V1 = 231.25 mL of 2.000 M NaCI was present in 500.0 mL 5XBPES.

D.3 600.0 mM Na_2HPO_4 Stock Solution Preparation

1. n (mol) Na_2HPO_4 = 0.600 M x 0.200 L gives n (mol) Na_2HPO_4 = 0.120 mol

m Na_2HPO_4 = 0.120 mol x 141.96 g/mol (MW of Na_2HPO_4) = 17.035 g

17.035 g Na_2HPO_4 was solubilized in H_2O and completed to 200.0 mL in a volumetric flask.

2. 0.600 M x V1 = 0.0300 M x 500.0 mL

V1 = 25.0 mL of 0.0300 M Na_2HPO_4 was present in 500.0 mL 5XBPES.

D.4 100.0 mM Na_2EDTA Stock Solution Preparation

1. n (mol) Na_2EDTA = 0.100 M x 0.200 L gives n (mol) Na_2EDTA = 0.0200 mol

m Na_2EDTA = 0.0200 mol x 372.24 g/mol (MW of Na_2EDTA) = 7.445 g

7.445 g Na_2EDTA was solubilized in H2O and completed to 200.0 mL in a volumetric flask.

2. 0.100 M x V1 = 0.00500 M x 500.0 mL

V1 = 25.0 mL of 0.100 M Na_2EDTA was present in 500.0 mL 5XBPES.

D.5 400.0 mM NaH_2PO_4 Stock Solution Preparation

1. n (mol) NaH_2PO_4 = 0.400 M x 0.200 L gives n (mol) NaH_2PO_4 = 0.0800 mol

m NaH_2PO_4 = 0.0800 mol x 119.98 g/mol (MW of NaH_2PO_4) = 9.598 g

9.598 g NaH_2PO_4 was solubilized in H_2O and completed to 200 mL in a volumetric flask.

2. 0.400 M x V1 = 0.0100 M x 500.0 mL

V1 = 12.50 mL of 0.400 M NaH_2PO_4 was present in 500.0 mL 5XBPES.

10.0 g SDS (Sigma Aldrich, 862010) was solubilized in H_2O, and volume was completed to 100.0 mL to prepare 10%SDS.

E. Association Constant Measurements

1.0 µM of Azamethyl was titrated with c-MYC:Azametyl as given in Table E.1, and fluorescent intensities were plotted against wavelength (Figure E.1).

Table E. 1 Titration table of 1.0 µM Azamethyl solution with 400.0 µM c-MYC G4 with 1.0 µM Azamethyl

Quadruplex DNA (µM)*	**Added 400.0 µM c-MyC with 1.0 µM Azamethyl (µL)**	**Total Volume (µL)****
0.00	0.0	2500.0
1.00	6.3	2506.3
2.00	6.3	2512.6
3.00	6.3	2518.9
4.00	6.4	2525.3
5.00	6.4	2531.6
6.00	6.4	2538.1
7.00	6.5	2544.5
8.00	6.5	2551.0
9.00	6.5	2557.5
10.00	6.6	2564.1
11.00	6.6	2570.7
12.00	6.6	2577.3
13.00	6.7	2584.0
14.00	6.7	2590.7
15.00	6.7	2597.4

* 1.0 µM c-MYC were taken as 1.0 µM Quadruplex DNA.

** 1.0 µM Azamethyl solution was prepared from 100.0 µM stock solution.

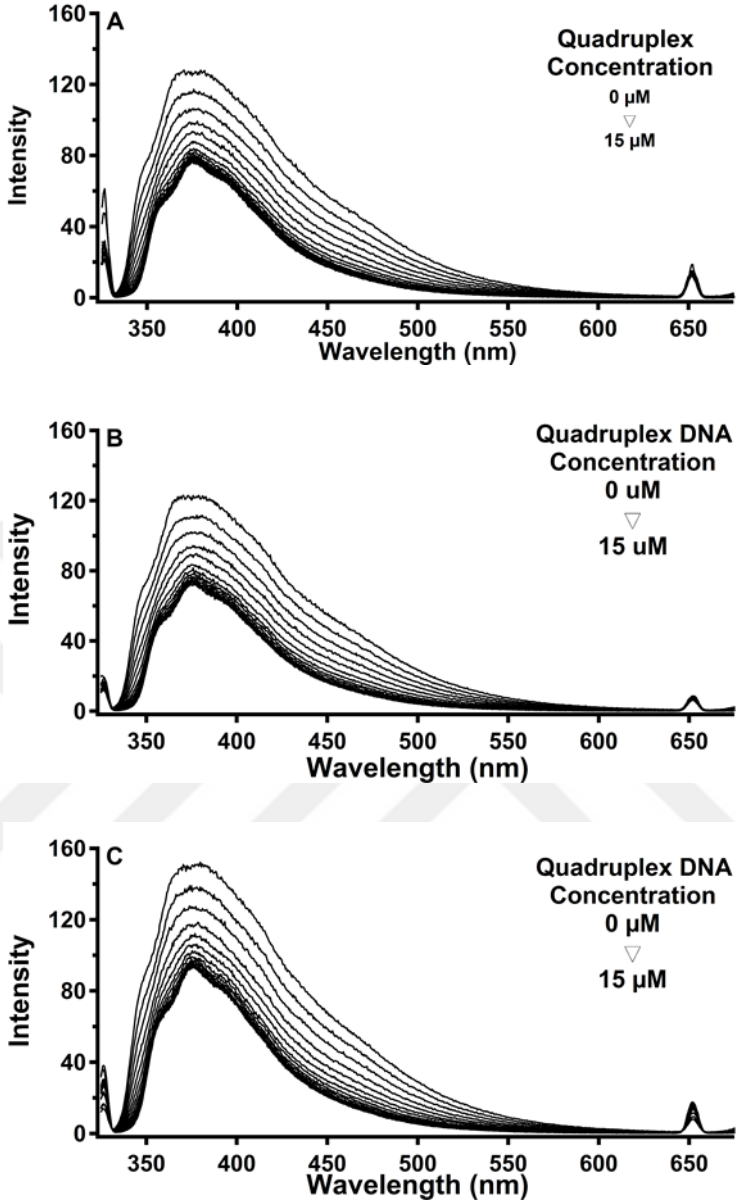

Figure E. 1. Fluorescence intensity vs Wavelength (nm) graphics for titration of 1.0 µM Azamethyl with c-MYC+Azamethyl solution.

F. Sample Preparation for Thermal Denaturation Experiments

The c-MYC solution was prepared according to the given example for c-MYC:Azamethyl 1:1 ratio. c-MYC concentration was calculated in G-Quartet (Ragazzon et al., 2007). And, one folded c-MYC G4 structure has three G-Quartets, therefore, 9.0 µM c-MYC G-Quartet responds to 3.0 µM in strand;

Table F. 1 c-MYC:Azamethyl 1:1 ratio sample preparation for annealing

Substance Name	**Initial Concentration**	**Final Concentration**	**Added Volume (µL)**
c-MYC	3848.0 µM	9.0 uM	9.3
5xBPES	5X	1X	800.0
Azamethyl (µM)	1000.0 µM	3.0 uM	12.0
H2O	-	-	3178.7
Total Volume			4000.0 µL

c-MYC solutions were prepared and annealed without Azamethyl at least one day before the experiment. Azamethyl solutions were freshly prepared just before the experiments and added onto c-MYC solutions.

G. Interactions of c-MYC:Azamethyl in UV-Vis spectrophotometer

Thermal denaturation experiments were performed for samples with varying c-MYC:Azamethyl concentrations. The UV-vis spectrum for the lowest temperature (15°C) and the highest (95°C) were compared as follows.

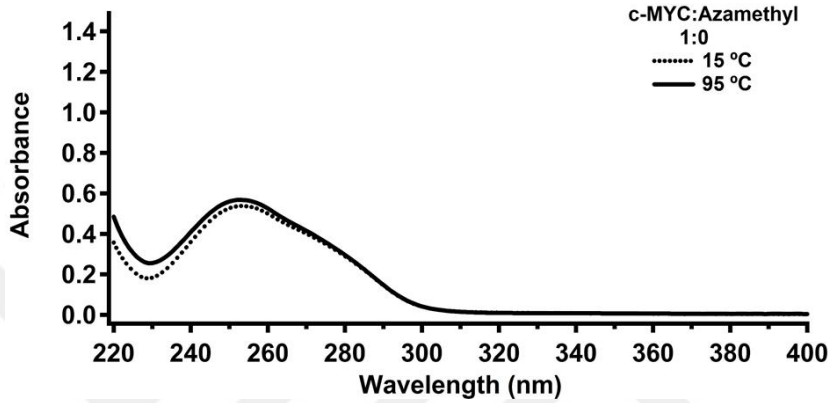

Figure G. 1. UV-Vis spectra of c-MYC:Azamethyl 1:0 sample at 15°C (dotted line) and 95°C (solid line).

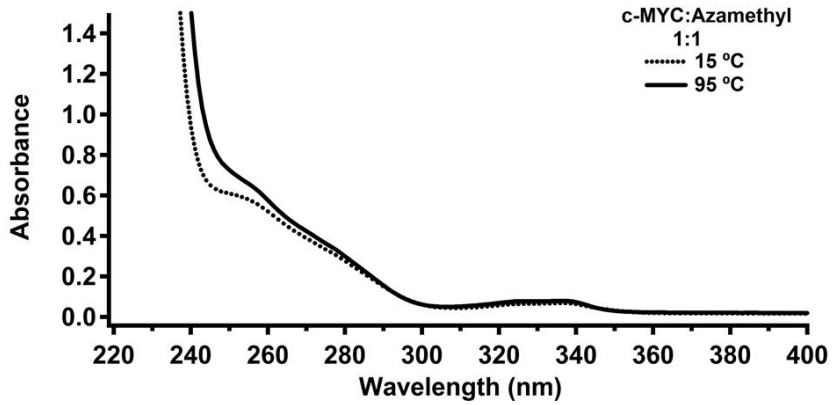

Figure G. 2. UV-Vis spectra of c-MYC:Azamethyl 1:1 sample at 15°C (dotted line) and 95°C (solid line).

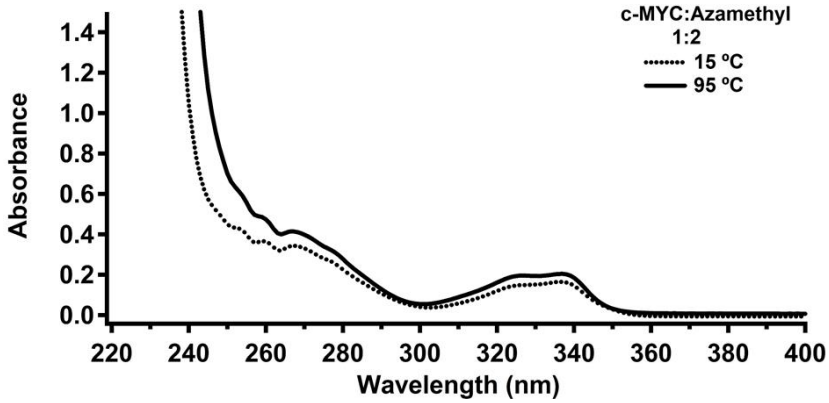

Figure G. 3. UV-Vis spectra of c-MYC:Azamethyl 1:2 sample at 15°C (dotted line) and 95°C (solid line).

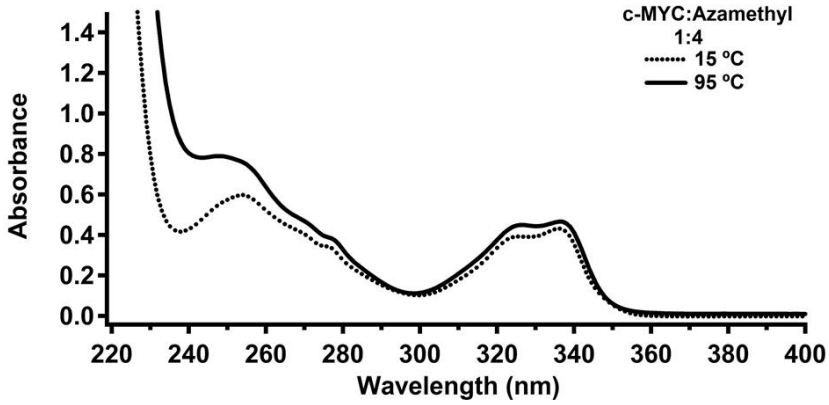

Figure G. 4. UV-Vis spectra of c-MYC:Azamethyl 1:4 sample at 15°C (dotted line) and 95°C (solid line).

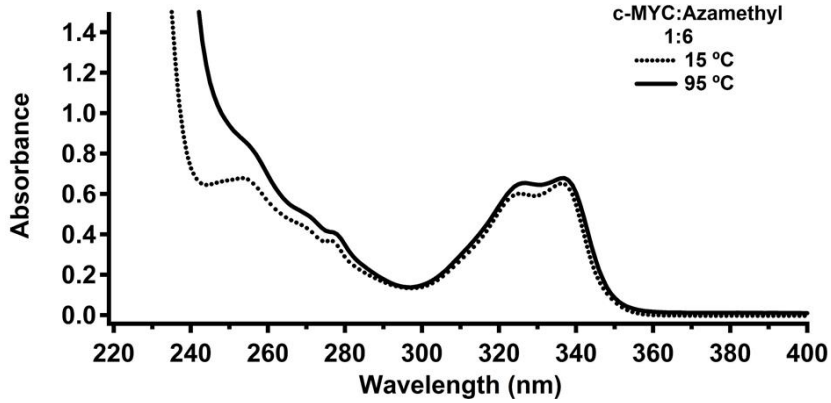

Figure G. 5. UV-Vis spectra of c-MYC:Azamethyl 1:6 sample at 15°C (dotted line) and 95°C (solid line).

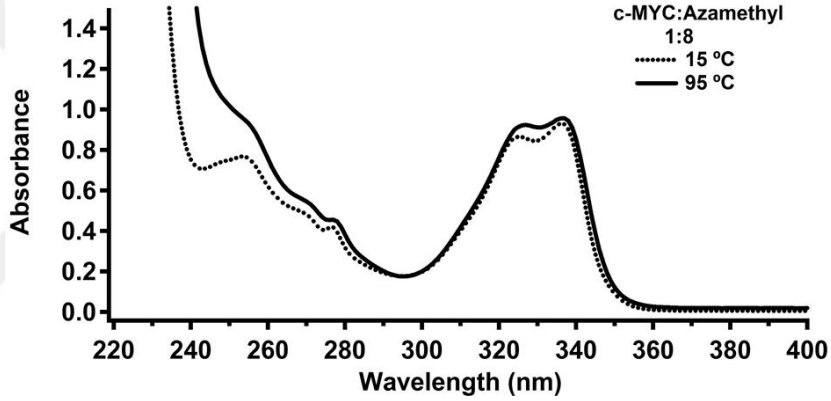

Figure G. 6. UV-Vis spectra of c-MYC:Azamethyl 1:8 sample at 15°C (dotted line) and 95°C (solid line).

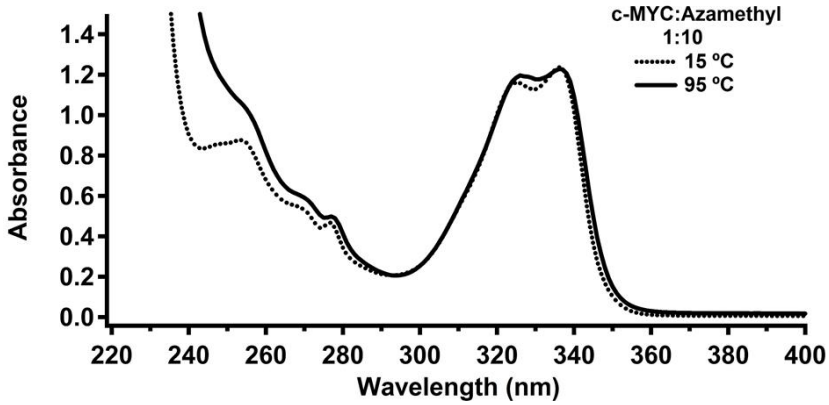

Figure G. 7. UV-Vis spectra of c-MYC:Azamethyl 1:10 sample at 15°C (dotted line) and 95°C (solid line).

H. CD spectra between 15°C and 95°C

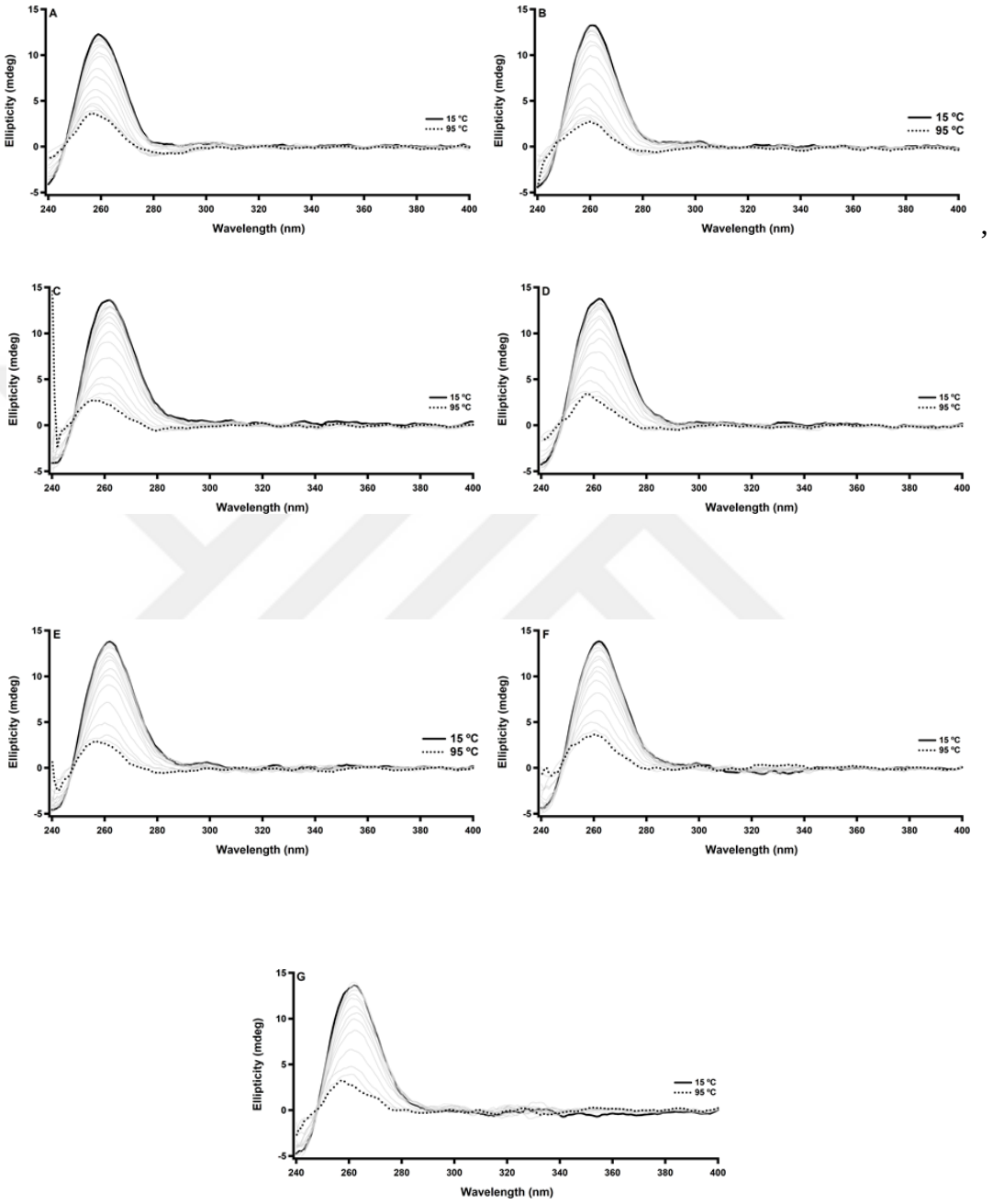

Figure H. 1. CD spectra of c-MYC:Azamethyl samples (A) 1:0, (B) 1:1, (C) 1:2, (D) 1:4, (E) 1:6, (F) 1:8 and (G) 1:10 with 5°C intervals from 15°C (solid line) to 95°C (dotted line).

I. UV-Vis spectra of c-MYC:Azamethyl samples between 15°C and 95°C

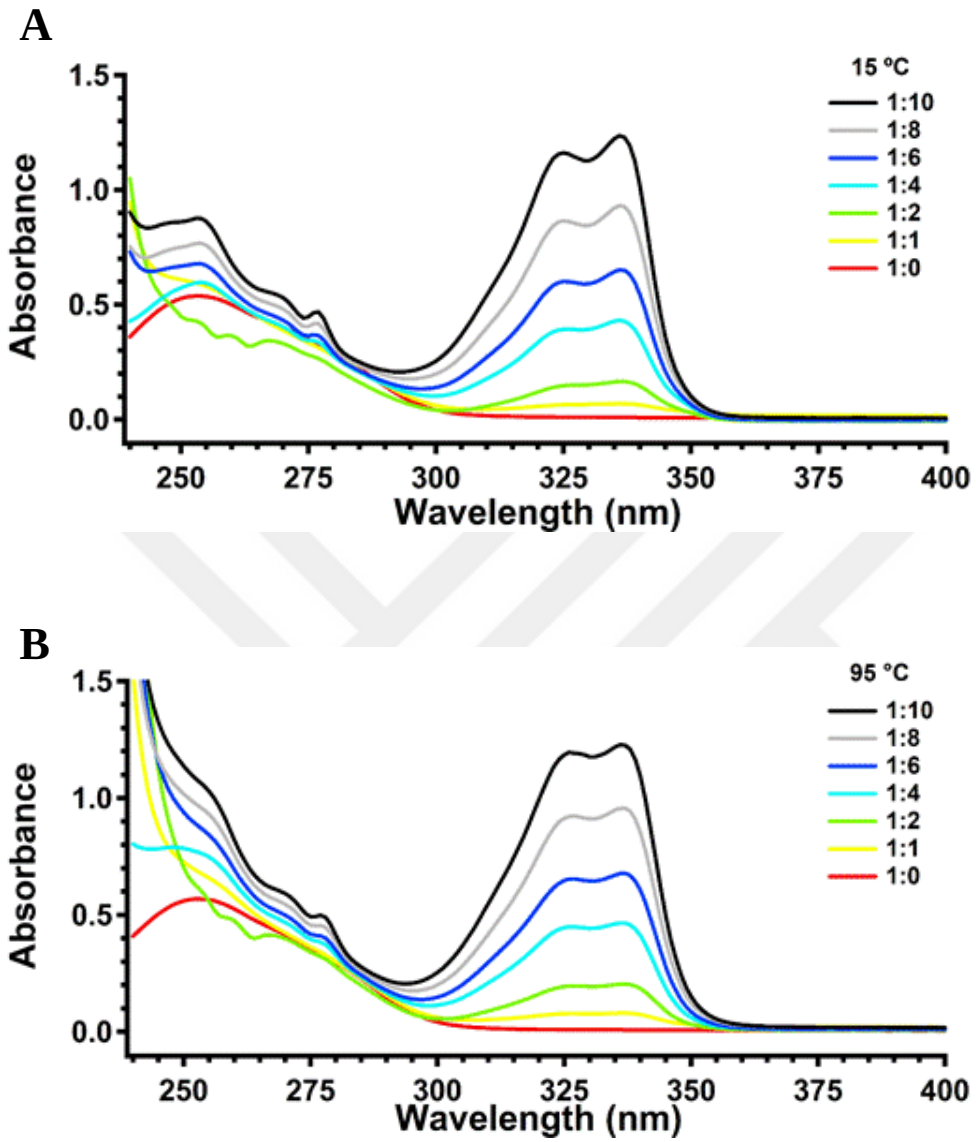

Figure I. 1. UV-Vis spectra of different c-MYC:Azamethyl samples in the range of 240-400 nm at 15°C (A) and 95°C (B).